

©2019

Aseel Shaban Mansi

ALL RIGHTS RESERVED

**Development of Low-Shrinkage Rapid Set Composite and Simulation of
Shrinkage Cracking Distribution in Repaired Concrete Members**

By

ASEEL SHANAN MANSI

A Dissertation submitted to the

School of Graduate Studies

Rutgers, The State University of New Jersey

In partial fulfillment of the requirements

For the degree of

Doctor of Philosophy

Graduate Program in Civil and Environmental Engineering

Written under the direction of

Yook-Kong Yong

And approved by

New Brunswick, New Jersey

May 2019

ABSTRACT OF THE DISSERTATION

Development of Low-Shrinkage Rapid Set Composite and Simulation of Shrinkage Cracking Distribution in Repaired Concrete Members

ASEEL SHABAN MANSI

Dissertation Director:

Dr. YOOK-KONG YONG

As the global transportation infrastructure aged, the need for effective maintenance has become necessary to maintain not only strength but also durability. Although many materials used in repair provide adequate strength, they can suffer early failure and degradation as a result of several phenomena such as rigidity and rapid shrinkage. In instances where such repair materials are used, cracking and debonding can quickly occur because of the high stresses developed in the system. The Portland cement repair material considered reliable repair materials; however, they require sufficient curing time which leads to detours or lane closures. Hence, the efficient repair and replacement of concrete pavements often require a rapid setting material that can be placed, cured, and opened to traffic in a relatively short period of time. Rapid-hardening cementitious repair materials have been widely used. The use of very early strength materials will minimize the out-of-service time of the effective repairs.

In this dissertation, experimental and analytical programs were carried out. The experimental program included three phases. The first phase was conducted to design and test the fresh and shrinkage properties of high early strength rapid set materials (HES-RSM) and high early strength fiber reinforced rapid set materials (HES-FR-RSM)

mixtures. These mixtures were developed for concrete repair applications in transportation infrastructures with low cracking potential. For this purpose, three of the most common ready patch repair materials and approved from the most of DOT'S were selected, the samples were cured using dry curing to simulate the critical condition in the repair process. As a fiber reinforcement, three types of fibers (steel, carbon, and basalt) with different percentages were prepared to select the best mix designs that satisfy various requirements. The second phase was performed to investigate the mechanical properties of the optimized mixtures which selected from the first phase depending on its shrinkage strain and flowability requirements. The third phase contains the validation of the model. The analytical part of this research included the development of a finite element model (FEM) that can be used for the analysis and prediction of the structural behavior of the composite repaired beams due to the shrinkage effect of the repair materials.

The results showed that the developed HES-FR-RSM can achieve high early compressive strength more than 3000 psi and modulus of rupture more than 1400 psi at the age of 4hrs. The free shrinkage strain values were below than 500 microstrains for the most optimized mixtures. The best performance mixture was C1S0.5 with 268 microstrains which is less than the tensile strain capacity of concrete which ranges from 200 to 300 microstrains. The model establishes the development of a good basic tool to study the effects of free shrinkage of the repair materials on the repaired composite and make the selecting repair materials easiest for the engineers for practical purpose. The model is also capable of simulating the crack initiations and could describe the real structural behavior.

DEDICATION

*This Humble Work
is Dedicated to my
Beloved Family.*

Abeel

ACKNOWLEDGMENT

I would like to express my cordial thanks and deepest gratitude to my advisor Dr. Yook-Kong Yong for his help and kind attention to complete this work. It was an honor to work with him and be exposed to his engineering and life experience.

I would also like to thank Dr. Basheer Al-gohi and Dr. Hao Wang for being on my committee and for their valuable advice. I would also like to thank Dr. Husam S. Najm for being on my committee as well as his guidance as a graduate director.

Deepest thanks are expressed to my husband Dr. Haider for his help and support along my career and Ph.D.

My deep and sincere thanks to my father, mother, my brothers and sisters, and my kids for their love and support at all times.

My sincere thanks to the Higher Committee for Education Development in Iraq (HCED) prime minister office for awarding my Ph.D. scholarship.

Table of Contents

| | |
|--|-----------|
| ABSTRACT OF THE DISSERTATION | ii |
| DEDICATION..... | iv |
| ACKNOWLEDGMENT | v |
| CHAPTER 1 INTRODUCTION | 1 |
| 1.1 PROBLEM STATEMENT | 1 |
| 1.2 RESEARCH OBJECTIVES | 4 |
| 1.3 DISSERTATION ORGANIZATION..... | 5 |
| CHAPTER 2 LITERATURE REVIEW | 7 |
| 2.1 INTRODUCTION..... | 7 |
| 2.2 TYPES OF CONCRETE SHRINKAGE | 8 |
| 2.2.1 Plastic Shrinkage | 9 |
| 2.2.2 Autogenous Shrinkage..... | 10 |
| 2.2.3 Thermal Shrinkage | 11 |
| 2.2.4 Drying shrinkage | 11 |
| 2.3 HOW DOES THE SHRINKAGE CRACKING LEAD TO REPAIR FAILURE? | 13 |
| 2.4 PREDICTION MODELS OF DRYING SHRINKAGE | 17 |
| 2.4.1 AASHTO LFRD Model (2014)..... | 18 |
| 2.4.2 ACI 209.2R (2008) | 19 |
| 2.4.3 CEB-FIP Model [1990] | 22 |
| 2.4.4 SAKATA Model [1993]..... | 22 |
| 2.5 THE REPAIR PROCESS..... | 24 |
| 2.6 REPAIR MATERIALS TYPES..... | 29 |
| 2.6.1 Ordinary Portland Cement Mortar and Concrete | 30 |
| 2.6.2 High Rapid Setting Repair Materials..... | 30 |
| 2.6.3 Polymer Concrete | 33 |
| 2.6.4 Epoxy Polymer Concrete (EPC)..... | 34 |
| 2.7 PERFORMANCE EVALUATION OF REPAIR MATERIALS | 34 |
| 2.8 PREVIOUS WORK ON FE AND THEORETICAL MODELS ON THE EFFECT OF SHRINKAGE ON THE REPAIRED SYSTEM..... | 36 |
| CHAPTER 3 EXPERIMENTAL WORK | 41 |

| | |
|--|-----------|
| 3.1 INTRODUCTION..... | 41 |
| 3.2 FIRST PHASE | 41 |
| 3.3 SECOND PHASE | 42 |
| 3.4 THIRD PHASE..... | 44 |
| 3.5 MATERIALS | 48 |
| 3.5.1 CEMENT ALL High Strength, Non-Shrink Grout Multi-Purpose Repair Material..... | 48 |
| 3.5.2 MORTAR MIX High-Strength Structural Repair | 48 |
| 3.5.3 RAPID ROAD REPAIR –EXTENDED | 48 |
| 3.5.4 Aggregate..... | 49 |
| 3.5.5 Fibers | 49 |
| 3.5.6 High Range Water Reducing Admixture..... | 51 |
| 3.6 TESTING OF FRESH MORTAR AND CONCRETE..... | 53 |
| 3.6.1 Slump Flow Test..... | 53 |
| 3.6.2 Slump Test..... | 53 |
| 3.7 TESTING OF HARDENED CONCRETE..... | 54 |
| 3.7.1 Compressive Strength Test..... | 54 |
| 3.7.2 Splitting Tensile Strength Test | 55 |
| 3.7.3 Flexural strength | 56 |
| 3.7.4 Static Modulus of Elasticity Test..... | 57 |
| 3.7.5 Drying Shrinkage..... | 57 |
| CHAPTER 4 EXPERIMENTAL RESULTS | 60 |
| 4.1 INTRODUCTION..... | 60 |
| 4.2 FRESH PROPERTIES | 60 |
| 4.3 HARDENED PROPERTIES | 60 |
| 4.3.1 Compressive Strength..... | 60 |
| 4.3.2 Tensile strength..... | 62 |
| 4.3.3 Flexural Strength | 64 |
| 4.3.4 Modulus of Elasticity..... | 66 |
| 4.3.5 Free Shrinkage Test | 68 |
| 4.4 Strain for Composite Repaired Prisms | 71 |

| | |
|--|------------|
| CHAPTER 5 FINITE ELEMENT MODEL DEVELOPMENT..... | 77 |
| 5.1 INTRODUCTION..... | 77 |
| 5.2 ADAPTIVE MESH REFINEMENT | 78 |
| 5.3 DEVELOPING THE FINITE ELEMENT MODEL | 79 |
| 5.3.1 First Step:Shrinkage Prediction Equation | 80 |
| 5.3.2 Second Step:Material Models Development..... | 81 |
| 5.3.3 Failure Criteria (Ind)..... | 83 |
| 5.3.4 Element Type Used | 85 |
| 5.4 RESULT AND MODEL VALIDATION | 86 |
| 5.4.1 Experimental conducted by Beushausen & Alexander, [2007]..... | 86 |
| 5.4.1.1 Case A..... | 86 |
| 5.4.1.1.1 Stress Development prediction..... | 90 |
| 5.4.1.2 CASE B..... | 97 |
| 5.4.2 The Experimental was carried out by Casting of Nine Composite Prism. 100 | |
| 5.4.2.1 Cracking Predictions | 101 |
| 5.4.3 Parametric Studies | 105 |
| 5.4.3.1 Dimension of the Repair | 105 |
| 5.4.3.1.1 Thickness of the Repair (Tr) | 105 |
| 5.4.3.1.2 Length of the Repair (Lr) | 107 |
| 5.4.3.2 Modulus of Elasticity (Er) | 109 |
| 5.4.3.3 The Shape of Repair (Sr) | 111 |
| CHAPTER 6 CONCLUSIONS..... | 113 |
| 6.1 CONCLUSIONS | 113 |
| APPENDICES | 116 |
| APPENDIX A MANUFACTURER PRODUCT SPECIFICATIONS..... | 116 |
| 1. CEMENT ALL MULTI-PURPOSE REPAIR MATERIAL & NON-SHRINK GROUT | 116 |
| 2. MORTAR MIX HIGH-STRENGTH STRUCTURAL REPAIR MORTAR DESCRIPTION..... | 119 |
| 3. QUIKRETE® RAPID ROAD REPAIR® - EXTENDED PRODUCT DESCRIPTION | 123 |
| REFERENCES..... | 126 |

LIST OF TABLES

| | |
|---|-----|
| Table 2.1 $\gamma_{(sh,tc)}$ for Moist Curing Type | 20 |
| Table 2.2 Properties governing compatibility of concrete Patch repair..... | 29 |
| Table 2.3 Types of Repair materials [Emberson and Mays, 1990] | 30 |
| Table 3.1 Mixtures Proportion and Identification..... | 42 |
| Table 3.2 Grading of the Aggregate Used | 49 |
| Table 3.3 Physical/Mechanical of Basalt Chopped Fiber | 51 |
| Table 3.4 Technical Information of Copper Coated Micro Steel Fiber | 51 |
| Table 3.5 Technical Information of Carbon Fiber | 51 |
| Table 4.1 Mechanical Properties Results..... | 61 |
| Table 4.2 Strain Profile for the Repaired Composite Prisms..... | 61 |
| Table 5.1 Restraint Factor in Different Restraint Condition..... | 83 |
| Table 5.2 Mixture Proportions and Material Properties for Substrate and Overlay | 87 |
| Table 5.3 Predicted vs. Modified Statistic Values Determined using ACI model..... | 101 |
| Table 5.4 Strain Profile and Cracking Strain | 103 |
| Table 5.5 Strain Profile for the Experiment, Plane-stress, and Plane-strain..... | 104 |

LIST OF FIGURES

| | |
|---|----|
| Figure 1.1 Flow Chart of the Research | 5 |
| Figure 2.1 Typical Deterioration Process of Concrete Repair | 8 |
| Figure 2.2 Cracking of Concrete Due to Cracking Shrinkage | 15 |
| Figure 2.3 Effect of Creep | 17 |
| Figure 2.4 Flowchart Demonstrate the Selection Process of the Repair Material | 25 |
| Figure 2.5 Characteristics of a Suitable Repair Material | 27 |
| Figure 2.6 shrinkage Test Results | 27 |
| Figure 3.1 Flow Chart of Phase One..... | 43 |
| Figure 3.2. Sketch of Composite Prism. | 45 |
| Figure 3.3. Composite Prism | 46 |
| Figure 3.4. Locations of Strain Measuring Discs | 47 |
| Figure 3.5. (a) Composite Prism after Repairing and Strain Measuring discs (b) A multi- Length Strain Gauge (c) Readings Measurement | 47 |
| Figure 3.6 Copper Coated Micro Steel Fiber..... | 50 |
| Figure 3.7 Basalt Chopped Fiber | 50 |
| Figure 3.8 Carbon Fiber..... | 50 |
| Figure 3.9 Mixing Process by Using Paddle Mixer..... | 52 |
| Figure 3.10 Slump Flow Test for Mortar Mixtures | 53 |
| Figure 3.11 Slump Test for Concrete Mixtures | 54 |
| Figure 3.12 1-Million lbs. Forney Testing Machine..... | 55 |
| Figure 3.13 Splitting Tensile Test Setup..... | 56 |
| Figure 3.14 Static Modulus of Elasticity Test Setup | 57 |
| Figure 3.15 Drying Curing..... | 58 |
| Figure 3.16 Free Drying Shrinkage Test Setup | 59 |
| Figure 4.1 Compressive Strength for C1S Mixtures..... | 61 |
| Figure 4.2 Compressive Strength for C2S Mixtures..... | 62 |
| Figure 4.3 Compressive Strength for Q Mixtures..... | 62 |
| Figure 4.4 Tensile strength for C1S Mixtures | 63 |
| Figure 4.5 Tensile strength for C2S Mixtures | 64 |
| Figure 4.6 Tensile Strength for Q Mixtures..... | 64 |
| Figure 4.7 Flexural Strength for C1S Mixtures | 65 |
| Figure 4.8 Flexural Strength for C2S Mixtures | 65 |
| Figure 4.9 Flexural Strength for Q Mixtures | 66 |
| Figure 4.10 Modulus of Elasticity for CTS1 Mixtures | 67 |
| Figure 4.11 Modulus of Elasticity for CTS2 Mixtures | 67 |
| Figure 4.12 Modulus of Elasticity for Q Mixtures | 68 |
| Figure 4.13 Free Drying Shrinkage CTS1 Mixtures..... | 69 |
| Figure 4.14 Free Drying Shrinkage CTS2 Mixtures..... | 70 |

| | |
|---|-----|
| Figure 4.15 Free Drying Shrinkage Q Mixtures | 70 |
| Figure 4.16 Picture Taken Using Digital Microscope for the C1R Repair Material | 73 |
| Figure 4.17 Picture Taken Using Digital Microscope for the C1S25 Repair Material..... | 70 |
| Figure 4.18 Picture Taken Using Digital Microscope for the C1S50 Repair Material..... | 70 |
| Figure 4.19 Picture Taken Using Digital Microscope for the C2R Repair Material..... | 70 |
| Figure 4.20 Picture Taken Using Digital Microscope for the C2S25 Repair Material..... | 70 |
| Figure 4.21 Picture Taken Using Digital Microscope for the C2C25 Repair Material.... | 70 |
| Figure 4.22 Picture Taken Using Digital Microscope for the C2B50 Repair Material.... | 70 |
| Figure 4.23 Picture Taken Using Digital Microscope for the QR Repair Material..... | 70 |
| Figure 4.24 Picture Taken Using Digital Microscope for the QS25 Repair Material..... | 70 |
| Figure 5.1 Nonuniform Element size changed by Global Adaptive Mesh Refinement ... | 80 |
| Figure 5.2 Flowchart for Calculating the Proposed Model..... | 85 |
| Figure 5.3 2D Triangular Element..... | 85 |
| Figure 5.4 Comparison Between Predicted and Modified Shrinkage for ACI 209.2R | 87 |
| Figure 5.5 Interface Strains in Overlay | 88 |
| Figure 5.6 Free Drying Shrinkage | 89 |
| Figure 5.7 The DF at the End of the Analysis | 90 |
| Figure 5.8 Prediction of Failure Modes | 91 |
| Figure 5.9 Variation of Stress σ_{xx} Along the Length at the Top of the Overlay (t=90) .. | 91 |
| Figure 5.10 Stress Distribution σ_{xx} (90 days) | 92 |
| Figure 5.11 Variation of stresses σ_{yy} Along the Length at the Bottom of the Overlay (t=90) | 92 |
| Figure 5.12 Stress Distribution σ_{yy} (90 days) | 93 |
| Figure 5.13 Variation of Stresses σ_{xy} Along the Length at the Bottom of the Overlay at (t=90) | 93 |
| Figure 5.14 Stress Distribution σ_{xy} (90 days) | 94 |
| Figure 5.15 Variation of Stress σ_{xx} Along the Length at the Top of the Overlay (t=90) due to Shrinkage and Creep Effect | 95 |
| Figure 5.16 Stress Distribution σ_{xx} (90 days) Due to Shrinkage and Creep Effect | 95 |
| Figure 5.17 Variation of Stress σ_{yy} along the Length at the Top of the Overlay (t=90) due to Shrinkage and Creep Effect. | 96 |
| Figure 5.18 Stress Distribution σ_{yy} (90 days) Due to Shrinkage and Creep Effect | 96 |
| Figure 5.19 Variation of Stress σ_{xy} Along the length at the Top of the Overlay (t=90) due to Shrinkage and Creep Effect | 97 |
| Figure 5.20 Stress Distribution σ_{xy} (90 days) Due to Shrinkage and Creep Effect | 97 |
| Figure 5.21 DF During Analysis Period | 100 |
| Figure 5.22 Cracks in Composite Prism Repaired by C2R: a) Experiment at 32 days, b) FEM at 28 days | 102 |
| Figure 5.23 Flowchart for the Parametric Study | 105 |
| Figure 5.24 Reference Repair Thickness (0.75 in) | 106 |

| | |
|---|-----|
| Figure 5.25 Repair Thickness (0.80 in) | 106 |
| Figure 5.26 Repair Thickness (0.90 in) | 107 |
| Figure 5.27 The Tensile Stresses at 24 Days Varied with Repair Thickness | 107 |
| Figures 5.28 The Tensile Stress at 24 days at Interface Varied with Length of Repair | 108 |
| Figures 5.29 The Shear Stress at 24 Days at Interface Varied with Length of Repair .. | 109 |
| Figure 5.30 Strain Variation at 24 Days Due to the Modulus of Elasticity Variation... | 109 |
| Figure 5.31 Repair Damage Factor with 1.0E | 110 |
| Figure 5.32 Repair Damage Factor with 0.95E | 110 |
| Figure 5.33 Repair Damage Factor with 0.9E | 110 |
| Figure 5.34 Suggestions of Layouts | 111 |
| Figure 5.35 The Strain Along the Length of The Beam at The Interface | 112 |
| Figure 5.36 The Crack Distribution for the Rectangle Shape of the Repair | 112 |
| Figure 5.37 The Crack Distribution for the Trapezoidal Shape of the Repair | 112 |

CHAPTER 1 INTRODUCTION

1.1 PROBLEM STATEMENT

There is a significant number of aging transportation infrastructures worldwide that are suffering from surface deterioration and distress. This is due to either mechanical loading or environmental exposure, and that results in extensive repair and maintenance. The repairing process should provide integration between the new repair material and the existing old substrate to form a composite system. This system should withstand both mechanical loads and environmental conditions. However, this goal is hard to achieve due to difficulties in matching the properties and performance of both materials. A premature failure usually happens in the repair system as a result of such differences. When the repair material is cast, it will be subjected to both ambient temperature and relative humidity. The newly applied repair material is prone to shrink due to evaporation of water and hydration process.

The main cause for the early age crack initiation and progress in the repair system is the drying shrinkage. Cracking in the repair system is an economic exhaustion due to an increase in rehabilitation cost and durability issues of chemical penetration agents, like chloride ions penetration which leads to corrosion damage. Consequently, a shorter service life or repair was required. Matthews [2007] conducted a study on the case histories of the behavior of the repair materials, many failure modes of the repair materials were recorded. He found that cracking was the principle cause of failure, and could result from the restrained shrinkage at 32% in concrete systems, followed by de-bonding at 25%, reinforcement corrosion at 22%, aggregate reaction at 4%, and various others at 17%.

Assessment of the tensile stresses is an effective technique that used to evaluate the ability of repair materials to crack. These tensile stresses are generated in the repair system due to restrained shrinkage. Many properties of the repair materials affect the shrinkage stress resulting from restrained shrinkage such as drying shrinkage, creep, and modulus of elasticity. Furthermore, the substrate concrete's individual properties can affect the imposed stresses.

Portland cement can be considered a reliable repair material; however, they require sufficient curing time which leads to detours or lane closures. Hence, the efficient repair and replacement of concrete pavements often require a rapid setting repair material (RSRM) that can be placed, cured, and opened to traffic in a relatively short time. Rapid-hardening cementitious repair materials have been widely used, and these materials were proven to minimize the out-of-service time due to the repairing process.

The transportation authorities often use prepackaged repair materials, such as rapid-set, cement-based, and resin-based mortar or concrete. Rapid-set cement-based materials are easy to mix and compatible with the substrate. However, they are more tending to dimensional instability [ACPA 1999]. Abdulhameed [2010] Abulhameed et al. [2018], Hassan et al. [2010], and Mansi [2010] have demonstrated that selecting the appropriate repair materials is the key for the successful repair. Increase in autogenous shrinkage, stiffness, and brittleness; also, a decrease in the creep is the main responsible factors for instability. These factors are aggravating in the RSRM since the last has a high rate of strength development and high paste volume. Consequently, it will tend to crack due to the inability of these materials to redistribute the stresses [Barde et al. 2006]. Therefore, the limitation of the magnitude of shrinkage has been specified in several standards and literature. ASTM

C928-00 gives a limit of shrinkage at 28 days at about 0.15 % (1500 microstrains). While, ASTM C1600-07 specifies a maximum value of shrinkage in the range of 600-1200 microstrains for rapid hardening cement-based material overlay/patching. A limit of 300 microstrains free shrinkage at seven days under 27° C and 55 % RH was assigned by the Hong Kong Housing Authority [Kristiawan 2013]. On the other hand, Mc Donald et al. [2000] recommended a limit for the drying shrinkage of 400 and 1000 microstrains at 28 days and one year, respectively.

Fibers have been used at a low volume fraction (less than 0.5 %) to mitigate shrinkage cracking [Raoufi et al., 2010]. When the matrix shrinks, shear stresses develop along both the matrix interface and the fiber. Matrix shrinkage in a particular direction is restrained by a fiber with an effective length parallel to that shrinkage strain direction [Mangat and Azari, 1984]. The use of fibers can improve the ductility of brittle material by transferring the load from the matrix to the fibers; besides, bridging and arresting the cracks [Ghazy et al., 2016]. Fibers do increase the fracture toughness of concrete and limit the width of the cracks that form [Raoufi et al., 2010]. Consequently, fiber reinforcement of concrete/mortar can reduce the damage in the repair system [Li et al., 2000].

Although concrete shrinkage cannot be prevented, it can be minimized. When concrete shrinkage is minimized, restrained cracking is less likely to be a problem. When concrete is maintained, and precautions are taken, the occurrence of cracking will be substantially reduced. With the control of cracking, the cost and necessity of maintenance would be reduced. Cracks in concrete occur when there is a combination of shrinkage, restrain condition, and low tensile strength. A free unrestrained sample of concrete will experience a reduction in the overall volume, but this shrinkage will not cause cracking because

restraint is not present. Similarly, a restrained sample of concrete with high enough tensile stress will resist cracking even while shrinking.

Recent infrastructures' studies highlighted the cracking resulted from restrained shrinkage; moreover, measuring and evaluating the restrained shrinkage due to its significant role in durability issue. Despite the complex nature of shrinkage parameters interaction, many numerical analysis techniques were established to study the cracks in the repair system and control it. Develop mixtures with low cracking potential and propose FEM that can predict the actual time of cracking, is a good way to increase the service life of a structure and reduce maintenance requirements.

1.2 RESEARCH OBJECTIVES

In this research, the goal is to modify some of the widely used ready batches to develop high early strength rapid set materials (HES-RSM). These materials are suitable for a wide range of repair applications for transportation infrastructures with low cracking potential. The development goal is to minimize the shrinkage strain to be less than 300 microstrains and increase the tensile strain capacity. Also, the research included developing a FEM that could verify the ability of the finite element method to describe the real structural behavior. Such as, computing the time-dependent restrained shrinkage stresses by measuring the free shrinkage values and tensile stresses at various depths of the repair layer. Also, predict the actual time of cracking, representation, and distribution of cracks. Therefore, such a model will be extremely useful in the repair design for concrete systems. Experimental and analytical programs were conducted for this purpose as shown in Figure 1.1. to achieve this primary goal.

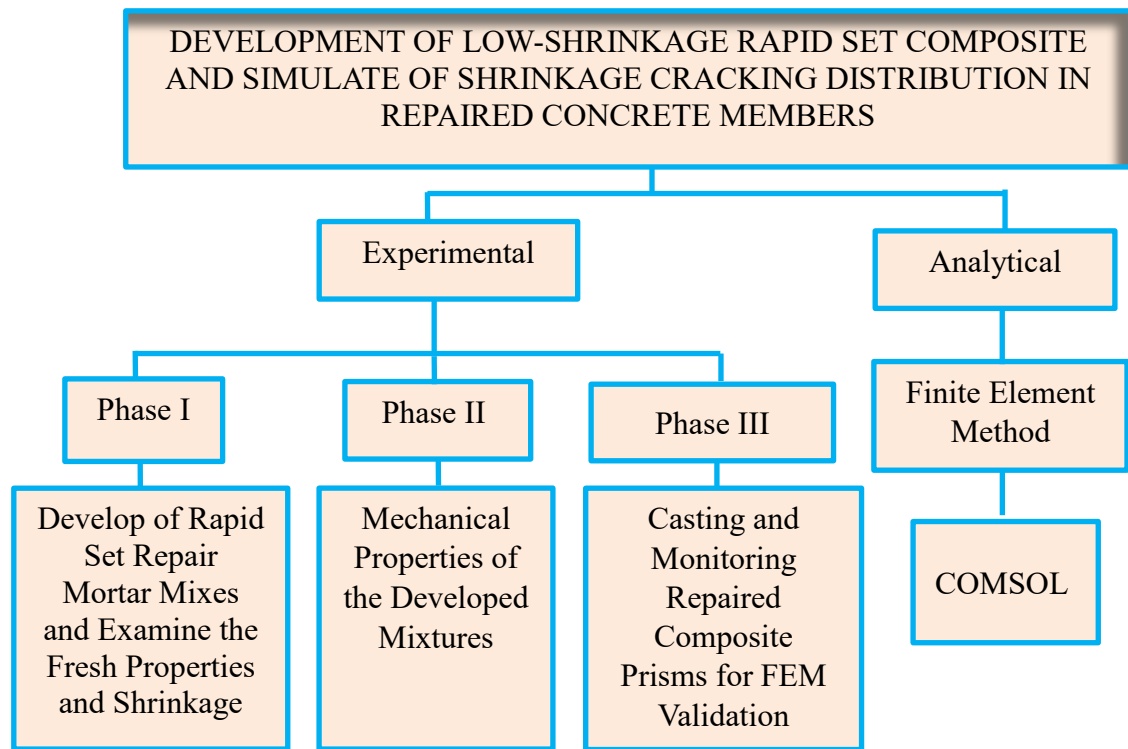


Figure 1.1 Flow Chart of the Research

1.3 DISSERTATION ORGANIZATION

The research work done and presented in this dissertation is divided into six chapters as the following:

Chapter one represents an introduction consisting of the problem statement, research objective, and thesis organization.

Chapter two includes the background, cracking and shrinkage in concrete, types of concrete shrinkage, the repair processes, types of repair materials, and literature review for experimental and FEM.

Chapter three covers the conducted experimental program in this research which includes the selected materials and their properties, mixtures proportions, and testing procedures.

Chapter four contains the results of the experimental tests. This includes mechanical properties in fresh and hardened states. The mechanical tests are flow, slump, free shrinkage, compressive strength, splitting tensile strength, flexural strength, and modulus of elasticity.

Chapter five covers the introduction, adaptive mesh refinement technique, developing a FEM. Discusses and verified the model with Experimental conducted by Beushausen & Alexander, [2007]. In addition, strain measurement and cracking monitor for the validated composite repaired prisms. Stresses analysis and parametric studies were studied.

Chapter six provides general conclusions.

CHAPTER 2 LITERATURE REVIEW

2.1 INTRODUCTION

As the global transportation infrastructure implemented throughout the last few decades, the need for effective maintenance has become necessary to maintain not only strength but also durability [Wang et al., 2003]. According to the Road Information Program, approximately 32% of key roads in the United States require serious maintenance or renewal due to their poor conditions [TRIP, 2012]. The most causes of the reducing strength or durability of the repair system are cracking and debonding. In results, water and aggressive solution penetrate into concrete, which in turn leads to accelerating the deterioration process. Although many materials used in repair provide adequate strength, they can suffer early failure and degradation as a result of properties such as rigidity and rapid shrinkage [Barde et al., 2006]. Figure 2.1. illustrates the failure of the concrete repair system due to the incorporation of mechanical, physical, and chemical processes. Generally, the repair deterioration process starts with delamination and crack of the repair/old interfacial caused by restrained volume change such as dry shrinkage or thermal deformation, when there exists a dimensional incompatibility between the repair and existing concrete [Vaysburd et al., 2004_a; Banthia et al., 2006; Cusson et al., 2006; Vaysburd et al., 2004_b]

In instances where incompatible repair materials are used, cracking and debonding can quickly occur as a consequence of the high stresses present in the system. Deterioration of concrete will lead to a shorter service life for the concrete element; and hence, for the entire structure. The combination of drying shrinkage of the new applied repair and the

restraint in the repair system will often lead to cracking. Therefore, the restrained shrinkage in the repaired system due to applying the new repair material becomes a major concern in the repair concrete industry.

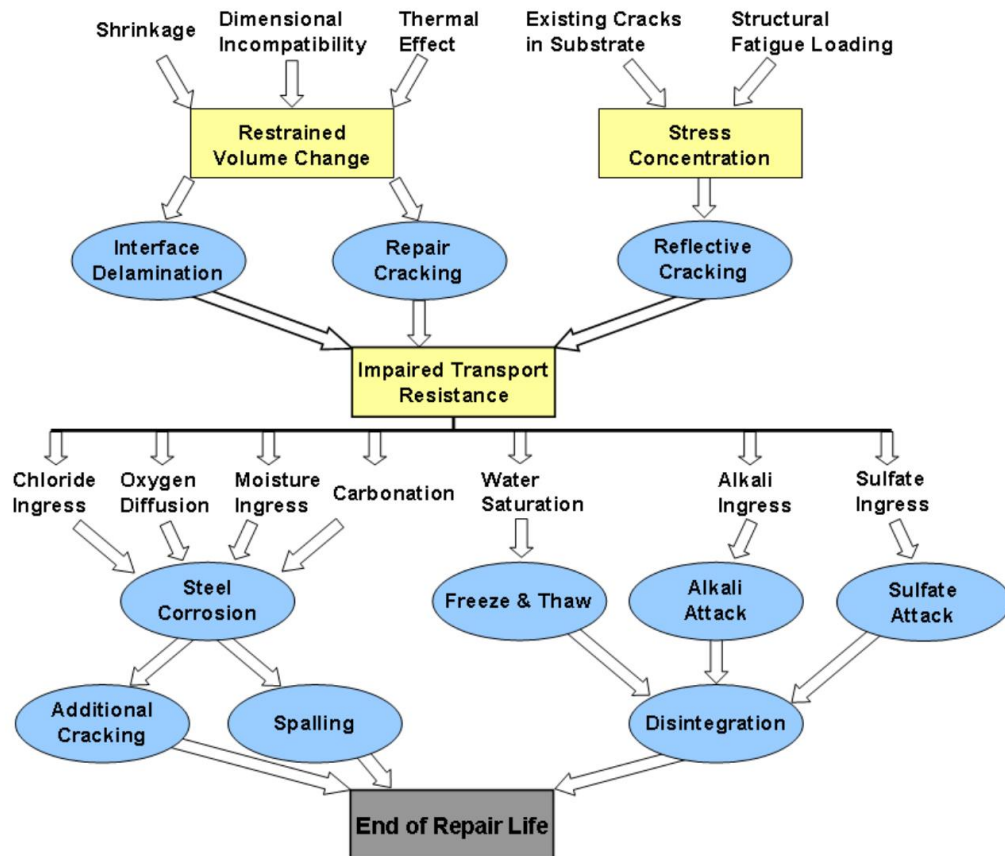


Figure 2.1 Typical Deterioration Process of Concrete Repair [Banthia et al., 2006]

2.2 TYPES OF CONCRETE SHRINKAGE

Concrete is a multi uses construction material which has the ability to take the shape of the form it is cast into. While concrete is hardening, some of the mixture water is evaporated. Consequently, concrete undergoes a change in the volume known as shrinkage. Several types of shrinkage can change the volume of concrete. They can occur at various periods of time during the

useful life of concrete. The shrinkage rates will be affected by the proportions of the mixture. The different types of shrinkage will be discussed below.

2.2.1 Plastic Shrinkage

The movement of water from concrete before its hardening start in the plastic state leads to a contraction in the volume known as plastic shrinkage. The water movement either by hydration process or such environmental conditions causes water evaporation which stays on the wet concrete surfaces. Therefore, increasing the bleeding of concrete leads to an increase in plastic shrinkage. Neville concluded that plastic shrinkage increases with the increase and decrease in cement and w/c ratio, respectively. One common observation is that the cracks induced by plastic shrinkage once fresh concrete surface dries. This leads to open water channels that produce tensile stress in surface tears and cracks that destroy the surface integrity and impair durability.

Although of the developing in rehabilitation techniques, cracking problem due to plastic shrinkage still a big challenge. In practice, many applications which have a big surface area, such as tunnel lining, slabs on grade, patching, and thin repair surface. Consequently, for the overlay material, the exposed surface area per unit volume is high. In addition to the high constraint of the substrate concrete or rock surface roughness. In order to reduce cracks of plastic shrinkage, continue additional curing is one of the best technique which prevents water diffusion from the surface of the concrete. Besides curing, there are many factors like controlling of temperature, minimizing using of preventing bleeding admixtures and shrinkage reducing admixtures, and using high wind protection. From the other hand, there is a need for many additional studies and measures to be considered [Weiss and Shah, 1990; Shah et al., 1992].

Using fibers in concrete mixtures is one of the most efficient technique to reduce plastic shrinkage. Addition of steel, polypropylene, or other types of fibers with different volumes prevents cracks growing due to their bridging forces [Grzybowski and Shah, 1997; Qi, et al., 2003].

According to research studies the high-performance concrete has the rate of bleeding lower than normal concrete thus it has the ability to show high plastic shrinkage. However, controlled evaporation by some techniques like windbreaks, fogging, shading, plastic sheet cover, and wet burlap can minimize cracking due to plastic shrinkage.

2.2.2 Autogenous Shrinkage

Autogenous shrinkage resulted from the hydration process between cement with water, which can also be called basic shrinkage. It does not affect by environmental and moisture effects. In concrete mixtures with w/c higher than 0.40, the autogenous shrinkage can be neglected [ACI 209.1 R-05]. On the other hand, it might be significant in concrete mixtures with w/c lower than 0.4 [Tazawa, 1999]. Lamond and Pielert, [2006] concluded that the autogenous shrinkage is influenced by the expansion resulting from adsorption of water from C-S-H in the cement matrix that known as disjoining pressure. In addition to shrinkage caused by disjoining pressure due to self-desiccation in the cement matrix as a result of self-desiccation.

Many factors affect autogenous shrinkage such as the dosage and type of mineral admixture and water/binder ratio. When the w/c ratio decreases, the autogenous shrinkage increases [Tazawa and Miyzawa 1995a; Tazawa et al., 1991]. While increasing in the Fly ash in concrete leads to reduce the autogenous shrinkage [Termkhajornkit et al., 2005]. However, the concrete mixtures incorporating blast furnace slag or silica fume showed higher autogenous shrinkage compared to reference concrete, and the autogenous

shrinkage increases due to substitution led with higher percentage [Tazawa and Miyzawa 1995a; Lee et al., 2006; Tazawa and Miyzawa 1995b]. Leivo and Holt [1997] conducted an experimental study to measure the autogenous shrinkage of concrete specimens with relative humidity (RH) 100%, the RH maintained by hood covering. They concluded that concrete mixture proportion like proportion and type of cement, w/c ratio, and chemical admixtures affect the autogenous shrinkage value.

The restraint of the aggregates in the cement paste leads to tensile stress which results by Autogenous shrinkage [Dela, 2006]. Consequently, cracking increases. Limitation of the Autogenous shrinkage values is the best way to reduce microcracking or macrocracking, and improvement in quality control of the concrete [Paillere et al., 1989].

2.2.3 Thermal Shrinkage

Concrete as a solid material is subjected to contraction due to cooling and expansion due to heating. This temperature fluctuation leads to a strain rate that affects by the thermal expansion coefficient of the materials. These volume changes due to temperature changes are referred to as thermal shrinkage or swelling. Thermal shrinkage is a concern at an early age with the low tensile strength of concrete and in a massive concrete structure where the heat of hydration produced is very high.

2.2.4 Drying shrinkage

Drying shrinkage is defined as the loss of the water from the pores of the concrete. As the evaporates to the outside, concrete shrinks. Drying shrinkage is similar to the autogenous shrinkage where both occur due to loss of water. For drying shrinkage, the water is transferred to the outside; whereas, for autogenous shrinkage, the water is transferred within the pore structure.

The concrete starts losing the free water in it when there is a difference in the relative humidity between the environment and the concrete due to the exposure to dry conditions. Little shrinkage or no is recorded in the large capillary pores. While in the fine capillary pores, the capillary is filled with water by moisture losing and formed a curved meniscus. Consequently, the pores walls are pulled by the surface tension of water. Once the meniscus is formed, the internal negative pressure is developed in the capillary pores which leads to concrete shrinkage. From the other hand, adsorbed water losing by continued drying leads to a contract of unrestrained of the cement paste. Plus to the additional shrinkage from the increase in the forces of attraction between the calcium silicate hydrate products [Mindess et al., 2003]. The increase in humidity leads to an increase in the thickness of the layer of the adsorbed water [Mindess et al., 2003]. Consequently, concrete with high w/c ratio leads to high drying shrinkage.

The factors that affect the drying shrinkage are divided into two categories; external and internal. The external factor is the curing method [CCAA, 2002]. The internal factors include the cement composition such as the proportion of C3A and S03, the aggregate properties and proportions in the mixture design, and water content or w/c ratio [Smadi et al., 1987].

The addition of chemical admixtures such as super-plasticizer modifies the internal structure of concrete. Since it breaks the large agglomerates into a smaller one, superplasticizer tends therefore to increase the rate of shrinkage strain [Omar et al., 2008]. The rate of shrinkage is also affected by the volume to surface ratio since greater surface yields more drying operations. Drying shrinkage can be mitigated by [CCAA, 2002; Bentz and Weiss, 2008; Mehta and Meterio, 2006]:

- Establishing a minimum required water-to-cement ratio in the concrete mixture.
- Utilizing the highest possible fraction of aggregate and the maximum possible aggregate size.
- Avoiding the use of admixture that enhances drying shrinkage such as admixtures that contains calcium chloride, ensuring proper curing and placing on site,
- Adopting expansive cement, and using shrinkage reducing admixture that can reduce the surface tension of the pore solution.

The role of the fibers to reduce shrinkage in the cementitious matrix has been identified and studied by many researchers [Swamy and Stavrides, 1979; Mangat and Azari, 1988; Filho and Sanjuan, 1999]. The restraint of shrinkage resulting from fibers differs than that from particles of the coarse aggregate due to their high aspect ratio [Zhang and Li, 2001].

Drying shrinkage is measured in accordance with ASTM C157. Classifying shrinkage in three basic categories: Any material with drying shrinkage less than 0.05% is called low shrinkage. Materials with shrinkage between 0.05% and 0.10% are called moderate shrinkage. On the other hand, materials with shrinkage greater than 0.10% are called high shrinkage [Emmon, 1993].

2.3 HOW DOES THE SHRINKAGE CRACKING LEAD TO REPAIR FAILURE?

Cracking and delamination are insidious causes of many repair durability problems [Vaysburd et al., 2004; Banthia et al., 2006; Cusson et al., 2006]. The presence of cracks dramatically alters the transport properties of the repair material [Hearn et al., 1999; Lepech et al., 2005; Sahmaran et al., 2007]. It also facilitates the ingress of aggressive agents into the repaired system and eventually causes premature deterioration and repair failure (such

as corrosion and disintegration). The loss of structural integrity reduces load transfer between the repair and substrate concrete structure. Both cracking and interfacial delamination caused by restrained volume change can reduce the durability and load-carrying capacity of the repaired structure. The ability of the repair material to withstand restrained volume change without cracking and interfacial delamination depends on the dimensional compatibility in the composite repair system [Czarnecki et al., 1999]. Among these properties, dimensional compatibility includes strain capacity, drying shrinkage, the coefficient of thermal expansion, creep, modulus of elasticity, and Poisson's ratio.

An ideal repair material should undergo zero shrinkage, and have the same amount of thermal deformation, creep, modulus of elasticity, and Poisson's ratio as the existing surrounding concrete. However, in reality, shrinkage always takes place in a new repair as soon as it is installed, and is considered as the most adverse factor [Babaei et al., 1999]. Among those described above, that promotes dimensional incompatibility of cement-based repair materials. It should also be noted that the interaction between the new repair and the existing concrete is a time-dependent process. Repair material shrinkage, elastic modulus, tensile strength, and the repair/old interfacial bond are all age-dependent properties and develop at different rates once the new repair is applied.

In the concrete patch repair, drying shrinkage is essential since it makes the most critical portion of all shrinkage strains or in other words, the deformation which is observable in practice [Shazali et al., 2012]. When the concrete is free to move, there is no risk from drying shrinkage. However, restraining the concrete will make drying shrinkage induce tensile stresses. The crack will occur as shown in Figure 2.2 when the tensile stresses higher the tensile capacity of the concrete. The reduction of the drying shrinkage

cannot prevent cracking which is also affected by restraining as well as the detailing and design of the concrete member. The new repair material starts shrinking considerably; however, the substrate concrete does not. The difference in shrinkage between repair material and substrate concrete will lead to restrain the deformation of the repair material. When the restraint is a maximum will lead to high values of differential shrinkage. As the drying shrinkage continues inducing tensile stress with time, the repair material tensile stress becomes greater than the tensile strength. This will, eventually, cause the repair material to crack. [ACI 224R-01].

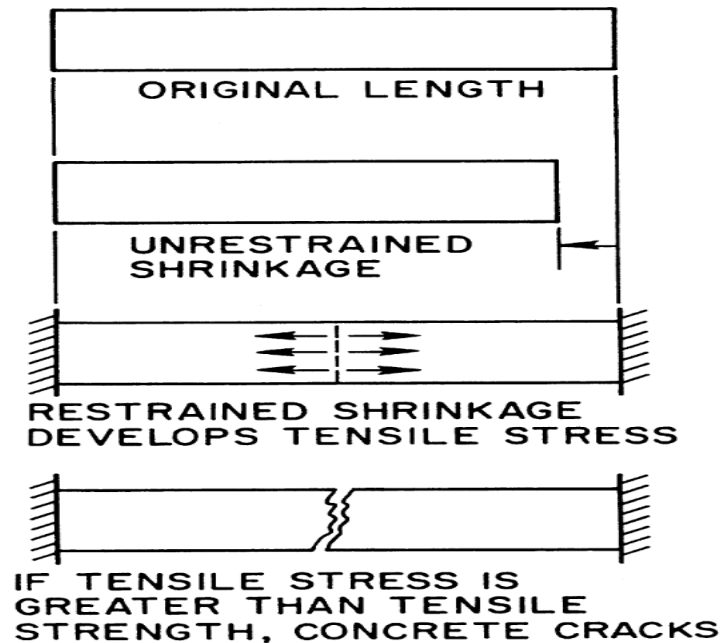


Figure 2.2 Cracking of Concrete Due to Cracking Shrinkage [ACI 224R-01]

Once the concrete is loaded, the elastic deformations are initiated. No increase with time in elastic deformations under sustained loading. Concrete is affected by the dead load which represents the sustained is loading. Consequently, it is subjected to two types of deformation. The creep is a nonelastic deformation, which increases with decreasing in the

loading rate through the loading period. The creep starts after few seconds of loading and continue for 25 years. Creep can be divided into two parts; the first is about $(1/3-1/4)$ of total creep, which occurs in the first month of sustained loading, the second is about $(1/2-3/4)$ of the total creep, which occurs in moderate size concrete section through the first half year of sustained loading. Although the recovery occurs once the sustained loading is removed, the concrete cannot return to its basic state. When releasing the loading at the late age of concrete, the deformation under load is higher than elastic and creep recoveries.

To understand the elastic and creep deformation effects at an exact time, the sustained modulus of elasticity, which represents the sum of the elastic and creeps deformation can be used. The experimental studies have recorded that beyond two years of sustained loading, the concrete modulus of elasticity is about one to half of the initial secant modulus of elasticity. This reduced modulus of elasticity usually used to represent the creep effect for design consideration [Kumar and Kumar 2014].

The reduction in concrete modulus of elasticity with time happens simultaneously with the long-term deflection increase. This reduction mainly occurs because of different variables such as creep, humidity, temperature, and other variables during concrete industry manufacturing. Although under the environmental condition and using ordinary construction material, the modulus of elasticity is taken as 40 to 50 percent of the initial modulus of elasticity value [Kumar and Kumar 2014].

The tension stiffening is reduced due to the creep effect and the cyclic loading, which induces an additional excessive slip between the steel and concrete. Then it is reduced about $1/2$ of its initial value in the long term loading [ACI Committee 224R-01]. It should be mentioned that the primary role of the concrete creeps is an associated stress

relief which eventually decreases cracking risk. As demonstrated in Figure 2.3, the interaction with creep relief is lowered down with age. Consequently, the increase in drying time leads to an increased cracking tendency [ACI Committee 224. 2001]. On the other hand, concrete tensile creep under restrained shrinkage is low compared to that under constant stress. Therefore, to properly investigate the cracking propensity of restrained concrete elements subjected to drying condition, using the characteristics of tensile creep for the constant loads' conditions can lead to a non-conservative prediction [see et al., 2003].

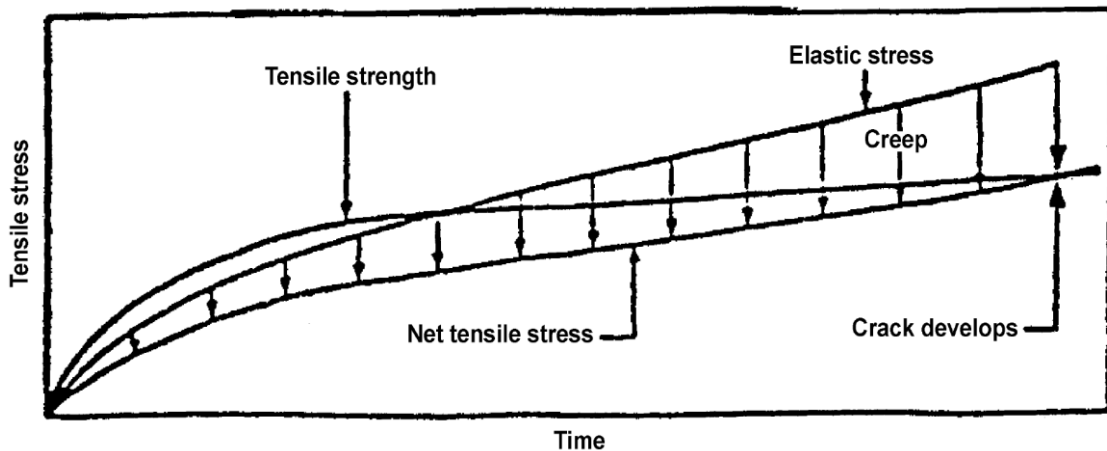


Figure 2.3 Effect of Creep

2.4 PREDICTION MODELS OF DRYING SHRINKAGE

Many of shrinkage prediction models are established to predict the unrestrained shrinkage. The researchers have used the free shrinkage values for many types of concrete under different conditions to fit these values and to meet certain guidelines. All the recent models were derived depending on AASHTO, ACI 209 and CEB_FIP models such as Sakata (Sakata, 1993), Gardner/Lockman (Gardner & Lockman, 2001) and Bazant B3 (Bazant & Baweja, 2000). All of these models have an ultimate shrinkage for a certain kind

of cement and strength values except for ACI 209 model is constant for all cement and concrete types [Kassimi 2013].

According to Nassif et al.[2003], the ACI 209 is a good prediction model for 28 days shrinkage, and it considers a conservative for later ages. Al-Manaseer and Prado [2015] concluded that the ACI 209R-92 shrinkage model is the best predicting model, followed by the B3 model, the CEB models, the GL 2000 model, and the AASHTO 2012 model. Hence, in this research, the ACI 209 was selected to predict shrinkage.

2.4.1 AASHTO LFRD Model (2014)

The following formula calculates the drying shrinkage strain:

$$\varepsilon_{sh} = k_s k_{hs} k_f k_{td} 0.48 \times 10^{-3} \quad (2-1)$$

$$k_s = \left[\frac{\frac{t}{26e^{0.36(\frac{V}{S})} + t}}{\frac{t}{45+t}} \right] \left[\frac{1064 - 94(\frac{V}{S})}{923} \right] \quad (2-2)$$

$$k_{hs} = (2.00 - 0.014 H) \quad (2-3)$$

$$K_f = \frac{5}{1 + f'_{ci}} \quad (2-4)$$

$$k_{td} = \left[\frac{t}{61 - 4f'_{ci} + t} \right] \quad (2-5)$$

Where: k_s : factor of the volume to surface ratio;

V/S : the ratio of volume to surface;

t : the concrete maturity factor;

k_{hs} : the humidity factor of shrinkage;

H : the relative humidity (%);

k_f : the concrete strength factor;

f'_{ci} : the concrete compressive strength;

$f'c$: the 28-d compressive strength of concrete; and

kt_d : the factor of time development.

Concrete shrinkage varied from 0 for the continuous curing to higher than 0.008 strain for the sections are made thin and contained aggregate with high shrinkage. The most important factors effect shrinkage as the following:

Characteristics and proportions of aggregate, the average humidity, the water/cement ratio, curing type, volume/surface area ratio, and air curing time [AASHTO, 2014].

2.4.2 ACI 209.2R (2008)

An empirical model suggested by ACI 209.2R (2008) as the following equation:

$$\varepsilon_{sh}(t, t_c) = \gamma_{sh} \times 780 \times 10^{-6} \times \left(\frac{t - t_c}{f + t - t_c} \right) \quad (2-6)$$

$$\gamma_{sh} = \gamma_{sh,tc} \gamma_{sh,RH} \gamma_{sh,vs} \gamma_{sh,s} \gamma_{sh,\phi} \gamma_{sh,c} \gamma_{sh,\alpha} \quad (2-7)$$

Where: $\varepsilon_{sh}(t, t_c)$ = the shrinkage strain (in/in);

t = concrete age (days);

t_c = concrete age when starting of the concrete drying (days);

$$f = 26.0 e^{\{0.36(\frac{v}{s})\}} \quad (2-8)$$

γ_{sh} = The correction factors cumulative product;

$\gamma_{sh,tc}$ = The initial moist curing coefficient is shown in Table 2.1 While for steam curing

$\gamma_{sh,tc} = 1$ with a curing time varied from 1 to 3 days;

$\gamma_{sh,RH}$ = The ambient relative humidity coefficient;

$$\gamma_{sh,RH} = \begin{cases} 1.40 - 1.02RH & \text{FOR } 0 \leq RH \leq 0.8 \\ 3.0 - 3.0RH & \text{FOR } 0.8 \leq RH \leq 1 \end{cases} \quad (2-9)$$

RH = The relative humidity;

$\gamma_{sh,vs}$ = The volume to surf the ace coefficient;

$$\gamma_{sh,vs} = 1.2 e^{\{-0.12(\frac{v}{s})\}} \quad (2-10)$$

$\gamma_{sh,s}$ = The slump correction factor;

$$\gamma_{sh,s} = 0.89 + 0.041s \text{ in in.-lb units} \quad (2-11)$$

$\gamma_{sh,tc}$ = The initial moist curing coefficient is shown in Table 2.1. While for steam curing,

$\gamma_{sh,tc} = 1$ with a curing time varied from 1 to 3 days

Table 2.1 $\gamma_{sh,tc}$ for Moist Curing Type

| Moist curing duration t_c , days | $\gamma_{sh,tc}$ |
|------------------------------------|------------------|
| 1 | 1.2 |
| 3 | 1.1 |
| 7 | 1.0 |
| 14 | 0.93 |
| 28 | 0.86 |
| 90 | 0.75 |

$\gamma_{sh,RH}$ = The ambient relative humidity coefficient;

$$\gamma_{sh,RH} = \begin{cases} 1.40 - 1.02RH & \text{FOR } 0 \leq RH \leq 0.8 \\ 3.0 - 3.0RH & \text{FOR } 0.8 \leq RH \leq 1 \end{cases} \quad (2-9)$$

RH = The relative humidity;

$\gamma_{sh,vs}$ =The volume to surface coefficient;

$$\gamma_{sh,vs} = 1.2 e^{\{-0.12(\frac{v}{s})\}} \quad (2-10)$$

$\gamma_{sh,s}$ = The slump correction factor;

$$\gamma_{sh,s} = 0.89 + 0.041S \text{ in in.-lb units} \quad (2-11)$$

S= the fresh concrete slump (mm or in);

$\gamma_{sh,\varphi}$ =The aggregates content factor;

$$\gamma_{sh,\psi} = 0.30 + 0.014\psi \text{ for } \psi \leq 50\% \quad (2-12)$$

$$\gamma_{sh,\psi} = 0.90 + 0.002\psi \text{ for } \psi > 50\% \quad (2-13)$$

ψ = percentage of the fine aggregate to total aggregate ratio by weight;

$\gamma_{sh,c}$ = The factor of cement content;

$$\gamma_{sh,c} = 0.75 + 0.00036c \text{ in in.-lb units} \quad (2-14)$$

c= The content of cement in lb/yd³;

$\gamma_{sh,\alpha}$ =The factor of air content;

$$\gamma_{sh,\alpha} = 0.95 + 0.008\alpha \geq 1 \quad (2-15)$$

α = The percent of content of air;

2.4.3 CEB-FIP Model [1990]

This model predicts shrinkage strains is given in the equation below:

$$\varepsilon_{cs}(t - t_s) = \varepsilon_{cso} \beta(t - t_s) \quad (2-16)$$

$$\varepsilon_{cso} = \varepsilon_s(f_{cm}) \beta_{RH} \quad (2-17)$$

$$\beta_{RH} = -1.55 \left[1 - \left(\frac{RH}{100} \right)^3 \right] \quad (2-18)$$

$$\varepsilon_s(f_{cm}) = \left[160 + 10\beta_{sc} \left(9 - \frac{f_{cm}}{1450} \right) \right] * 10^{-6} \quad (2-19)$$

$$\beta_s(t - t_o) = \sqrt{\frac{t - t_s}{350 \left(\frac{h}{4} \right)^2 + (t - t_s)}} \quad (2-20)$$

Where: β_{sc} is a factor accounting for cement type as following:

$\beta_{sc} = 4$ with slow setting concrete, 5 with normal to rapid setting concrete and 8 with the rapid setting for high strength cement;

2.4.4 SAKATA Model [1993]

Sakata (1993) represented the following equation to predict shrinkage strain:

$$\varepsilon_{sh}(t - t_0) = \varepsilon_{sh\infty} \left[1 - \exp\{-0.108(t - t_0)^{0.56}\} \right] \quad (2-21)$$

$$\varepsilon_{sh\infty} = -50 + 78 \left\{ 1 - \exp\left(\frac{RH}{100}\right) \right\} + 38 \ln W - 5 \left[\ln \left\{ \left(\frac{V}{S} \right) / 10 \right\} \right]^2 \quad (2-22)$$

Where: $\varepsilon_{sh}(t - t_0)$: predicted shrinkage strain ($\times 10^{-5}$);

$\varepsilon_{sh\infty}$: Maximum shrinkage strain ($\times 10^{-5}$);

W : Water content in the mixture (kg/m^3);

RH : Percentage of the relative humidity;

$\frac{V}{S}$: The volume surface area ratio;

t : Time (day);

t_0 : Drying time once started (day);

2.4.5 GL [2000] Model

The GL2000 model developed by Gardner and Lockman (2001). The model is applicable to all types of concrete mixtures including mixtures contain chemical admixtures or mineral by-product. In addition to the condition of casting like casting temperature, or curing regime [Gardner and Lockman 2001].

$$\varepsilon_{sh}(t - t_c) = \varepsilon_{shu} \beta(h) \beta(t) \quad (2-23)$$

$$\varepsilon_{shu} = 1000K \left(\frac{4350}{f'_{cm28}} \right)^{\frac{1}{2}} 10^{-6} \quad (2-24)$$

$$\beta(h) = 1 - 1.18h^4 \quad (2-25)$$

$$\beta(t) = \left(\frac{t - t_c}{t - t_c + 97 (V/S)^{\frac{1}{2}}} \right) 10^{-6} \quad (2-26)$$

Where:

ε_{shu} : maximum shrinkage strain, 10^{-6} ;

K : cement type correction factor;

f'_{cm28} : 28-d compressive strength of concrete (Psi);

$\beta(h)$: humidity correction factor;

h : relative humidity;

$\beta(t)$: time correction factor;

t : age of concrete (d);

t_c : age of concrete at moist curing end (d);

V/S : volume-to-surface ratio (in);

2.5 THE REPAIR PROCESS

The repair design controls the success of the repair process, the existing concrete deterioration, the substrate surface condition, the repair material selection process, the casting, and finishing work quality of the repair materials, and the effective inspection for the structure. Abdulhameed, [2010]; Abdulhameed et al., [2018]; Hassan et al., [2010]; and Mansi, [2010] proven that selecting the appropriate materials for any repair process is the main factor in the process. To develop the repair mechanism, many of questions are needed and shown in Figure 2.4 to demonstrate the best way to select the strategy and appropriate repair material during the analysis stage of existing damage structure. The designer engineer must determine the requirements to accomplish the compatible repair system with substrate structure, exposure conditions, and the final user needs. Also, the time of closing during the repairing process for the repaired structure.

Many of the researches are focusing on the repair materials which are used in pavement repair work that is exposed to surface deterioration. However, these optimized repair mixtures are appropriate to other different concrete structures. This repair materials

are often used in a hard environment condition such as cycles of freezing and thawing, exposure of chloride, and cycles of wetting and drying. Also, it can be cast and finished without any full road closure by using partial closure technique. Then after several hours (4-6 hrs), the road will re-open for normal traffic. On the other hand, it should be mentioned that the new applied repair material in the repair system may not be compatible with the substrate concrete. Therefore, special care in selecting the appropriate repair materials must be taken.

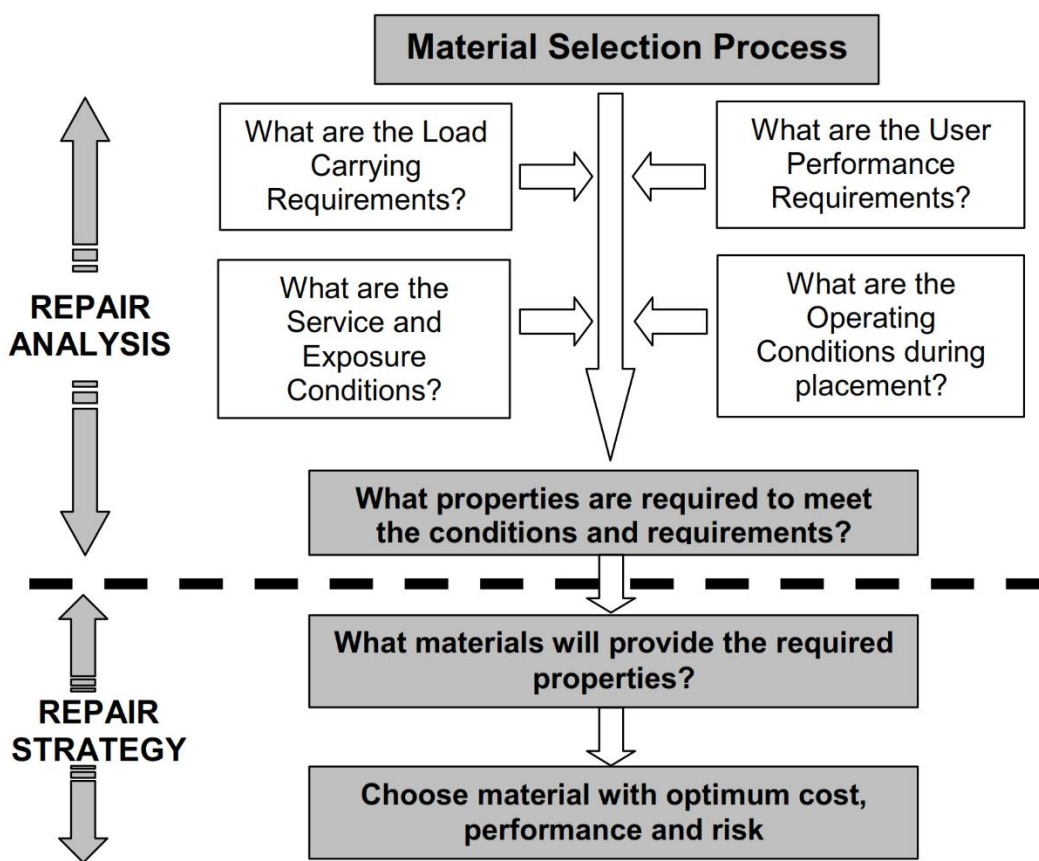


Figure 2.4 Flowchart Demonstrate the Selection Process of the Repair Material [Emmons, 1993]

The selection process of the optimum repair material considers a difficult task. There are many types of repair materials with a variety of prices and properties. Taking

time to select an optimal repair material is essential when the engineer take in consideration behavior expectation from the repaired system [Emmons, 1993; Poston et al., 2001].

There are four major performance criteria as shown in Figure 2.5, which are used to select the ideal repair material. First, the repair materials should have the structural ability to carry the load and successfully transfer the stresses through the repair system. This requires that the repair material must show perfect bonding with the parent concrete and should have the same modulus of elasticity or higher than the parent concrete. Second, the repair material should be easily cast with minimum requirements of curing, high followability, and workability in limited time, and high early strength so it can re-open the repaired structure. Third, the repair materials should meet the durability requirements, which includes dimensional compatibility of the repair material. Specifically choosing the repair materials that has approximately zero drying shrinkage (ideal material), so the material with drying shrinkage from 0.05% to 0.1% is classified as low shrinkage as shown in Figure 2.6. The materials with higher than 0.10% drying shrinkage, will not have the ability to stand against the harsh environmental conditions such as freezing, thawing, and chloride ion ingress. Finally, the repair materials safety requirements, which include the ability of the repair materials to finish with providing safe surface and smooth ride [Barde et al., 2006].

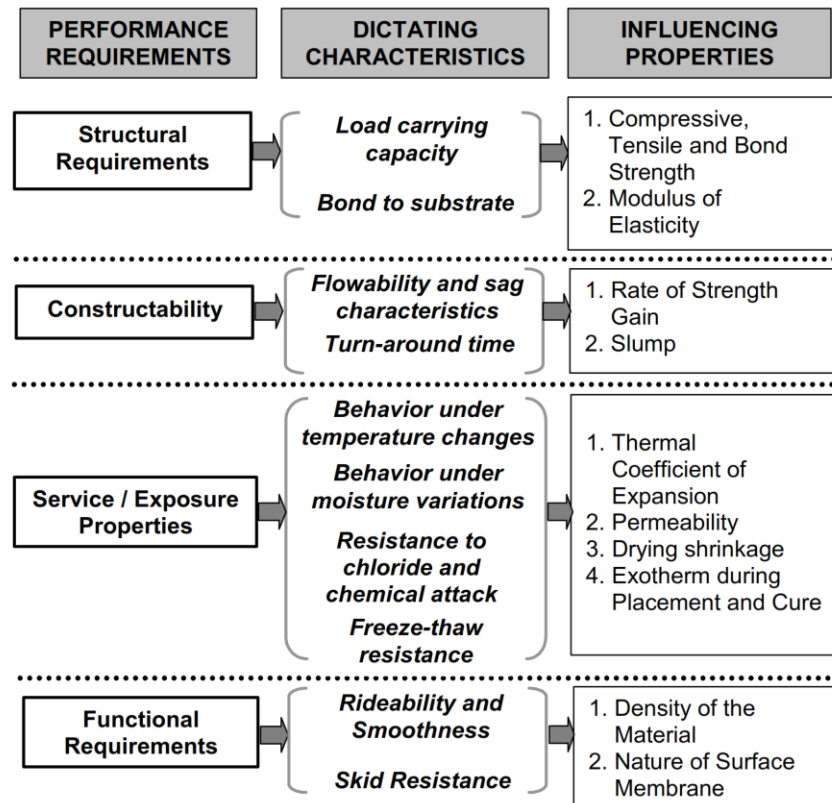


Figure 2.5 Characteristics of a Suitable Repair Material [Barde et al., 2006]

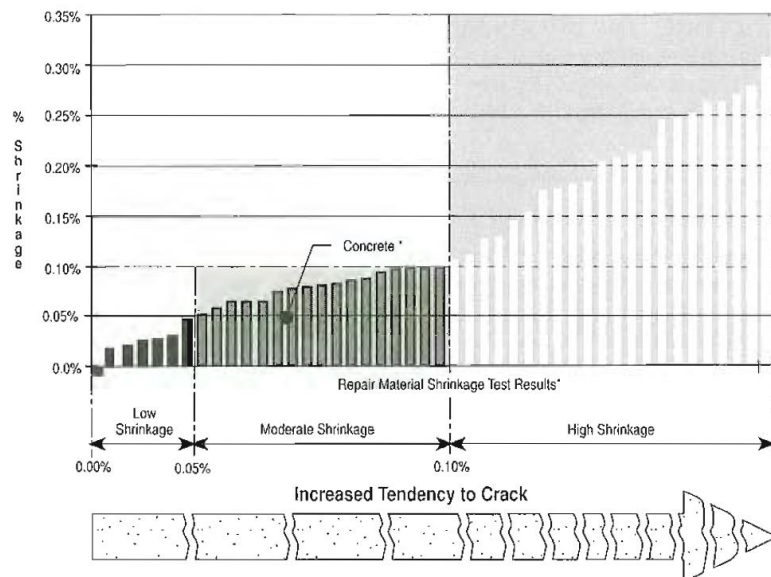


Figure 2.6 Shrinkage Test Results, Alberta Concrete Patch Evaluation Program, Report No.ABTR/RD/RR-87/05 [Emmons, 1993]

In general, most of the engineers try to use perfect materials in construction. However, the compatibility of the repair concrete system is still a big challenge in the repair concrete industry. Some of the properties for the typical material are demonstrated in Table 2.2 [Emmerson and Mays, 1990].

In an ideal situation, the repair material might have the same or higher strength than the substrate concrete so that, the structure can stand the design loads that supposed to carry without failure. Also, it is preferred that the modulus of elasticity for both the repair material and substrate to be close, so all the stresses and deformation are transferred through the composite system resulted by loading are similar. Additionally, the volume dimensional changes of the repair material should be stable compared to the substrate concrete [Emmons, 1993; Emmerson and Mays, 1990; Poston et al. 2001] such as low autogenous and drying shrinkage. Also, the thermal expansion coefficient for both repair and substrate materials should be similar. In addition, good bond strength between substrate and repair material is required. In conclusion, the repair materials are designed to provide the same properties of the parent concrete during the repair process. Consequently, it is expected to meet or exceed the minimum requirement for the structural design. On the other hand, it is not expected to behave like the substrate concrete under the same condition of loads and environmental changes. In conclusion, the selection of the ideal repair material is the rational process [Emmons, 1993].

Table 2.2 Properties Governing Compatibility of Concrete Patch Repair [Emberson and Mays, 1990]

| Property | Relationship of repair material (R) to the concrete substrate (C) |
|---|--|
| Strength in compression, tension, and flexure | $R \geq C$ |
| Modulus in compression, tension and flexure | $R \sim C$ |
| Poisson's Ratio | Dependent on modulus and type of repair |
| The coefficient of thermal expansion | $R \sim C$ |
| Adhesion in tension and shear | $R \geq C$ |
| Curing and long-term shrinkage | $R \leq C$ |
| Strain capacity | $R \geq C$ |
| Creep and Relaxation | Dependent on whether creep causes desirable or undesirable effects |
| Fatigue performance | $R \geq C$ |

2.6 REPAIR MATERIALS TYPES

There are many types of commercially and custom mixture repair materials available in the markets. Back between 1994 and 1995, over 120 manufactures of concrete repair materials were listed by Aberdeen's sourcebook. Each manufacturer produces more than one type of repair materials and that Leeds to hundreds of repair materials in the markets since that time. Despite the fact that there are a lot of commercially repair materials available, they can be categorized into a small number of groups. Emberson and Mays, [1990] classified the repair materials into categories as shown in Table 2.3.

Table 2.3 Types of Repair Materials [Emberson and Mays, 1990]

| Resinous Materials | Polymer-Modified Cementitious Materials | Resinous Materials |
|---------------------------------|--|---------------------------|
| Ordinary Portland cement/mortar | Styrene-butadiene modified rubber | Epoxy mortar |
| High Alumina cement/mortar | Vinyl Acetate modified | Polyester mortar |
| | | Acrylic mortar |

2.6.1 Ordinary Portland Cement Mortar and Concrete

Ordinary Portland cement mortar and concrete are considered the main conventional materials in the repair concrete industry although it requires curing not less than seven days to continue gaining strength. Curing of Portland cement-based materials is critical in reducing early shrinkage and for future long-term performance [Emmons, 1993]. The most important of their characteristics is that they are compatible due to its similarities to the substrate concrete.

2.6.2 High Rapid Setting Repair Materials

High rapid setting repair materials are designed to achieve compressive strength of 3000 psi during the first eight hours as a minimum requirement [US Army Corps of Engineers, 1995]. The primary categories of rapid-set cement are magnesium phosphate cement, calcium sulfoaluminate cement, calcium aluminate cement, and other blended cement [Yang et al., 2016].

Magnesium phosphate cement develops strength based on the hydration reaction between magnesium oxides and phosphates. This reaction occurs quickly leading to a quick or flash setting, rapid strength development, and large amounts of heat generation [Yang et al., 2000, ACI 546, 2004]. Consequently, this material is not recommended for large-

volume repairs because there is insufficient time for a flash-set concrete to be mixed, placed, and finished. Also, the large heat release may cause rapid heat accumulation in the material, which may result in thermal cracking or debonding. Another limitation is that the magnesium phosphate chemically reacts with the carbonate aggregates or carbonated concrete surface. The reaction liberates carbon dioxide gas that weakens the bond [ACI 546, 2004]. However, this material does not require moisture curing after placement due to the fact that the magnesium phosphate cement paste has negligible shrinkage upon drying.

Similarly, calcium sulfoaluminate cement can also be characterized as a quick setting. It develops rapid early strength and high dimensional stability as a result of the fast hydration reaction of tetracalcium trialuminate sulfate (at an early age) and the formation of an expansive hydration product (ettringite) that compensates for shrinkage [Martin-Sedeno et al., 2010, Juenger et al., 2011]. Nevertheless, the widespread use of calcium sulfoaluminate cement-based materials is restricted by their relatively higher cost due to the limited availability of raw materials. In contrast, the calcium aluminate cement has the advantage of rapid setting and strength gain as well as enhanced resistance to high temperature, abrasion, and chemical attacks [Scrivener et al., 1999, Ideker et al., 2013]. The main disadvantages are the high cost due to the restricted sources of raw materials and the metastable hydration product that causes a decrease in the strength of mortars or concretes [Yang et al., 2016].

Rapid-set cement-based materials are easier to mix and more compatible with the substrate compared with conventional repair material, but they are costly and can be more prone to dimensional instability [ACPA, 1999]. While some other factors influence the

cracking behavior of concrete structures, including environmental effects, the magnitudes of loads, and the concrete mix design, a reduction in shrinkage induced cracking provides many benefits towards the longevity of a concrete structure.

In recent time, many high early-strength cement repair materials were developed which are more prone to cracking, lacking of good bonding, and extremely affected by environmental changes. Modern high strength concretes are generally made with relatively low water-cement ratios and high paste contents. It is commonly thought that the increased strength of more modern concretes results in improved performance. However, recent research has indicated that these concretes may be more susceptible to early-age cracking [Shah and Weiss, 2000]. This increased the susceptibility to cracking in high strength concrete can be explained by increases in the autogenous shrinkage at early-ages, stiffness, and brittleness along with reduced relaxation or creep [Weiss et al., 1999]. Also, shrinkage is related to the paste content [Pickett, 1956]; therefore, high strength concrete produced by increasing the cement content will result in a higher overall shrinkage. The interface between repair material and parent concrete is susceptible to internal stresses due to volume changes. Therefore, several techniques are required particularly to reduce stresses effects and choose the materials with stable volume changes [Poston et al., 2001].

One of the common past believes that the concretes with low w/c ratios have low drying shrinkage which means the lower ability for cracking. Consequently, the repair materials are not expected to crack due to their low w/c ratios which are selected to provide high strength. However, there are many recent studies concluded that the ability of early high strength concretes for cracking are high due to many factors. These factors are high autogenous shrinkage, high stiffness, low creep, and high brittleness which are the

properties of the rapid set repair materials due to the rapid rate development of the properties and the volume of the paste. The modulus of elasticity of the repair material is rapidly developed, and the creep is decreased. Consequently, stresses redistribution may be affected and increased their ability for cracking.

A common approach to mitigate shrinkage cracking is to use fiber reinforcement. Fibers are typically used in small volumes (i.e., less than 0.5 % by volume) of concrete [Raoufi et al. 2010]. When the matrix shrinks, shear stresses developed along both the matrix interface and the fiber. Matrix shrinkage in a particular direction is restrained by a fiber with an effective length parallel to that shrinkage strain direction [Mangat and Azari, 1984]. The use of fibers can improve brittle materials' ductility by transferring the load from the matrix to the fibers, besides, bridging and arresting the cracks [Ghazy et al. 2016]. Fibers do increase the fracture toughness of concrete and limit the width of the cracks that form [Raoufi et al. 2010]. Consequently, fiber reinforcement of concrete/mortar can reduce the damage to the repair system [Li et al. 2000].

2.6.3 Polymer Concrete

The main ingredients of the polymer concrete are monomer kinds such as methacrylate and ester resin. Any polymer system has the monomer compound includes an inhibitor which prevents the polymerization process occurs instantly, a catalyst for starting the process of polymerization, an accelerator for accelerating the process, and premixed aggregate. There are many applications for this type of concrete like industrial floors, thin and surface repair, etc. The polymer concrete characteristics are high abrasion resistance, low permeability, and early age mechanical properties developed. Although the monomer can be casted in the very low temperature (-6°C), the polymer concrete should not be exposed to sunlight or sudden changes of temperature.

2.6.4 Epoxy Polymer Concrete (EPC)

This category represents a wide variety of different types of repair materials. Epoxy which serves as the binder is part of the polymer family. Many different types of Epoxies can be extended with a variety of aggregate and fillers. The characteristics of the EPC repair material can be significantly influenced by using different types of epoxies or by the type and amount of aggregate or fillers that are used to extend the epoxy. The characteristics that can be modified are thermal expansion coefficient, modulus of elasticity, set time, and strength. EPC materials are compatible materials and have excellent durability materials, and it gives a wide range of compressive and flexural strength values with high early strength and provides excellent bond strength.

2.7 PERFORMANCE EVALUATION OF REPAIR MATERIALS

Concrete repair market includes a wide variety of many types of repair materials with different physical and mechanical properties. Therefore, the repair material selection process is a difficult task. The recent studies highlighted that the incorrect decision to select the repair material due to the lack in the investigation of the composite repair compatibility leads to repair system failure [Abdulhameed 2018, Abdulhameed et al., 2018, Hasan et al. 2010].

Pattnaik [2006] investigated the composite repair system of the eight repair materials and parent concrete in three experimental phases. In the first phase, the mechanical and durability properties of the repair materials were carried out. In the second phase, the compatibility of the composite repair system was studied. In addition, modeling it by using a FEM. The third phase included the prediction of repair materials durability by using the effect of the volume change and compatibility on it. The results of the first phase showed that the repair materials' properties (such as mechanical properties) are not

governed by the process of selection of repair materials. Also, the repair material bond strength and failure modes are controlled by the ratio between repair materials mechanical properties and the mechanical properties of the substrate. On the other hand, curing type and the texture of the surface affect the bond strength. Therefore, the researcher suggested that the ASTM C928 specification needs to be modified. In the second phase, it was observed that the incompatible failure occurred due to high values of compressive and flexural strength in the repair material compared to the parent concrete. The third phase results showed that no effective effect of the relation between the repair material properties and the compatibility.

Wipf et al. [2004] studied the effect of properties of the repair material on the durability of the repaired concrete system. Moreover, they identified factors that affect the performance of the repair materials during applications. Five cementitious repair materials were studied. These included the chemical additives that enhanced the tensile strength, bond strength, and/or reduce the weight compared to normal concrete. A simulation using beam specimens was used which casted and damaged then repaired. Also, compressive strength and bond strength (by using the wedge test) were carried out. They pointed out that the Modulus of Elasticity, Bond Strength, Coefficient of Thermal Expansion, and Compressive Strength are identified as the key factors for durable repair. The flexure, slant shear, and push out shear tests are applied on specimens under an aggressive condition such as freeze/thaw cycles. If the repair materials were applied in the concrete column, other materials' tests should be considered. They concluded that selecting a repair process is controlled by both the modulus of elasticity and bond strength properties. In addition, an engineer should have the expertise in the placing of the repair materials, preparing small

batches to be familiar how the repair material behaves, recognizing the performance of the repair materials within laboratory conditions, controlling casting time of RSRM, and hiring contractor who should be familiar with concrete repair and RSRM.

Amit et al. (2006) studied the performance of eleven types of repair materials in addition to a reference mix that was designed using ASTM type III Portland cement and 2% Calcium Chloride as an accelerator for comparison purposes. The experimental program included evaluation of materials properties to determine the developing rate of the mechanical properties. Also, measuring the ring test, the autogenous and drying shrinkage. In addition, evaluating the bond strength of the repair composite system. The researcher observed that all of the repair materials examined showed compressive strength over 4000 psi for a long-term, setting time between 10 min to 120 min and a modulus of elasticity of 3000 ksi. The results demonstrated that the bond strength of the repair materials in shear higher compared to tension.

From the previous review, it is evident that all the researches evaluated the performance of the repair materials. While In this research, modification and selecting the repair materials were carried out. This approach considers unique because no available research has studied that.

2.8 PREVIOUS WORK ON FE AND THEORETICAL MODELS ON THE EFFECT OF SHRINKAGE ON THE REPAIRED SYSTEM

The main reason for the repair system failure is the Differential shrinkage in the composite repair system [Martinola et al., 2001, Beushausen and Alexander 2007]. The induced stresses are controlled by the restraint quantity, gradients of moisture due to types of curing and drying situations, and repair material type. Once the tensile stresses exceed the tensile strength of the repair material or parent concrete, both of debonding and

cracking in the repair material or parent concrete will be taken place [Hadidi and Saadeghvaziri, 2005].

When evaluating various concrete systems, numerical analysis methods have proven to be extremely advantageous in assessing shrinkage in concrete. Yuan & Marosszeky [1994] generated such an analytical procedure intended to evaluate the restrained shrinkage of the repaired reinforced concrete system. It was found that repair materials that showed high shrinkage can lead to crack of the patch system and increase tensile strains in the substrate concrete. Inversely, cracking can be postponed due to the repair material expansion and the effect of creep, which is reducing the tensile stresses.

Weiss et al. [1998] used fracture mechanics to create a theoretical model that can estimate the time of the first cracking in restrained concrete systems. This method is based on the restraint environment and creep properties. The researchers also stated that admixtures like shrinkage reducing products could postpone and even avoid the occurrence of cracking.

Rahman et al. [2000] developed a FEM to study shrinkage stresses and creep in the patch repair system. A model simulated the restrained shrinkage by time-dependent moisture diffusion, then analyzed the stresses resulting from restrained shrinkage and creep. In the repair system, a repair layer with thickness 25 mm was cast on the parent concrete ($200 \times 200 \text{ mm}^2$). The temperature and relative humidity (RH) were controlled in the laboratory at $20 \pm 28^\circ\text{C}$ and $65 \pm 5\%$, respectively. Also, strain at critical points and free shrinkage of the repair material were recorded for two months after repair system was casted. This study identified the critical zones and failure modes in the patch repair system.

Moreover, the researchers developed guidelines for the repair design and limited the ultimate free shrinkage strain of the repair material to prevent stresses build up to the failure criteria.

Yuan and Yue Cai [2003] developed a model that predicts the chemical shrinkage or the shrinkage of concrete materials in response to exposure to certain chemicals. The model coefficients were developed with the help of experiments including tensile creep and free shrinkage tests. The shrinkage tests involved three different materials: styrene butadiene rubber (SBR) modified cement mortar, regular cement mortar, and Unsaturated Polyester. The results of the experiments proved that analysis obtained from the developed models could accurately predict tensile cracking as well as tensile strength. Furthermore, the experiments suggested that the region of concentrated tensile stress can be located along the transverse interface where the tensile stress is greater than tensile strength.

Another analytical model was proposed by Zhou et al. [2008] to analyze the various stresses and strains in various forms of concrete overlay materials. The model is based on the plate theory and relationships between interface slip and shear stress. This model intends to quantify imposed stresses in both the substrate concrete and the repair material. Techniques involved in determining stiffness vary; however, in this model is based on the judgment of engineers which may result in prediction error. Notably, in this model, the relationship between stress relaxation and tensile creep is not considered.

Sajedi et al. [2011] proposed a numerical simulation of bonded concrete overlays to investigate the cracking tendency under restrained shrinkage. Four different mix designs were chosen as a repair concrete when some part of cement is respectively replaced by

silica-fume (SF), ground granulated blast-furnace Slag (GGBS) and a combination of SF and GGBS (ternary system). The new method was used to determine the restrained shrinkage values by free shrinkage measurements. The results showed among the investigated overlays, the concrete C-SFS (32.5% of cement was substituted), GGBS (25% of cement weight) and SF (7.5% of cement weight)) had the lowest cracking tendency, due to the low free shrinkage and high tensile strength values. In all cases, the concentration of cracks at the center of overlay was high. In the mix design for the concrete CSF (SF is replaced cement by 7.5% of cement weight), the cracking tendency was so high. So, it seems that in the mixtures which made by this pozzolan, the use of fibers or increasing the curing time or overlay thickness is necessary for avoiding the cracking in early ages. Cracks also formed in the depth of overlay. However, no cracks were observed in the substrate.

Siavash et al. [2011] developed a theoretical method to calculate the restrained shrinkage and tensile stress grading with depth in the repaired concrete system. This method was based on the measuring of the free shrinkage of the repair material in the laboratory. The suggested method was validated by the experimental results performed by Beushausen and Alexander [2007]. The dimensions of overlay were (1600 x160x40 mm) with moderate surface roughness. The new method showed a good correlation with the experimental results and is considered as a simple technique to select appropriate repair material for the successful repair.

Lukovi´ et al. [2016] developed a 3D lattice model to study the deterioration of concrete repair system due to drying shrinkage. The simulation of drying shrinkage in the repair system was presented depending on moisture transport theory and used experimental results of brittle and ductile materials to predict the cracking tendency. The parameters in

this study were the surface texture of the substrate, bond strength, and repair materials thickness. Also, the study investigated the role of strain hardening cementitious composite (SHCC) to control the damage resulted in the repair system due to drying shrinkage. The proposed model predicted that the thinner overlays have more cracks under the same condition for drying and bond strength. Also, the cracks number increased with the increase in the bond strength and roughness of parent concrete. On the other hand, SHCC showed low drying shrinkage; hence, the small crack widths was observed, which is important for durability requirements.

Using COMSOL finite element modeling software, Shazali et al. [2012] worked to develop a model that estimates the reaction of the repair materials in response to moisture diffusion. The heat transfer module available in the COMSOL software is used to imitate the drying shrinkage that occurs when moisture dissipates from concrete. The model showed a good agreement with the result of the experiment conducted by Rahman et al. [2000].

CHAPTER 3 EXPERIMENTAL WORK

3.1 INTRODUCTION

The program of the experimental work was designed to modify the rapid set ready mix repair mortars and concrete that are used in repairing the damaged concrete structures. For this objective, the work was introduced into three phases. The first phase is to design the HES-FR-RSM mixtures. The second phase was conducted to select and test mixtures from the first phase for shrinkage and mechanical properties. While the last and third phase was performed to study the structural behavior of simple supported repaired prisms under the restrained shrinkage effect. This chapter provides information about materials used, mix proportions, mixing procedure, and methods of testing.

3.2 FIRST PHASE

The first part of the experimental work designed to develop HES-FR-RSM with shrinkage less than 300 microstrains. To achieve this goal, three types of fibers with different percentages were used. Also, three types of prepackaged RSRM were selected. These materials are, mortar mix (high-strength structural repair material (C1)), cement all (high strength and non-shrink grout multi-purpose repair material) (C2) from CTS Company. In addition, Quikrete rapid road repair–extended (Q) from Quikrete company. Table 3.1 shows the mixtures proportions and abbreviations. Flow slump, slump, and free drying shrinkage tests were conducted at this phase.

Table 3.1 Mixtures Proportion and Identification

| C1 | | | | C2 | | | | Q | | | |
|---------|----------------|------|-------|---------|----------------|------|-------|---------|----------------|------|-------|
| Mixture | Identification | w/c | HRWR% | Mixture | Identification | w/c | HRWR% | Mixture | Identification | w/c | HRWR% |
| C1R | Reference | 0.09 | 1.5 | C2R | Reference | 0.15 | 0.50 | QR | Reference | 0.09 | 0.0 |
| C1S25 | C1+0.25%SF | | 1.5 | C2S25 | C2+0.25%SF | | 1.00 | QS25 | Q+0.25%SF | | 0.0 |
| C1S50 | C1+0.50%SF | | 2.0 | C2S50 | C2+0.50%SF | | 1.00 | QS50 | Q+0.50%SF | | 0.5 |
| C1S75 | C1+0.75%SF | | 2.5 | C2S75 | C2+0.75%SF | | 1.00 | QS75 | Q+0.75%SF | | 1.0 |
| C1B25 | C1+0.25%BF | | 2.0 | C2B25 | C2+0.25%BF | | 0.50 | QB25 | Q+0.25%BF | | 2.0 |
| C1B50 | C1+0.50%BF | | 3.0 | C2B50 | C2+0.50%BF | | 0.75 | QB50 | Q+0.50%BF | | 3.0 |
| C1B75 | C1+0.75%BF | | 4.0 | C2B75 | C2+0.75%BF | | 1.00 | QB75 | Q+0.75%BF | | 4.0 |
| C1C25 | C1+0.25%CF | | 1.5 | C2C25 | C2+0.25%CF | | 1.00 | QC15 | Q+0.15%CF | | 1.0 |
| C1C50 | C1+0.50%CF | | 2.0 | C2C50 | C2+0.50%CF | | 1.00 | QC20 | Q+0.20%CF | | 2.0 |
| C1C75 | C1+0.75%CF | | 3.0 | C2C75 | C2+0.75%CF | | 1.00 | QC25 | Q+0.25%CF | | 3.0 |

3.3 SECOND PHASE

The second part of the experimental work was performing the mechanical properties for the optimized HES-FR-RSM mixtures that were selected from phase 1 that showed shrinkage strain below 600 microstrains and met the minimum structural requirement for the repair system. The mechanical properties studied are compressive strength, tensile strength, modulus of elasticity, and flexural strength. All samples were dry cured to simulate the curing condition in field applications where the repair was expected to be exposed to air and the structure re-open to traffic in a short time. Figure 3.1 shows the material testing of various mixtures.

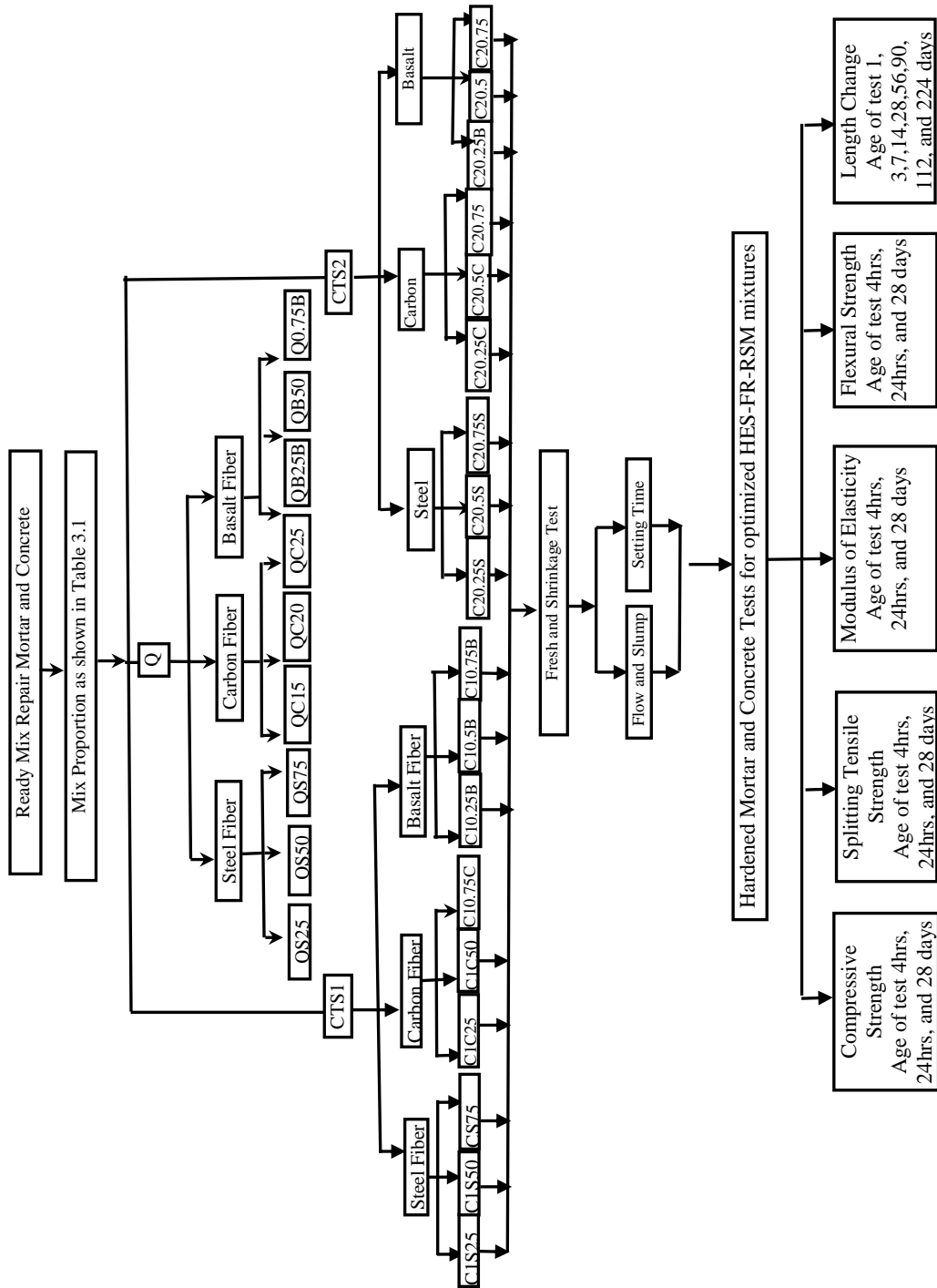


Figure 3.1 Flow Chart of Phase One

3.4 THIRD PHASE

The last part of the experimental program was performed to study the shrinkage of the repaired prisms. A total of nine composite repaired prisms were investigated. Figure 3.2 shows the composite prism dimensions which consist of a substrate with a notch to be repaired with the developed mixtures. The substrate part was initially casted and moist-cured until the age of 28-day. High strength concrete was selected for the substrate with a modulus of elasticity (E) = 4999, Compressive strength (f'_c) = 6816 psi, and tensile strength (f_t) = 523 psi. The notch part then was repaired by the nine selected mixtures.

At the time of repairing, the substrate was at least six months old to ensure that most of the substrate shrinkage had taken place before the repairing was applied as shown in Figure 3.3 a. This procedure was followed to simulate the actual repair conditions of old concrete structures. The measured strain on the members was accounted for the effects of repairing mixtures shrinkage. Substrate surfaces were roughened by using a steel brush to receive a rough and sound interface texture. Then, the substrate surfaces were kept moist for 24 hours using wet burlap and plastic sheets as shown in Figure 3.3 b. and left to air dry for approximately 30–60 minutes prior to repair application. This was done to produce a saturated surface-dry substrate (SSD), which represents optimum moisture conditions for bonding, SSD condition is most favorable for higher bond strength [Austin and Robins 1993, Austin et al., 1995). According to the data sheets for the repair materials [Appendix A], curing of the repair part was started as soon as it lost the moist sheen on the surface and kept wet for at least one hour. After 24 hours, composite prisms were demolded.

Figure 3.4 shows the locations of the strain measuring discs. Strain was measured at an approximately (0.11in) distance from the interface in both repair and substrate as

shown in Figure 3.5.a, and the mean value was used for the analysis. A multi-length strain gauge set equal to 100mm with a measuring accuracy of 0.0001mm was used as shown in Figure 3.5.b and 3.5.c. The elastic strain in the repair system due to restrained shrinkage is generated at various ages as shrinkage develop in the system from the total strain (ϵ_{tt}) that can be expressed as: $\epsilon_{tt} = \epsilon_{el} + \epsilon_{sh}$ in which ϵ_{el} is the elastic strain, ϵ_{sh} is the shrinkage strain (Shazali et al., 2012). A digital microscopic as shown in Figure 3.5.d. was used for crack monitoring.

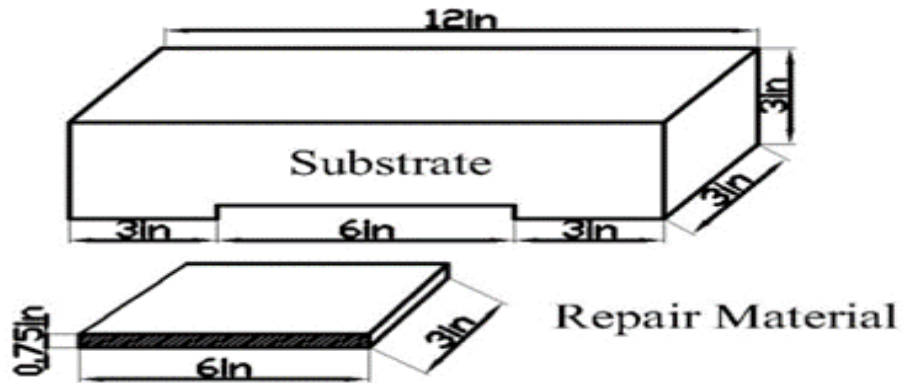


Figure 3.2. Sketch of Composite Prism. (Sketch Dimension are in Inches and Not to scale)



(a)



(b)

Figure 3.3. Composite Prism: (a) Dry Curing for Six Months, (b) Moist Curing Before Preparing.

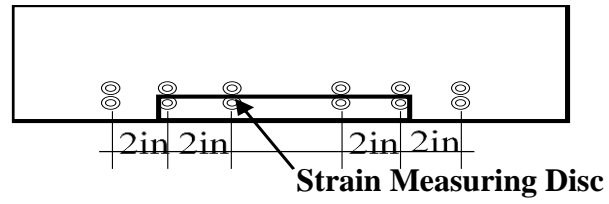


Figure 3.4. Locations of Strain Measuring Discs

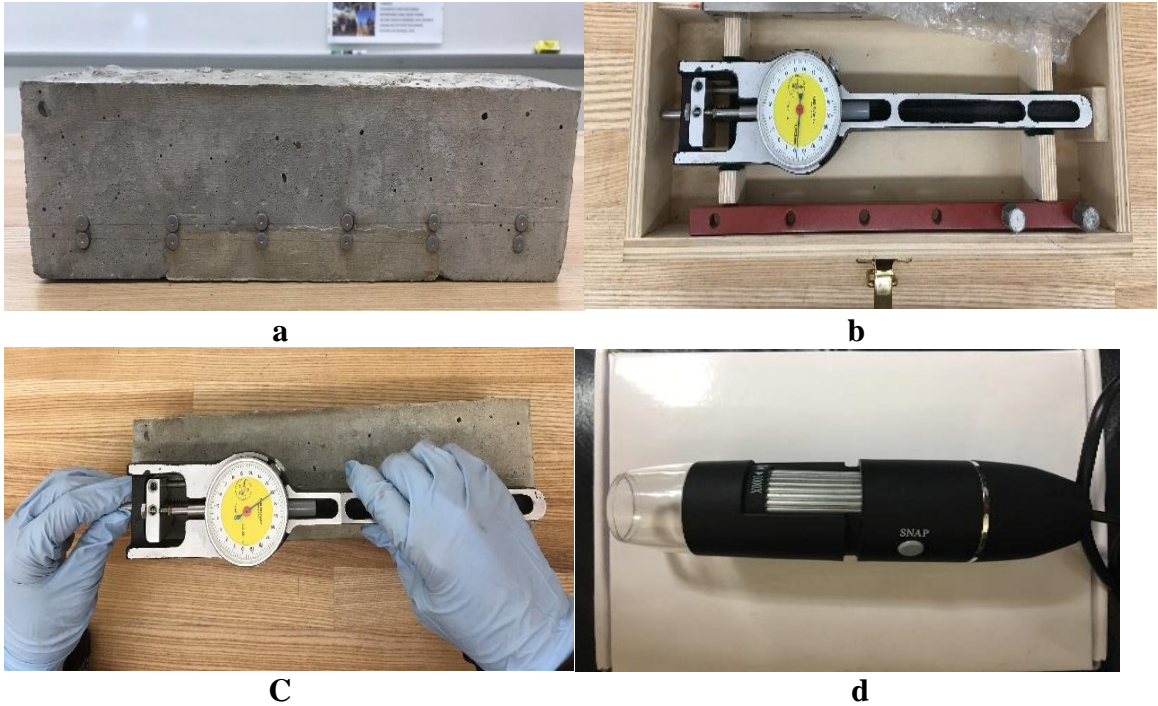


Figure 3.5. (a) Composite Prism After Repairing and Strain Measuring Discs, (b) A Multi-Length Strain Gauge, (c) Readings Measurement, (d) Digital Microscopic

3.5 MATERIALS

3.5.1 CEMENT ALL High Strength, Non-Shrink Grout Multi-Purpose Repair Material

Rapid Set® CEMENT ALL® is a high-performance, fast-setting, multipurpose concrete repair material, and non-shrink grout. Durable in wet environments, CEMENT ALL is a blend of Rapid Set hydraulic cement and specially graded fine aggregates. Use CEMENT ALL for general and structural concrete repair, doweling and anchoring, industrial grouting, formed work, vertical and horizontal trowel applications. CEMENT ALL is ideal for airport, highway, industrial, and marine applications.

3.5.2 MORTAR MIX High-Strength Structural Repair

Rapid Set® MORTAR MIX is a high-performance, fast-setting, multipurpose repair material. Durable in wet environments, MORTAR MIX is a blend of Rapid Set hydraulic cement and quality aggregates. Use MORTAR MIX for general and structural concrete repair, construction of pavements, stucco and plaster repair, one-coat exterior plaster, underlayment and formed work. MORTAR MIX is a versatile product that is suitable for vertical and overhead applications.

3.5.3 RAPID ROAD REPAIR –EXTENDED

QUIKRETE® Rapid Road Repair® - Extended is a very high strength, rapid hardening concrete designed to repair concrete highways, bridge decks, concrete parking lots, and concrete floors needing repairs exceeding 2” (50mm) in depth. QUIKRETE® Rapid Road Repair® - Extended is made from special blended cement with carefully graded sand and gravel to provide a permanent patch. It also contains alkali-resistant glass fibers for improved flexural performance essential for applications of severe vibration as in the repair of bridge decks.

3.5.4 Aggregate

Both fine and coarse aggregates were obtained from the Clayton Company located in Edison, NJ. The maximum coarse aggregate size was 3/4 in (#57) for the substrate concrete. The sieve analysis for the two types of aggregate was done according to ASTM C136. Table 3.2 shows the results of the sieve analysis. The results showed that all aggregates are conforming to ASTM C33 recommendations.

Table 3.2 Grading of the Aggregate Used

| Sieve No. | Sieve Size (inch) | Percent Passing (Fine) | Percent Passing (Coarse #57) |
|------------------|------------------------------|---------------------------------------|---|
| 1.5" | 1.5 | 100.00 | 100.00 |
| 1" | 1 | 100.00 | 100.00 |
| 3/4" | 0.75 | 100.00 | 80.08 |
| 1/2" | 0.5 | 100.00 | 20.28 |
| 3/8" | 0.375 | 100.00 | 3.03 |
| #4 | 0.187 | 99.23 | 0.50 |
| #8 | 0.0937 | 95.37 | 0.50 |
| #16 | 0.0469 | 82.65 | 0.50 |
| #30 | 0.0234 | 55.95 | 0.50 |
| #50 | 0.0117 | 15.73 | 0.50 |
| #100 | 0.0059 | 1.75 | 0.50 |
| #200 | 0.0029 | 0.17 | 0.50 |

3.5.5 Fibers

The Basalt chopped fiber used is filament diameter 13 microns with a length of 3 in, this type was made by Sudaglass Company. While the copper coated Micro steel fiber for ultra-high-performance concrete is 6 mm long, it was made by Ganzhou Daye Metallic

Fibers Company. The short carbon fibers were pitch-based and unsized. Tables 3.3, 3.4 and 3.5 indicate the technical information of the basalt chopped fibers, copper coated Micro steel fiber, and carbon fibers respectively. Figures 3.6, 3.7, and 3.8 show the three types of fiber.



Figure 3.6. Copper Coated Micro Steel Fiber



Figure 3.7 Basalt Chopped Fiber



Figure 3.8 Carbon Fiber

Table 3.3 Physical/Mechanical of Basalt Chopped Fiber

| | |
|------------------------------|---------------------------|
| Density | 2.75 (g/cm ³) |
| Filament diameter | 9-23 (microns) |
| Tensile strength | 4840 (MPa) |
| Compression | 3792 (MPa) |
| Elastic modulus | 89 (GPa) |
| Linear expansion coefficient | 5.5 (x10 /K) |

Table 3.4 Technical Information of Copper Coated Micro Steel Fiber

| | |
|------------------|---|
| Material | High strength steel wire, surface copper coated |
| Length | 6 (mm) |
| Diameter | 0.2 (mm) |
| Tensile Strength | 2850 (MPa) |
| shape | straight |

Table 3.5 Technical Information of Carbon Fiber

| | |
|---------------------|-----------------------|
| Filament diameter | 10 μ m |
| Tensile strength | 690 MPa |
| Tensile modulus | 48 GPa |
| Elongation at break | 1.4% |
| Specific gravity | 1.6 g/cm ³ |
| Carbon content | 98 wt. % |

3.5.6 High Range Water Reducing Admixture

A superplasticizer based on sulphonated melamine formaldehyde condensates, which is known commercially as Eucon 37 was used throughout this investigation as a high range water-reducing admixture; conforming to ASTM C 494, Type F admixture and AASHTO M 194 Type F admixture specifications. The superplasticizer used throughout

this study brought from Euclid chemical company. The HRWRA was used to maintain the workability and strength while maintaining a constant w/c.

For the C1, C2, and Q control mixes, the method of mixing that explained in the data sheet for each product was used. Paddle mixer was used for the experimental quantities as shown in Figure 3.9. HES-FR-RSM mixes were conducted as follow; the total mixing water was placed in the bucket and mixed for 30 seconds and then stopped. The mixer was restarted, the estimated HRWRA was added and the concrete was mixed for approximately three minutes. After that, the measured fibers were added at the end, and the mixing process was continued for a minimum of 1 minute to distribute fibers uniformly.

For the substrate concrete, the traditional method to mix concrete is as follow: First, add both fine and coarse aggregate to the mixer and start mixing for 30 seconds. After that add 1/3 of the mixing water to the mixer and start mixing for one minute. Next, the mixer was stopped, 2/3 of mixing water was added, and the mixer was restarted for three minutes, and then it was stopped. Finally, the HRWR was added to the mixer, and the mixture was mixed for three minutes.



Figure 3.9 Mixing Process by Using Paddle Mixer

3.6 TESTING OF FRESH MORTAR AND CONCRETE

3.6.1 Slump Flow Test

Typically, the repair materials are the cementitious mortar. Therefore, the flow of the repair materials was determined using a flow Table of mortar as per ASTM C230 standard practice. The flow was measured immediately after mixing, within 5 minutes from the time of addition of water into the mix, because of the rapid setting of the repair materials.

The specimen was subjected to 25 drops of one inch each in a period of 15 seconds. Four measures of the base diameter of the mortar along scribed lines in the table top were taken using a caliper, and these values were averaged and compared with the original base diameter as shown in Figure 3.10. The method calculates the increase in the average base diameter of the paste mass, expressed as a percentage of the original base diameter.

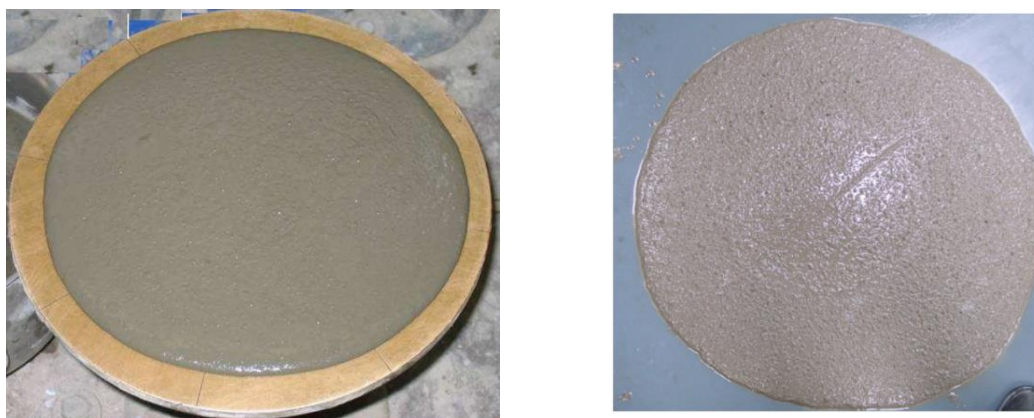


Figure 3.10 Slump Flow Test for Mortar Mixes

3.6.2 Slump Test

Slump test was carried out to determine the workability of concrete following the procedure described in ASTM C143–89a as shown in Figure 3.11. The w/c was adjusted to maintain the same workability, slump 3-5 in (76-127 mm).



Figure 3.11 Slump Test for Concrete Mixtures

3.7 TESTING OF HARDENED CONCRETE

3.7.1 Compressive Strength Test

The compressive strength test was carried out according to ASTM C 39, using 4X8 in cylinders. The compressive strength cylinders were tested using a standard testing machine with a capacity of 1 Million pounds as shown in Figure. 3.12. The loading was applied at a rate of 4000 lbs each 9 seconds. The average of three specimens was recorded for each testing age.



Figure 3.12. 1-Million lbs. Forney Testing Machine

3.7.2 Splitting Tensile Strength Test

The splitting tensile strength test was carried out according to ASTM C496. Cylinders of 4 in diameter and 8 in height were used, and tests were performed using a standard testing machine at a rate of 100 lbs per second. Figure. 3.13 shows the placement of the test cylinder in the machine. The average of three cylinders was taken at each test. The splitting tensile strength is given by the following equation:

$$f_t = \frac{2P}{\pi dL} \quad \text{ASTM C496 [2011]} \quad \dots (3.1)$$

Where

f_t = splitting tensile strength, (psi)

P = maximum applied load, (lbs)

d = diameter of the specimen, (in)

L = length of the specimen (in)



Figure 3.13 Splitting Tensile Test Setup

3.7.3 Flexural strength

This test was carried out on 2×2×10in prism specimens in accordance with ASTM C78, using MTS flexural strength test machine and the setup shown in Figure. 3.14. The theoretical maximum tensile stress reached in the bottom fiber of the test beam is known as the modulus of rupture. The fracture occurs within the central one-third of the beam for all specimens; therefore, the modulus of rupture was calculated using the following formula:

$$f_r = \frac{PL}{bd^2} \quad \text{ASTM C78 [2015]} \quad \dots (3.2)$$

Where

f_r = modulus of rupture, (psi)

P = maximum applied load, (lbs)

L = span length, (in)

d = depth of the specimen, (in)

b = width of the specimen, (in)

3.7.4 Static Modulus of Elasticity Test

Based on ASTM C469, the static modulus of elasticity was conducted on 4x8 inch cylinder specimens. In this test, the specimen is loaded up to 40 percent of the ultimate compressive strength. Hence, the compressive strength was required before starting the test. The load and deformation were recorded manually at regular intervals. The modulus of elasticity can be determined by plotting the strains against the stresses where the slope represents the modulus of elasticity. Figure 3.15 shows the setup of the test.



Figure 3.14 Static Modulus of Elasticity Test Setup

3.7.5 Drying Shrinkage

The drying shrinkage of repair materials was measured on 10-in length and 1-in x

1-in cross-sectional area of prismatic section as per ASTM C157 standard practice, three samples were sampled for each mixture. Steel gauge studs were screwed into the plates at each end of the mold. After demolding the specimens, they were dry cured as shown in Figure 3.15. At each age of test, the length of the reference bar, as well as the distance between two gage studs, is measured using a length comparator as shown in Figure 3.16. The free shrinkage strain can be obtained by dividing the change in length by the original length.



Figure 3.15 Drying Curing

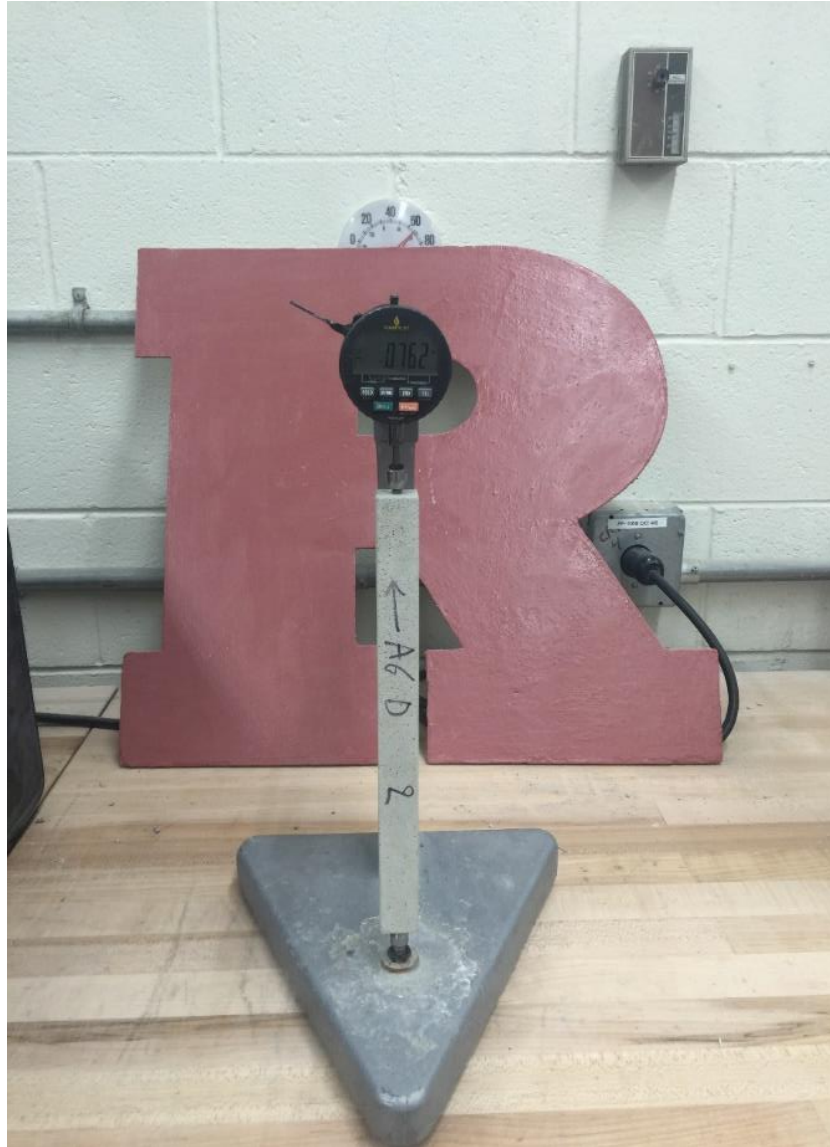


Figure 3.16 Free Drying Shrinkage Test Setup

CHAPTER 4 EXPERIMENTAL RESULTS

4.1 INTRODUCTION

This chapter summarized all the test results of the testing including fresh and hardened properties results of RSRM and HES-FR-RSM mixes. The fresh properties include the slump flow test and the slump test. While the hardened properties are compressive strength, splitting tensile strength, flexural strength, modulus of elasticity, and free shrinkage.

4.2 FRESH PROPERTIES

In general, the flow and slump for the mixtures were maintained to be acceptable for repair application by adjusting the high range water reducer (HRWR) dosage. Maintaining a sufficient flow and slump for the repair materials is vital to provide control through the repairing process since RSRM set in a short time. The flow ranged between 149 to 165mm and 134 to 165mm for CTS1 and CTS2 mixtures, respectively. While, the slump for Q mixtures ranged between 101 and 127mm.

4.3 HARDENED PROPERTIES

Table 4.1 shows the summary of the test results at different ages. The strength development for all mixtures showed the ability of the mixtures to timely gain the design strength and the ability to immediate service.

4.3.1 Compressive Strength

The federal highway administration (FHWA) (1999) recommends for rapid-setting cementitious concrete minimum compressive strength of 1000 and 3000 psi at 4 and 24 hours, respectively. The compressive strength development at various curing ages for all types of concrete are presented in Table 4.1. At 24 hours, the compressive strength values for the RSM and HES-FR-RSM were between 4120 and 6915 psi which exceeded this minimum requirement. The

compressive strength of the mixtures containing SF is slightly higher than the BF and CF for the three types of developed HES-FR-RSM mixtures as shown in Figures 4.1, 4.2, 4.3.

Table 4.1 Mechanical Properties Results

| Mixture | Compressive Strength, psi (ASTM C39) | | | Splitting Tensile Strength, psi (ASTM C496) | | | Flexural Strength, psi (ASTM C78) | | | Modulus of Elasticity, ksi (ASTM C469) | | |
|---------|--------------------------------------|-------|-------|---|-------|------|-----------------------------------|-------|------|--|-------|------|
| | Age | | | Age | | | Age | | | Age | | |
| | 4hr. | 24hr. | 28D | 4hr. | 24hr. | 28D | 4hr. | 24hr. | 28D | 4hr. | 24hr. | 28D |
| C1R1 | 4785 | 5577 | 8917 | 358 | 490 | 597 | 917 | 1147 | 1960 | 1150 | 3750 | 5000 |
| C1S25 | 4864 | 5664 | 8958 | 369 | 510 | 637 | 972 | 1222 | 1970 | 1165 | 3765 | 5007 |
| C1S50 | 4993 | 5857 | 8997 | 388 | 534 | 657 | 1108 | 1333 | 2015 | 1300 | 4138 | 5593 |
| C1B25 | 4900 | 5991 | 8921 | 467 | 609 | 717 | 1044 | 1284 | 2012 | 1133 | 3692 | 4858 |
| C1B50 | 4928 | 5676 | 8968 | 430 | 671 | 850 | 1292 | 1317 | 2355 | 1187 | 3390 | 4530 |
| C1C25 | 4796 | 5610 | 8858 | 360 | 500 | 637 | 1255 | 1498 | 2178 | 1290 | 4067 | 5552 |
| C1C50 | 4800 | 5633 | 8902 | 360 | 512 | 640 | 1105 | 1340 | 1992 | 1187 | 3879 | 4887 |
| C2R2 | 5356 | 6564 | 10063 | 505 | 620 | 790 | 863 | 1099 | 2111 | 1064 | 3463 | 4681 |
| C2S25 | 5450 | 6010 | 10700 | 519 | 656 | 912 | 845 | 1088 | 2010 | 1130 | 3497 | 4711 |
| C2S50 | 5524 | 6123 | 10975 | 546 | 747 | 958 | 1124 | 1364 | 2178 | 1300 | 3650 | 4980 |
| C2B25 | 5384 | 6643 | 10340 | 612 | 778 | 1038 | 1379 | 1599 | 2292 | 1034 | 3220 | 4473 |
| C2B50 | 5405 | 6915 | 10543 | 635 | 872 | 1235 | 1093 | 1333 | 2123 | 1057 | 3425 | 4510 |
| C2B75 | 5416 | 6213 | 10664 | 653 | 791 | 1106 | 900 | 1134 | 1950 | 1011 | 3024 | 4206 |
| C2C75 | 5390 | 6188 | 10435 | 512 | 632 | 893 | 1116 | 1356 | 2136 | 1005 | 3007 | 4211 |
| QR | 2087 | 4120 | 6500 | 374 | 520 | 646 | 742 | 976 | 1815 | 1120 | 3654 | 4841 |
| QS25 | 2112 | 4566 | 6777 | 403 | 540 | 687 | 807 | 1040 | 1870 | 1150 | 3700 | 4900 |
| QS50 | 2203 | 4875 | 6908 | 423 | 576 | 702 | 850 | 1095 | 1945 | 1230 | 3620 | 4932 |

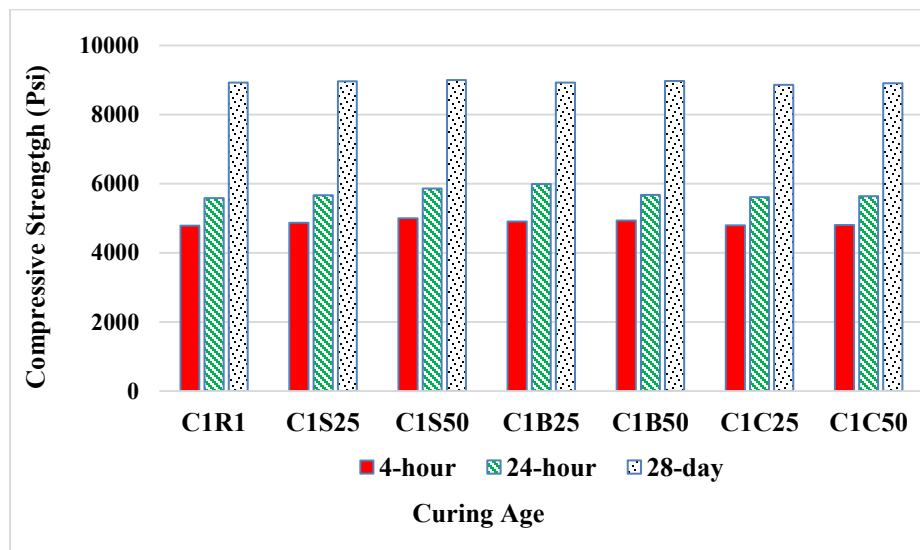


Figure 4.1 Compressive Strength for C1S Mixtures

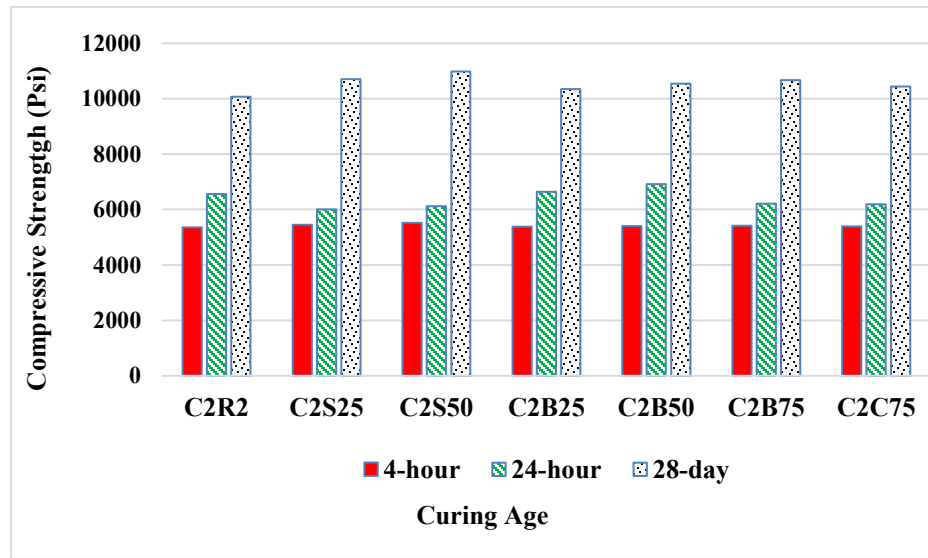


Figure 4.2 Compressive Strength for C2S Mixtures

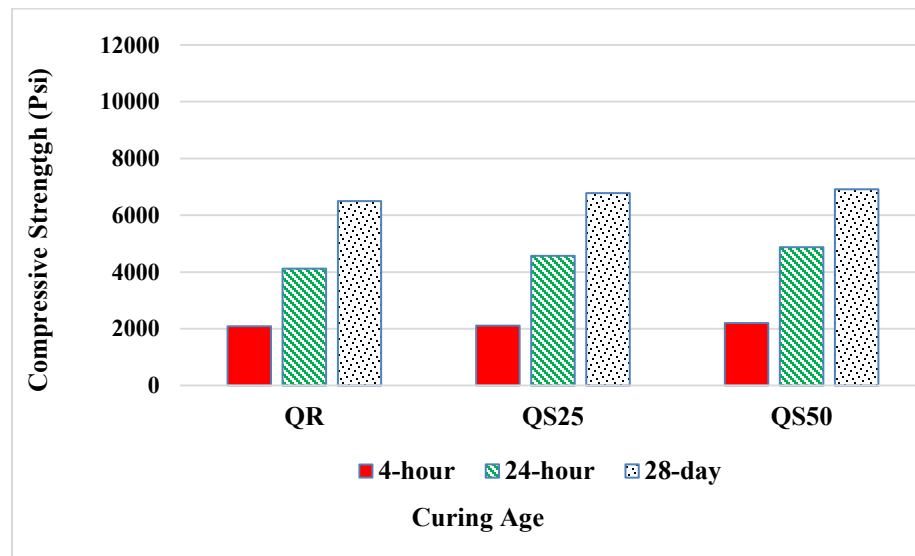


Figure 4.3 Compressive Strength for Q Mixtures

4.3.2 Tensile strength

The results in Table 4.1 indicated that, in general, all types of concrete exhibited a continuous increase in splitting tensile strength with time of the curing. The results showed that the tensile strength for C1B50, C1S50, and C1C50 were increased by 42, 10, and 7%,

respectively compared with C1R as shown in Figure 4.4. On the other hand, the maximum percentage increase for C2B50 was 39% as shown in Figure 4.5. This improvement is mainly due to the higher tensile strength of BF (702 ksi) compared to those of SF (413 ksi) and CF (100 ksi). The Q mixtures showed a slight increase in the compressive and tensile strength with an increasing percentage of SF volume fraction as shown in Figure 4.6. In general, the increase in compressive/tensile strength of cement-based repair materials, e.g., high strength concrete, is typically achieved through a very dense microstructure by employing low water/cement ratios [Mehta 1986].

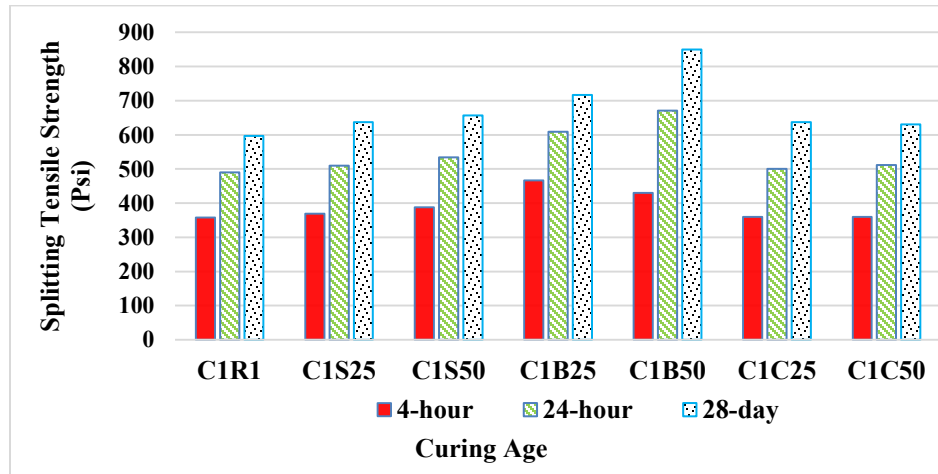


Figure 4.4 Tensile strength for C1S Mixtures

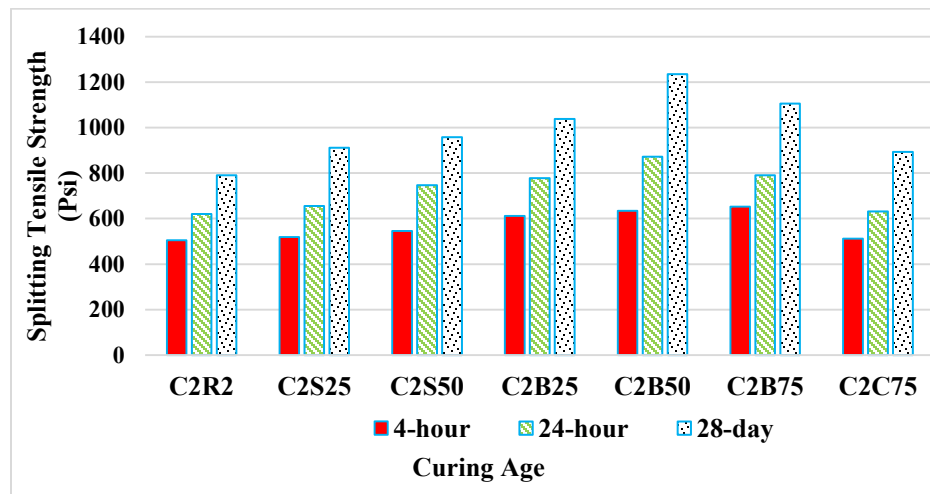
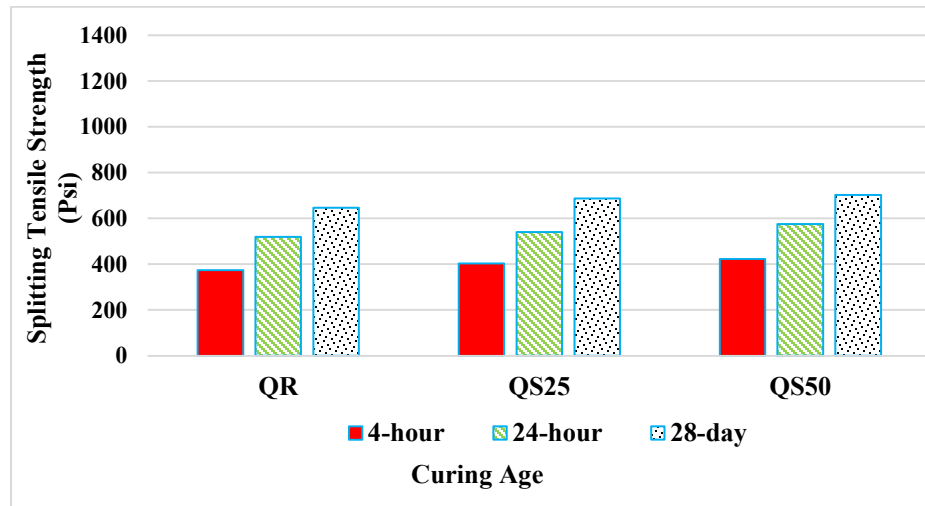


Figure 4.5 Tensile strength for C2S Mixtures**Figure 4.6 Tensile Strength for Q Mixtures**

4.3.3 Flexural Strength

Engineers usually specify the minimum flexural strength of repair material as the requirements for the time before opening to traffic. The FHWA [1999] recommends a minimum flexural strength of 450 Psi according to ASTM C78 for rapid-setting cementitious concretes. It can be seen from Table 4.1 that the flexural strengths for all the optimized mixtures satisfy all the requirements above. For the fibers used in this study, the maximum values for flexural strength were 2015, 2012, and 2176 Psi for C1S50, C1B25, and C1C25, respectively as shown in Figure 4.7. While for C2 were 2176 and 2292 Psi for C2S50 and C2B25, respectively as shown in Figure 4.8. For Q mixtures, the highest obtained flexural strength was 1949 Psi for QS50 as shown in Figure 4.9.

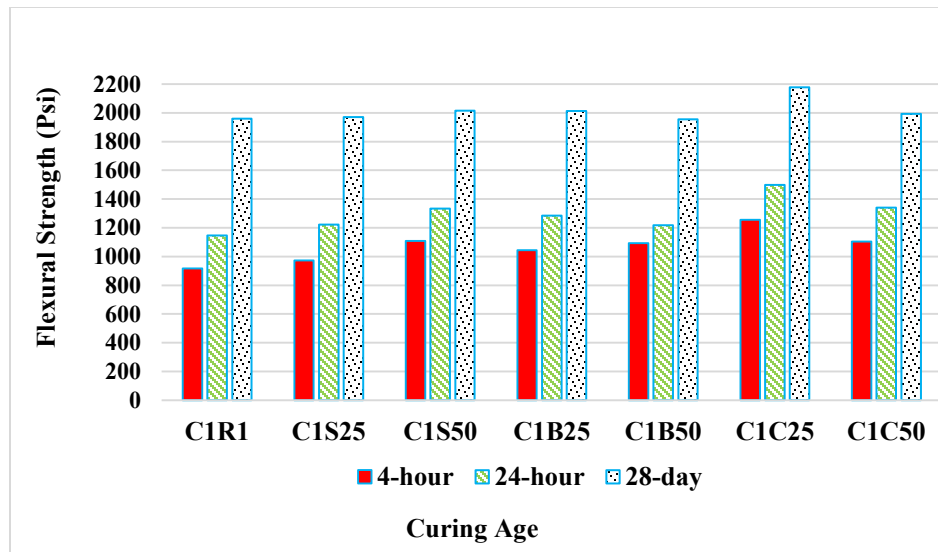


Figure 4.7 Flexural Strength for C1S Mixtures

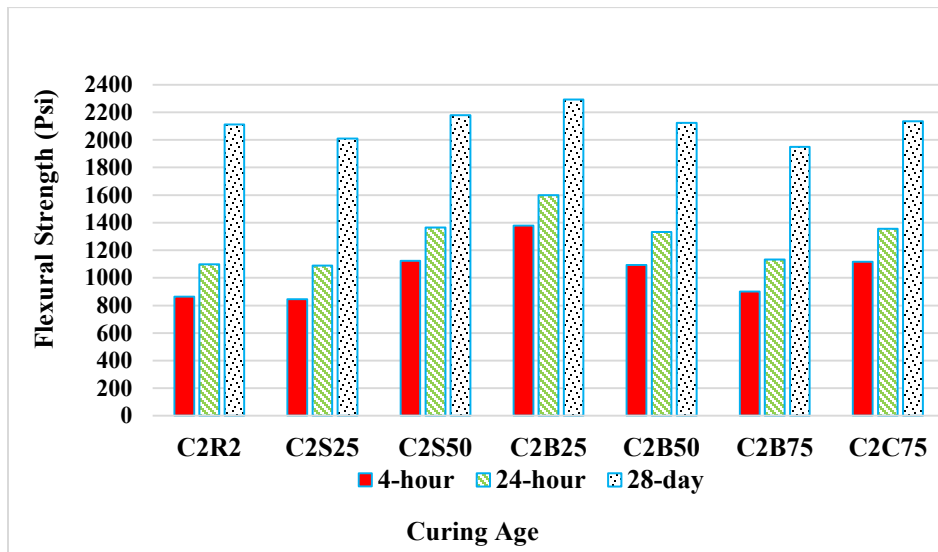


Figure 4.8 Flexural Strength for C2S Mixtures

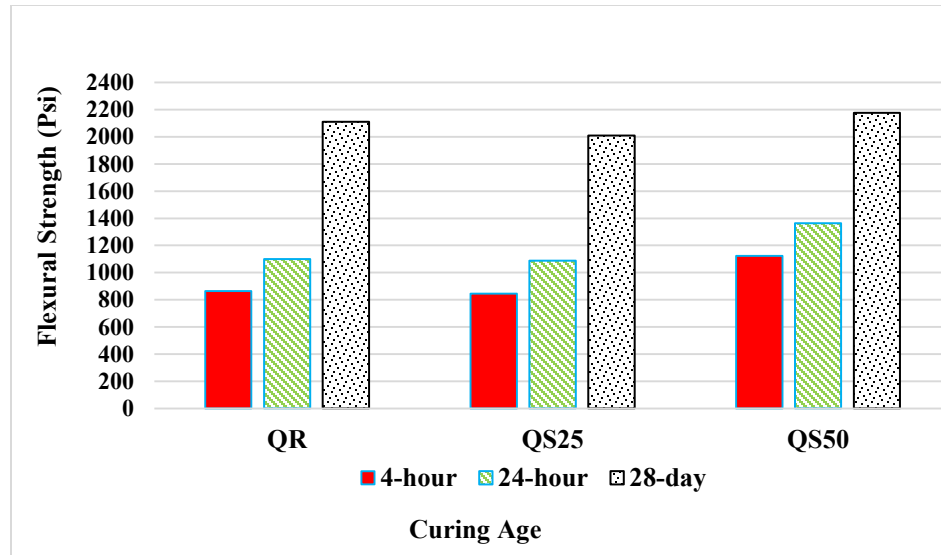


Figure 4.9 Flexural Strength for Q Mixtures

4.3.4 Modulus of Elasticity

The modulus of elasticity for the whole optimized mixtures showed a slight increase compared to the corresponding reference mixtures as shown in Figures 4.10, 4.11, 4.12. The main reason for the slight increment is fibers addition. The desired modulus of elasticity for the repair material is a little higher (stiffer) than that for the substrate. The repair material is most likely in the tension zone. Hence, if the modulus of elasticity higher than that for the substrate, the stress will not be distributed and concentrate on the interface. As a result, bond failure may happen. On the other hand, if the modulus of elasticity for the repair material is too low, the repair patch will sag or creep [Kurtz et al., 1997]. A lower modulus repair material is desirable in limiting the tensile stress induced by restrained drying shrinkage [Wipf et al., 2004].

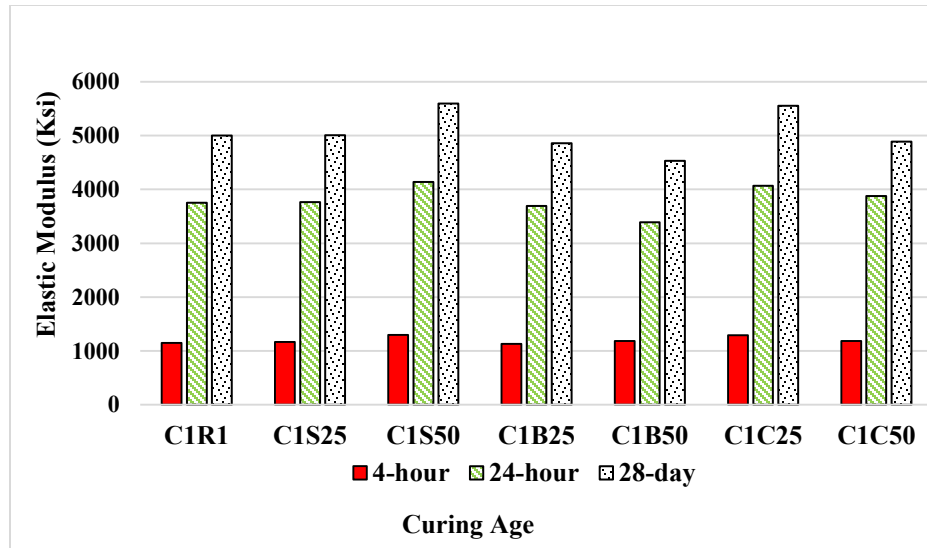


Figure 4.10 Modulus of Elasticity for CTS1 Mixtures

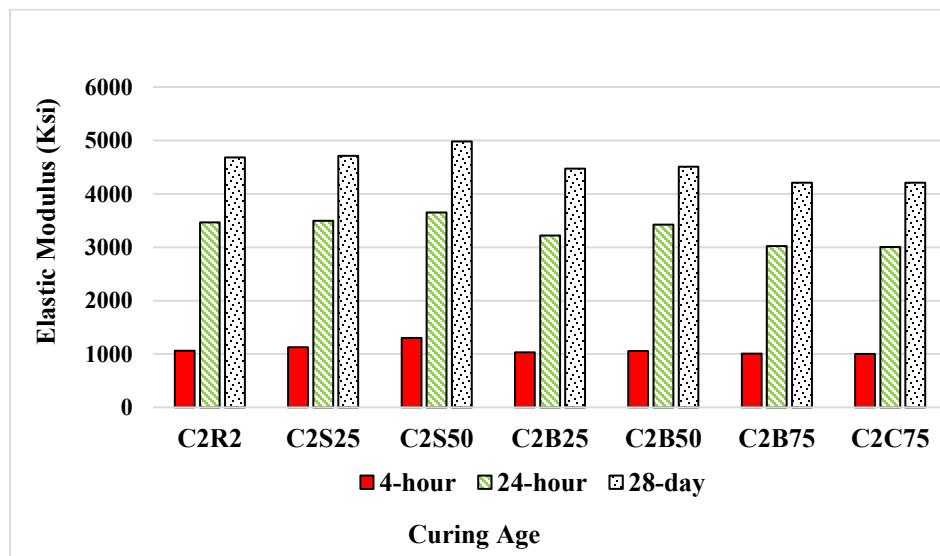


Figure 4.11 Modulus of Elasticity for CTS2 Mixtures

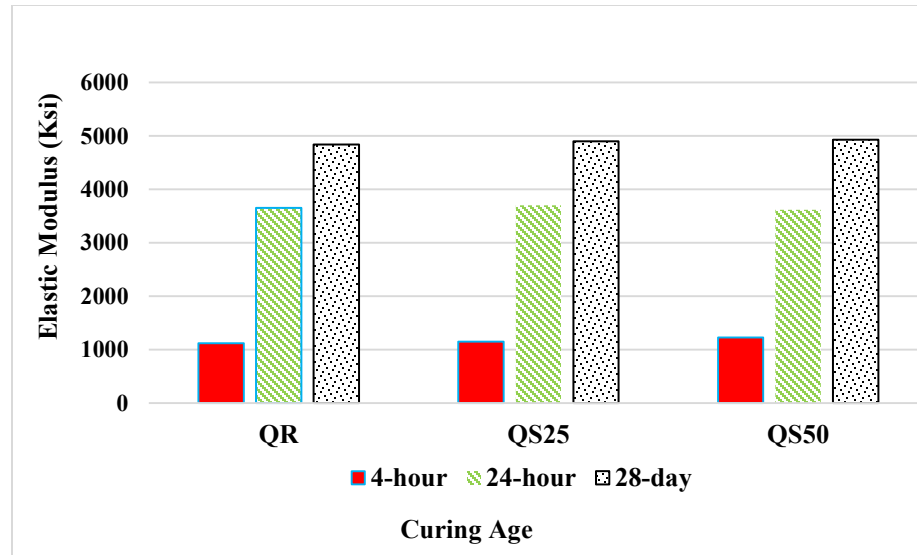


Figure 4.12 Modulus of Elasticity for Q Mixtures

4.3.5 Free Shrinkage Test

The free shrinkage results of CTS1, CTS2, and Q mixtures are shown in Figures 4.13, 4.14, and 4.15, respectively. The results showed that the mixtures contain SF in three types of products exhibited lower shrinkage compared to mixtures contain CF and BF. It is important to mention a decrease in the percentage reduction of free shrinkage as SF content increases by about 36% and 30% for C1S50 and C1S25 compared with the reference (C1R), respectively. The best performance mixture was C1S50 with 268 microstrains, while C1S75 mix showed an increase in shrinkage by 15% compared with C1R. Increasing in fibers volume fractions required to increase the HRWR dosage to maintain the flow of the mixture. Ghosh and Malhotra (1979), Brooks, Wainwright, and Neville (1979), and Feldman and Swenson (1975) demonstrated that using high-range water-reducing admixtures increases shrinkage. According to Ytterberg (1987), high-range water-reducing admixtures do not necessarily reduce shrinkage in proportion to their ability to reduce water content. Tokuda et al. [1981] and Alexander et al. [1980] concluded that the addition of admixture-free control to concretes leads to increase in shrinkage and creep

about 20% although the mixture proportions are constant. The reason is due to the ability of admixture to entrain air, thus making the hardened paste weaker and more prone to deformation. While for CF, the reduction percentage was 29% for C1C50 mixture. On the other hand, BF did not show significant shrinkage reduction. For CTS2 mixtures, the reduction percentage was 13% for C2S25. However, no significant reduction was observed in the other volume fraction or other fiber types. For Q mixtures, there is no significant shrinkage reduction compared to the reference mixture. The mixtures that showed free drying shrinkage lower than 500 microstrains are QR, QS25, and QS50.

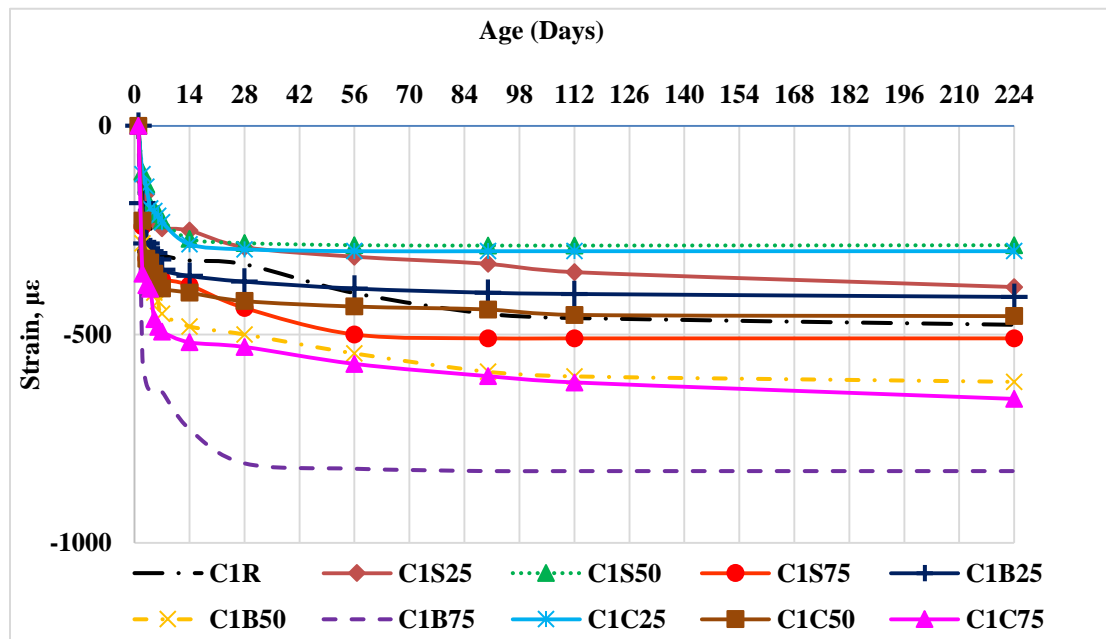


Figure 4.13. Free Drying Shrinkage CTS1 Mixtures

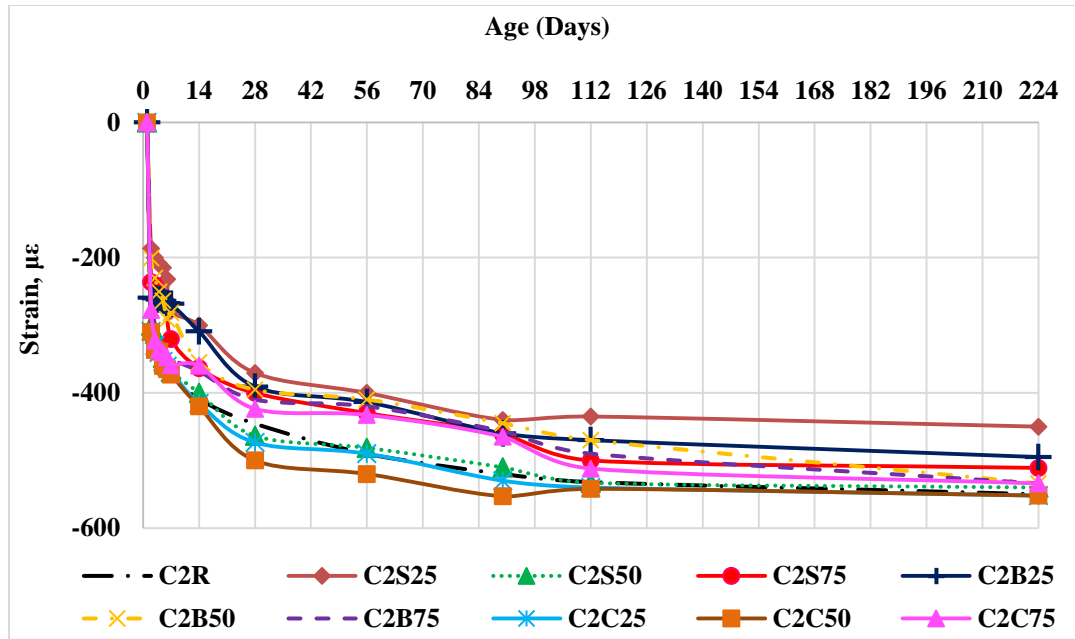


Figure 4.14. Free Drying Shrinkage CTS2 Mixtures

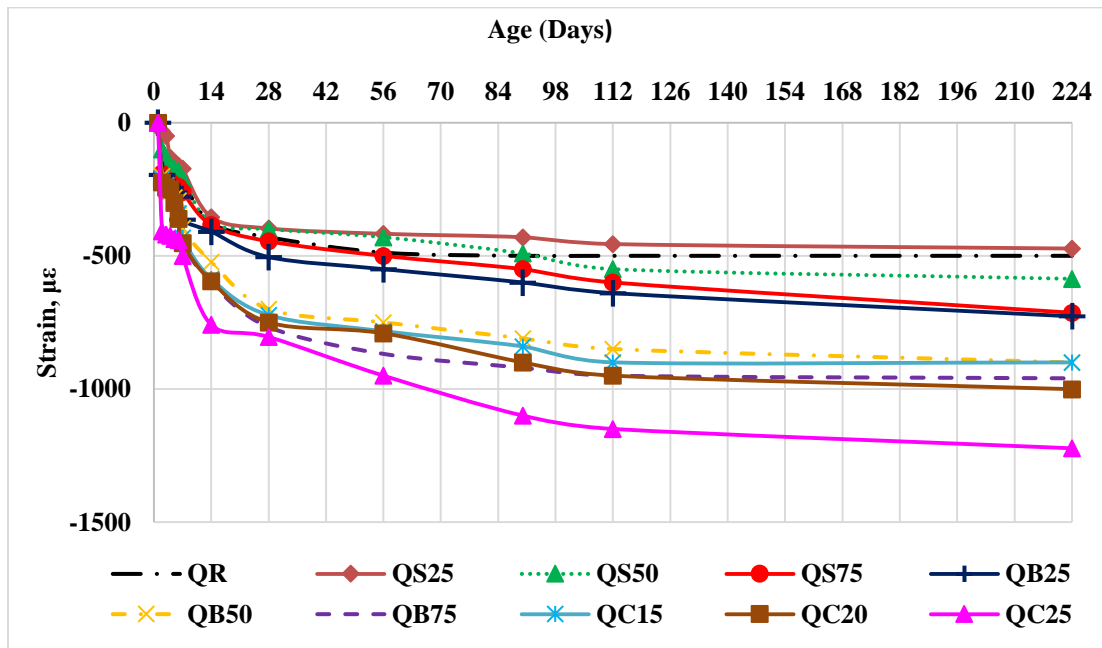


Figure 4.15. Free Drying Shrinkage Q Mixtures

4.4 Strain for Composite Repaired Prisms

The strain profiles for the composite repaired prisms at 56 days are shown in Table 4.2. The strain in the composite repaired prisms was measured using multi-length strain gauge as explained in Chapter Three. The results showed that the recorded strain was low and consistent in all mixtures except in C2R. The reason why the strain is higher in C2R compared with other prisms repaired with other mixtures is due to the high shrinkage of this repair material. During this test, the crack also was monitored using a digital microscope. Figures 4.16 through 4.24 show the observed cracks for all of the repaired prisms. It is noted that the crack initiated only in the prism repaired with C2R. This is mainly due to the reason mentioned above.

Table 4.2 Strain Profile for the Repaired Composite Prisms

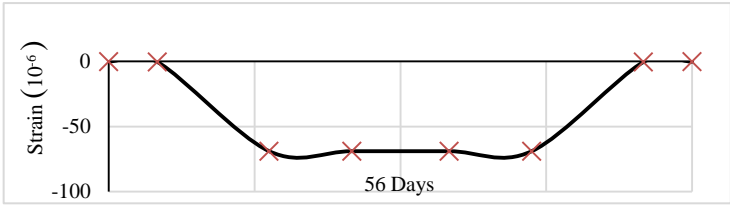
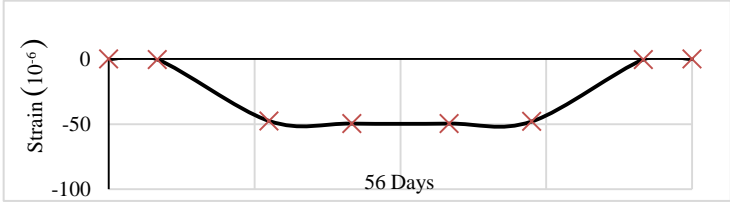
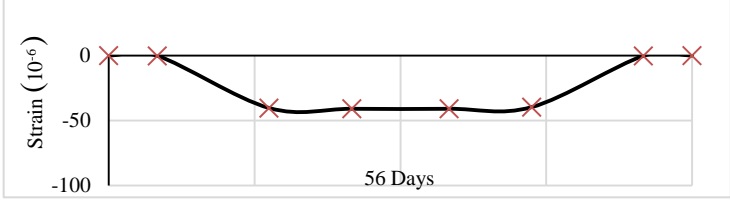
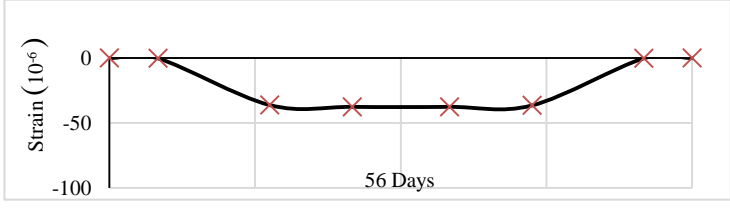
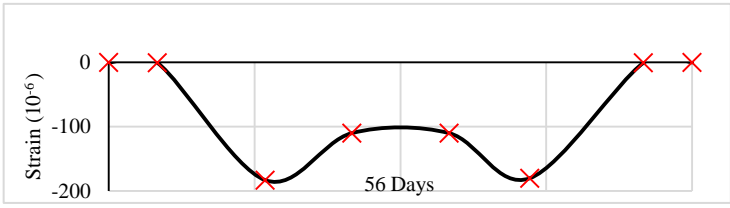
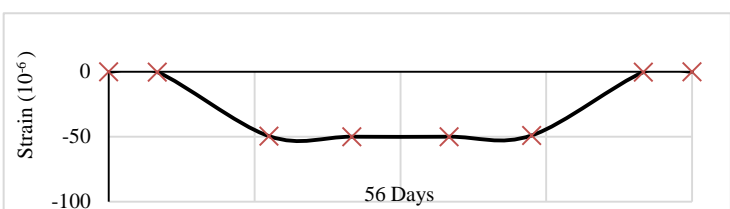
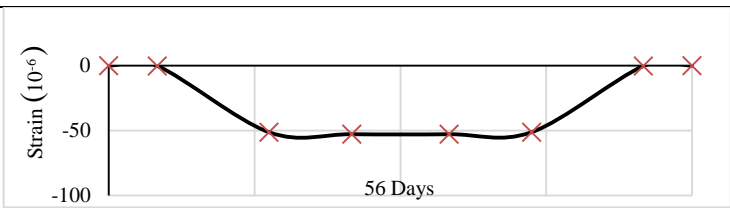
| Mixture ID | Strain Profile Along the Length of Prism |
|------------|--|
| C1R |  |
| C1C25 |  |
| C1S25 |  |
| C1S50 |  |
| C2R |  |
| C2S25 |  |
| C2B50 |  |

Table 4.2 Continued

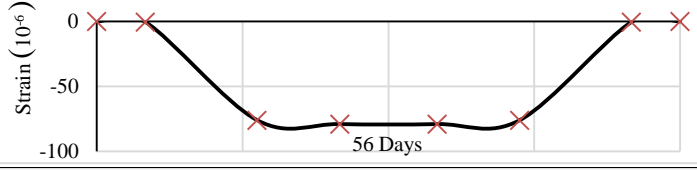
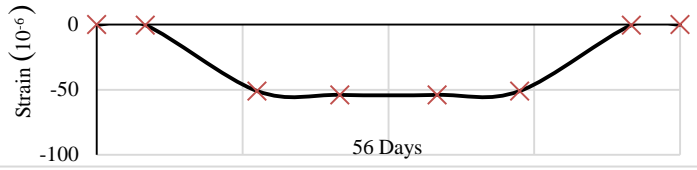
| Mixture ID | Strain Profile Along the Length of Prism | |
|------------|--|--|
| QR |  | |
| Q25S |  | |



Figure 4.16 Picture Taken Using Digital Microscope for the C1R Repair Material



Figure 4.17 Picture Taken Using Digital Microscope for the C1S25 Repair Material



Figure 4.18 Picture Taken Using Digital Microscope for the C1S50 Repair Material



Figure 4.19 Picture Taken Using Digital Microscope for the C2R Repair Material



Figure 4.20 Picture Taken Using Digital Microscope for the C2S25 Repair Material

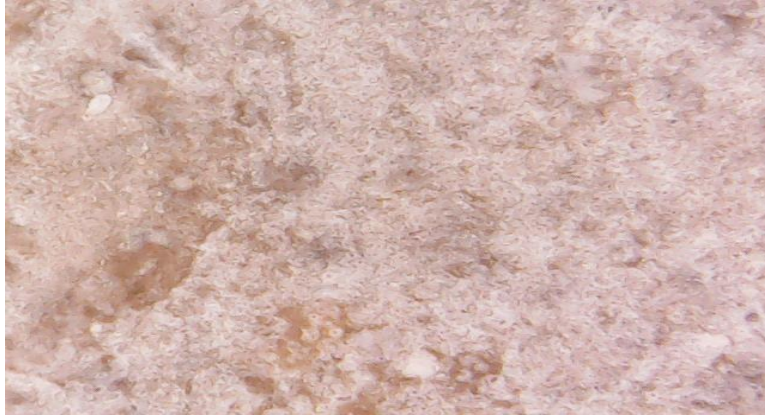


Figure 4.21 Picture Taken Using Digital Microscope for the C2C25 Repair Material



Figure 4.22 Picture Taken Using Digital Microscope for the C2B50 Repair Material



Figure 4.23 Picture Taken Using Digital Microscope for the QR Repair Material



Figure 4.24 Picture Taken Using Digital Microscope for the QS25 Repair Material

CHAPTER 5 FINITE ELEMENT MODEL DEVELOPMENT

5.1 INTRODUCTION

FEM is a valuable tool used by engineers to analyze the real complex problem by developing numerical models. This technique saves time and money by using their solutions to confirm experimental results. Consequently, the number of experiments can be reduced. In this study COMSOL 5.2 program was used to perform the FEM analysis. This program was used to build two-dimensional models, simulate a developed free shrinkage strain with time applied to the models, predict the actual time of cracking and analyze the effects of the free shrinkage strain on the structural performance of the repaired composite prism. The free shrinkage strain is introduced into the program as a time-dependent module. The results from the FEA were then compared to experimental data. This section will overview the settings and initial setup of COMSOL for this research.

The simulation accuracy of any modeling depending on its parts such as constitutive equations which represent physical performance, numerical solution, and model geometric including the shape, finite element meshing, and adaptive mesh refinement technique.

This chapter first introduces the reader to what the finite element method is and the possibilities that come with it. Main purpose of the chapter is to explain in a short manner how the model was created and what settings were adjusted to ensure the convergence of the analyses and to calibrate the model according to the experimental data.

This research demonstrates the procedure to refine the domain elements by using adaptive mesh refinement technique according to the failure criteria which can put instead of error estimation.

Also, this numerical model has been proposed to represent the damage of structural members based on empirical damage definitions.

5.2 ADAPTIVE MESH REFINEMENT

This section mainly follows the development given in adaptive mesh refinement by COMSOL with some changes for the model developed. The accuracy of the FEA model is based on the selection of the finite element mesh. This mesh is useful in subdividing the CAD model into smaller portions known as elements, over where the solution of equations is set. The equations represent the principle equation of interest through a polynomial function set which is defined over each element. As the mesh is refined, elements continue being smaller and smaller, and the computed solution approaches the true value.

The refinement of the mesh is a key step to validate the simulation and gain enough certainty in the model, software, and results. The analyst can start with preliminary mesh when all the required information is gathered into the FEA model. It is advisable, to start with, a coarse mesh (large elements) in the early computation stage. The coarse mesh is easy to compute since it requires little computational resources. Although coarse mesh can give an inaccurate solution, it is used for rough estimation and also as a checkpoint for applied constraints and loads[COMSOL, 2017].

The mesh refinement process starts after the computation of the solution on the coarse mesh. Basically, mesh refinement refers to a process of resolving the model with progressively better-quality meshes and making a comparison between the different meshes. The contrast can be achieved by two ways first through analyzing one point or more in the field model, second by the field integral evaluation of the area over some boundaries or domains[COMSOL, 2017].

Through comparisons made between the scalar values, it can examine solution convergence regarding refinement of the mesh. When comparing with at least three sequent solutions have accomplished, the asymptotic characteristic of the solution emerges, and the solution changes in meshes become smaller. The changes continue becoming smaller, and eventually, the analyst will assume the model to be converged. Adaptive mesh refinement was used in the proposed model as shown in Figure 5.1. In general, it applies an error assessment approach to limit the points in the model domain where there is a large local error. FEA software uses the information from error estimates to generate a whole new mesh. Small elements are employed in areas which have a significant local error. Therefore, the local error in the entire analysis takes into consideration [COMSOL, 2017].

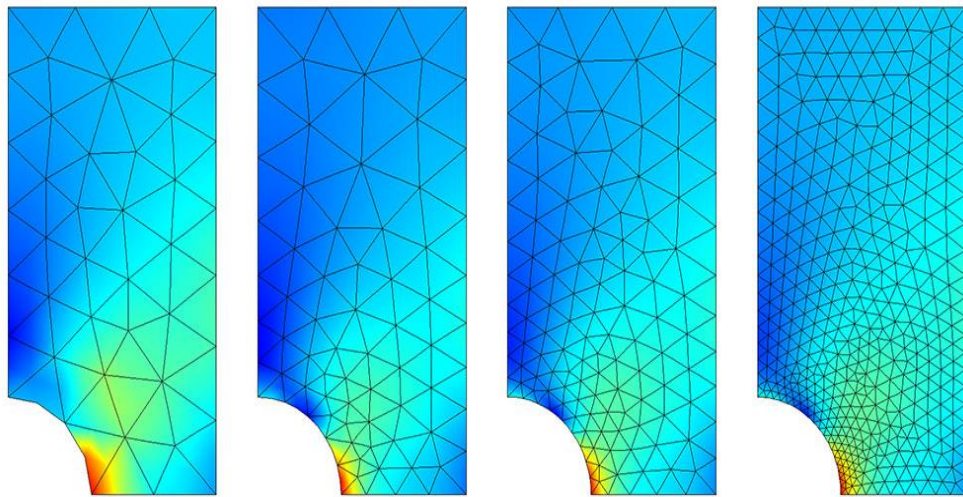


Figure 5.1 Nonuniform Element Size Changed by Global Adaptive Mesh Refinement [<https://cdn.comsol.com/cyclopedia/mesh-refinement/image7.jpg>]

5.3 DEVELOPING THE FINITE ELEMENT MODEL

Numerical simulation of stress development in a composite repaired system due to restrained shrinkage strain was developed. A two-steps computation were used for this purpose by using finite element program COMSOL 5.2.

5.3.1 First Step: Shrinkage Prediction Equation

This step includes computing of the shrinkage gradient by developing an equation to estimate the drying shrinkage of concretes and mortars as a time-dependent and grading with depth. Eq. 5.1 presents the proposed ACI 209.2R [2008] empirical model that was used.

$$\mathcal{E}_{sh}(t, t_c) = \gamma_{sh} \times 780 \times 10^{-6} \times \left(\frac{t - t_c}{f + t - t_c} \right) \quad (5.1)$$

$$\gamma_{sh} = \gamma_{sh,tc} \gamma_{sh,RH} \gamma_{sh,vs} \gamma_{sh,s} \gamma_{sh,\phi} \gamma_{sh,c} \gamma_{sh,\alpha} \quad (5.2)$$

Where: $\mathcal{E}_{sh}(t, t_c)$ = the shrinkage strain (mm/mm); t = concrete age (days), t_c = concrete age when starting of the concrete drying (days); γ_{sh} = The correction factors cumulative product; $\gamma_{sh,tc}$ = the coefficient of moist curing; $\gamma_{sh,RH}$ = the coefficient of ambient relative humidity; $\gamma_{sh,vs}$ = the volume to the surface coefficient.

$$\gamma_{sh,RH} = 1.40 - 1.02RH \quad \text{FOR } 0 \leq RH \leq 0.8$$

$$\text{Or} \quad (5.3)$$

$$\gamma_{sh,RH} = 3.0 - 3.0RH \quad \text{FOR } 0.8 \leq RH \leq 1$$

$\gamma_{sh,s}$ = the slump correction factor; $\gamma_{sh,\phi}$ = the factor of fine aggregates content; $\gamma_{sh,c}$ = the factor of cement content; $\gamma_{sh,\alpha}$ = the factor of air content.

Internal relative humidity (RH) is calculated at a gradient depth of concrete, depending on varying moisture gradient at gradient depth due to the evaporation process. Parrot [1988] based on ambient relative humidity suggested the equation below:

$$RH = RHA + \frac{(100 - RHA) \times [d^x (Y - e)(w - z)]}{d^x (Y - e)(w - z) + tW} \quad (5.4)$$

Where: RHA = the ambient relative humidity (%);

d = the depth from the drying surface (mm);

e = the percentage of pozzolanic materials %;

w = the percentage of water/binder ratio;

and W, X, Y , and Z = constants.

The study conducted by McDonald & Roper [1991] proofed that results can be more accurate by using the values of W, X, Y , and Z are 11.4, 0.85, 128, and 128 respectively. When substituting Eq. 5.4 into Eq. 5.3 [Sajedi et al., 2011]; the model will be capable of predicting the shrinkage strain as a constant or varying with depth. Also, constant shrinkage throughout the repair depth is the simple approach, which is usually used by the most analytical models. To modify the ACI equation in order to fit the experimental data, statistical method [Least Square] was used. The statistical method calculates a factor (C) that is achieved the minimum difference between the theoretical and experimental data. A linear correlation between experimental and predicted shrinkage values represented by the slope of the correction and the correlation factor (R^2) was achieved.

5.3.2 Second Step: Material Models Development

In this step, the solid mechanics module under the structural mechanics section was employed to model the materials analysis and the shrinkage strain.

Plane stress was assumed in the model since the repair layer thickness is small compared with the other two dimensions.

The repair material shrinkage (ε_{sh}), elastic modulus (E), and tensile strength (f_t) are all age-dependent properties and develop at different rates once the new repair is installed. Hence, a time-dependent analyses are carried out.

The $E(t)$ and $f_t(t)$ were calculated by using the models provided by ACI 209.2R[2008] and ACI 318 [2014] as shown in equation 5.5 and 5.6 respectively. The material models were fitted to match the experimental properties.

$$E(t) = E_{28} \sqrt{\frac{t}{a+b \times t}} \quad \text{psi} \quad (5.5)$$

E_{28} = A 28 days modulus of elasticity.

- t = age of concrete (days).
- a and b are constant from Table A4 ACI 209.2R [2008].

$$f_t(t) = 6.7 \times \sqrt{f_{c28} \frac{t}{a+b \times t}} \quad \text{psi} \quad (5.6)$$

f_{c28} = compressive strength at 28 days

Concrete tensile creep due to restrained shrinkage is smaller than due to constant stresses [See et al., 2003]. Using tensile creep characteristics of members subjected to drying shrinkage can lead to un-conservative prediction. Therefore, the creep relaxation effect in the repaired composite system was not considered in this research. The Interface surface roughness (R) has been considered with degree of restrain to determine the restrain factor that shown in Table 5.1 [Abbasnia et al., 2005]. A fully bonding between repair materials and the substrate is also assumed.

Table 5.1 Restraint Factor in Different Restraint condition [Abbasnia et al., 2005]

| Restraint Condition | Position | Restraint Factor (R) | Average of R |
|----------------------------|-----------------|-----------------------------|---------------------|
| 1 (highest) | At near surface | 0.76-0.94 | 0.83 |
| | At center | 0.72-0.93 | |
| 2 (high) | At near Surface | 0.57-0.83 | 0.69 |
| | At center | 0.54-0.78 | |
| 3 (low) | At near Surface | 0.38-0.53 | 0.52 |
| | At center | 0.42-0.56 | |
| 4 (lowest) | At near Surface | 0.10-0.32 | 0.22 |
| | At center | 0.25-0.34 | |

5.3.3 Failure Criteria (Ind)

Modeling cracking behavior in nonlinear FE analysis can be done with two different approaches, smeared or discrete crack approach. The main difference between the two is how the cracks are represented in the model. For the discrete approach, the geometry of the crack must be known while for smeared it does not. Tension stiffening can be defined as the contribution of concrete between cracks to the net stiffness of a member [Göraner et al., 2015], and it considers as reinforced concrete property while tension softening is a plain concrete property. The gradual reduction in stiffness due to progressive cracking is referred to as strain softening. In finite element analysis of concrete structures involves a progressive reduction of the effective modulus of elasticity of concrete with increased cracking [ACI 224R.2R, 2004]. The smeared crack model introduces the effect of cracks by making changes to the coefficients of the material stiffness matrix, not changing the geometry or the mesh [Selby and Vecchio, 1993]. In this model, tension softening is modeled by using a stiffness reduction factor concept.

In general, the model seeks to create a more reliable and accurate numerical solution by using the feedback technique and integrating the error estimates and reference solutions. Error estimations are substituted with failure criteria (Ind) in the proposed model, which involves a comparison of standard stresses engendered with tensile strength. The failure criteria that was developed for the repair material is the maximum stress criterion. This criterion assumes the cracking in that element happens when the element maximum principal stress exceeds the tensile strength. This criterion was developed by using adaptive mesh refinement technique. In the proposed model, the error estimations in the adaptive mesh refinement technique are substituted with failure criteria (Ind), which involves a comparison of standard stresses engendered with tensile strength. On every shrinkage strain increment and convergence limit, the elements are tested to identify the elements which are damaged sufficiently (those parts where the damage variable has reached its failure criterion). When it happens, the linear elastic analysis is applied to the elastic-softening problem via setting the E of the entire damaged component approach to zero (0.001, to avoid numerical singularity problems). The damage processing is representing by cracking initiation. To simulate the cracks in the model, damage factor (DF) is introduced as [Lemaitre, 2012] by the following expression:

$$DF = 1 - \frac{E_{ind}}{E_0} \quad (5.7)$$

Where: E_{ind} = the new modulus of elasticity of element and E_0 = the initial modulus of elasticity of element. If the element does not reach the failure criteria, $DF = 0$. Otherwise, $DF \approx 1$ when the element reaches Ind; and consequently, the crack is initiated. As the crack propagates with a node patch which is grounded on super error-estimation convergent, the refined meshes are obtained. The flowchart of the model is shown in Figure 5.2.

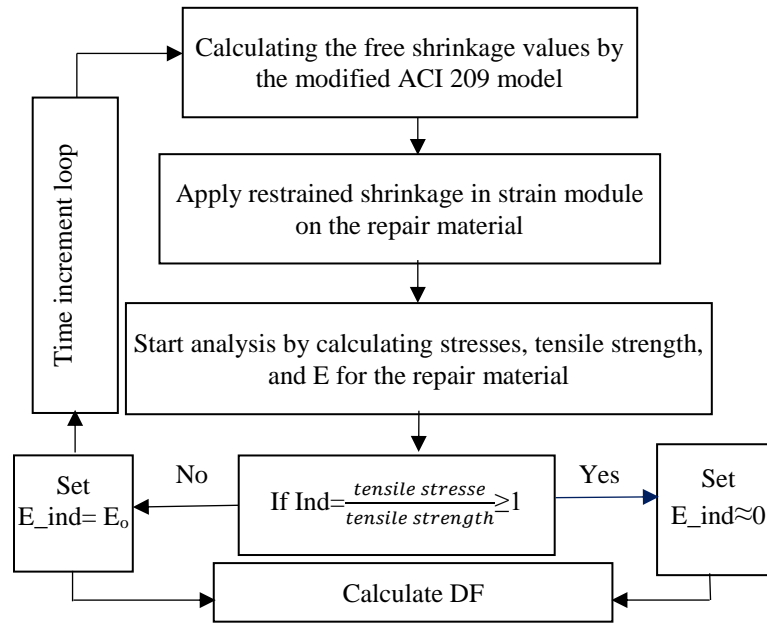


Figure 5.2 Flowchart for Calculating the Proposed Model

5.3.4 Element Type Used

Different element families are available to be employed in COMSOL. One of the major distinctions between the various element families is the geometry type that each family assumes.

Free triangular elements are used for both substrate and repair. The triangular finite element is a local and global two-dimensional element, as shown in Figure 5.3. It can be used in elasticity problems for both plane stress and plane strain.

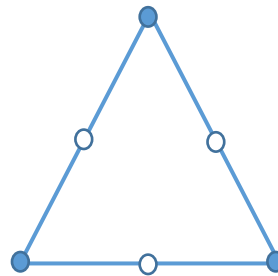


Figure 5.3 2D Triangular Element

5.4 RESULT AND MODEL VALIDATION

The FE model prediction was validated with two experimental results as follow:

5.4.1 Experimental conducted by Beushausen & Alexander, [2007]

The experimental results for bonded concrete overlays are shown in Table 5.2. Specimen A.

5.4.1.1 Case A

The overlay dimensions of 1600 x 160 x 40 mm. In general, the predicted shrinkage models approximately fit the free shrinkage values measured. Hence, the ACI code equation was modified to fit the experimental data as shown in Figure 5.4. The relative humidity is ranging from 55 to 75 %. In this case, a value of 60 % was chosen. A restrained factor of a value equal to 0.37 was selected [Sajedi et al. 2011]. A constant shrinkage throughout the repair depth is the simple approach, which is usually used by the most analytical models, especially it is consistent with shin [2000]. He concluded that it is reasonable to assume that the pore RH is constant for the locations deeper than 1.0". Also, it is reasonable to assume that the RH between the top surface and the depth of 0.25" is linear.

A statistical method (least square) was used to modify the ACI equation to fit the experimental data. A correction factor (C) was obtained which gives the best fit. The obtained correlation between the measured and the predicted data was linear in terms of the slop and the correlation factor (R^2). Figure 5.4 shows the modified ACI 209.2R and the correction factor (C), which is used to get a better fitting of the data. The mean correction factor (C) is 1.16. The Linear correlation and R^2 for the overlay mix were obtained. The R^2 value of the relationship for the modified model is 0.97 which is greater than of the original model (0.90). Consequently, it showed a better prediction of the experimental shrinkage values.

Table 5.2 Mixture Proportions and Material Properties for Substrate and Overlay

| | Substrate | Overlay |
|--|-----------|---------|
| Cement CEM I (Kg/m ³) | 350 | 510 |
| Water (kg/m ³) | 175 | 235 |
| 19 mm Greywacke stone (kg/m ³) | 1025 | - |
| 9 mm Greywacke stone (kg/m ³) | - | 940 |
| Sand (2 mm max) (kg/m ³) | 875 | 660 |
| W/C ratio (-) | 0.50 | 0.46 |
| Slump (mm) | 90 | 80 |
| 28-d Compressive strength (MPa) | 48.4 | 53.3 |
| 28-d Tensile strength (MPa) | - | 3.0 |
| 28-d Elastic modulus (GPa) | 82.1 | 29.6 |
| 28-d Free shrinkage strain (10 ⁻⁶) | - | 290 |

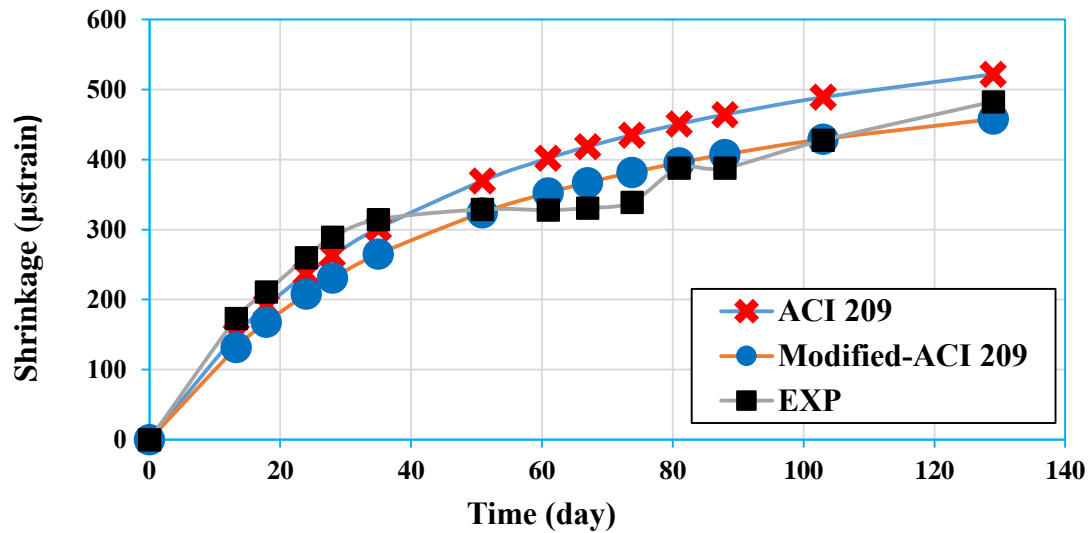
**Figure 5.4 Comparison between Predicted and Modified Shrinkage for ACI 209.2R**

Figure 5.5 shows the comparison between the FEM results of the interface strain in the overlay with experimental results. The developed model showed a good agreement with experimental results. On the other hand, the FEM predicted that there is no crack depending

on the proposed damage factor. This prediction agreed with experimental findings which were observed by visual assessment using a magnifying glass during the test time. Figures 5.6.a, 5.6.b show the free drying shrinkage predicted by the model and deformed shape, respectively. Figure 5.7 illustrates the DF (equal to 0) which is an indication for crack has not been formed. It can be seen how the DF does not change during the test period (from day 2 to day 129).

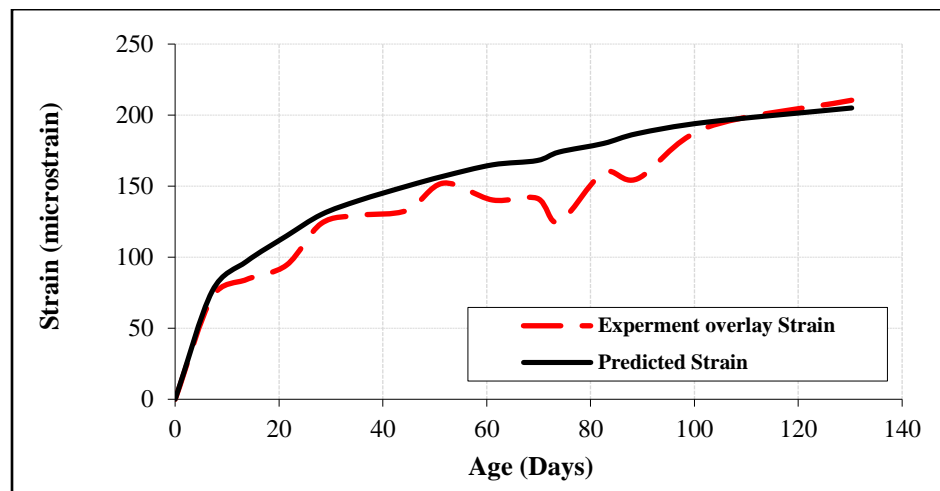


Figure 5.5 Interface Strains in Overlay

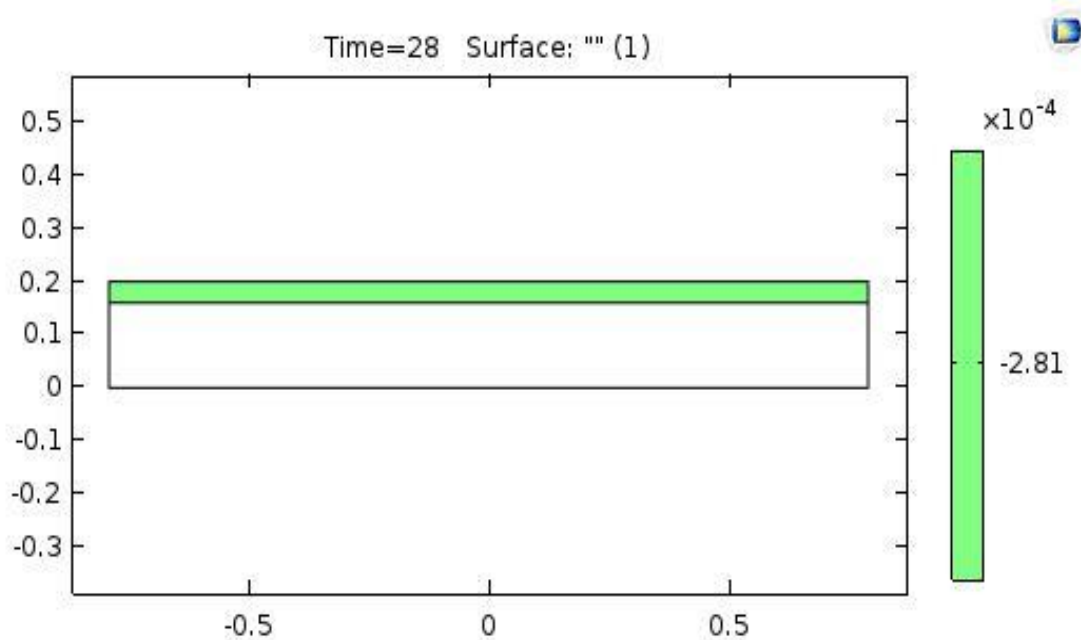


Figure 5.6.a Free Drying Shrinkage

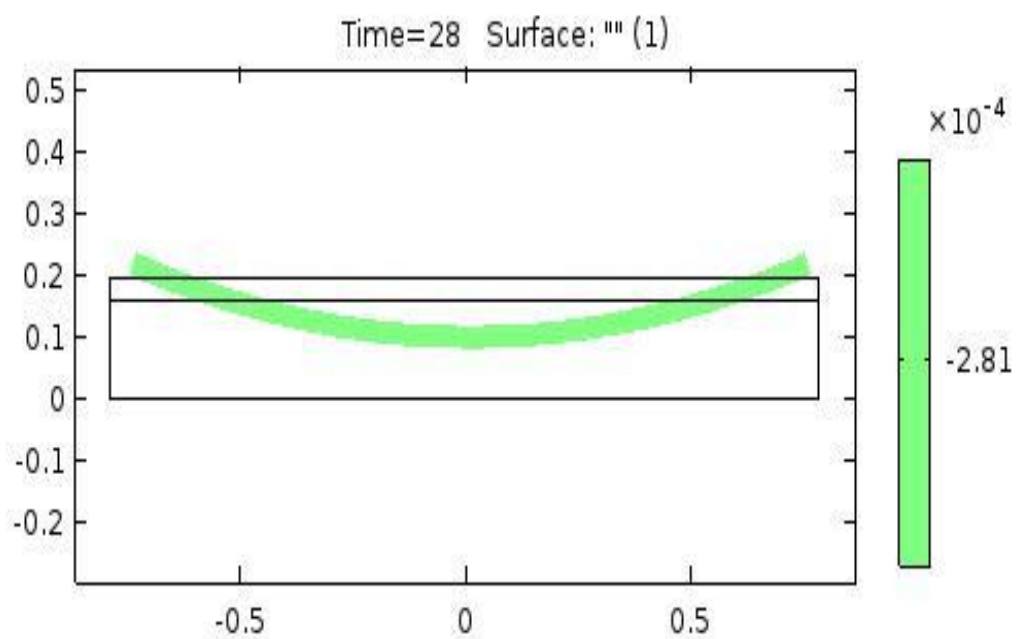


Figure 5.6.b Free Drying Shrinkage (Deformed Shape)

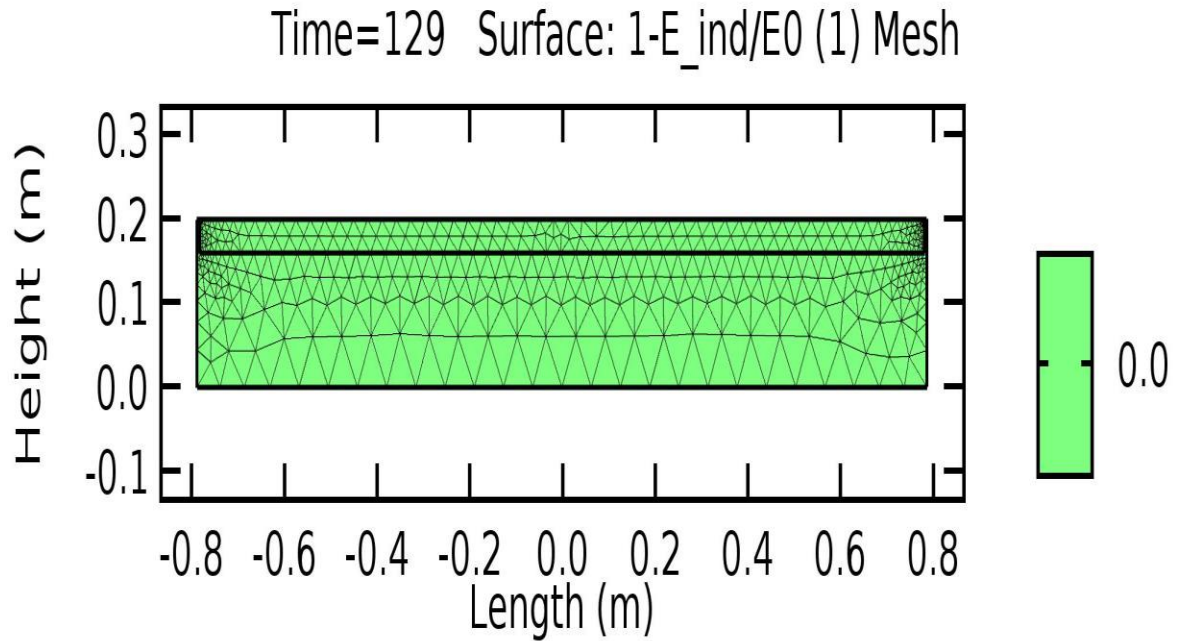


Figure 5.7 the DF at the End of the Analysis

5.4.1.1.1 Stress Development prediction:

Three important types of failure repair modes can be defined as follows[Rahman et al., 2000]:

- Cracks due to tensile stresses through repair part thickness
- Shear failure in the substrate part under the interface between substrate and repair layer
- Peeling due to transverse tension in the interface part of the patch repair system, which leads to delamination due to the combined effect of tensile stresses, shear stress, and peeling. All the previous failure modes are shown in Figure 5.8.

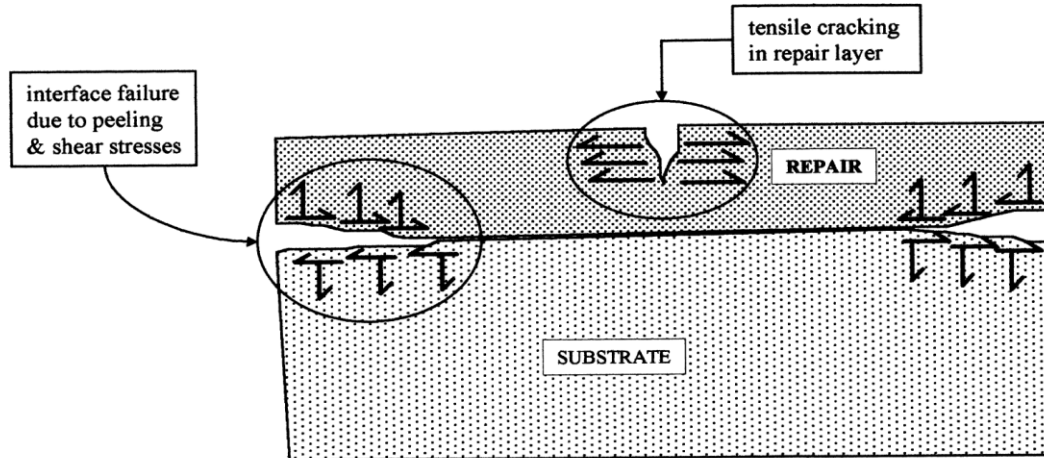


Figure 5.8 Prediction of Failure Modes

The proposed model predicts restrained shrinkage stress. Figure 5.9 demonstrates σ_{xx} variation along the length of the beam at time 90 days; in addition to that, Figure 5.10 shows the stresses in overlay repair system, the development of these stresses can be seen using stress contours distribution. There is a buildup of tensile stress in the repair layer whereas the substrate is subjected to compressive stress.

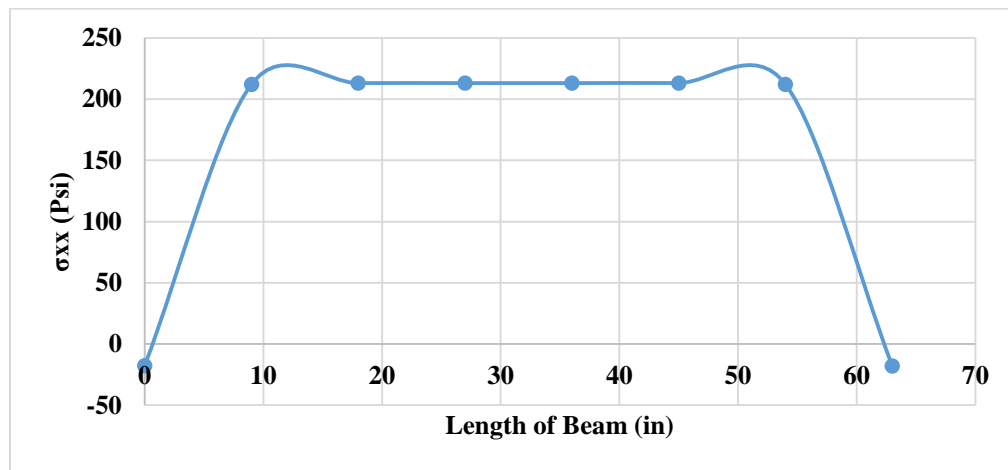


Figure 5.9 Variation of Stress σ_{xx} Along the Length at the Top of the Overlay (t=90)

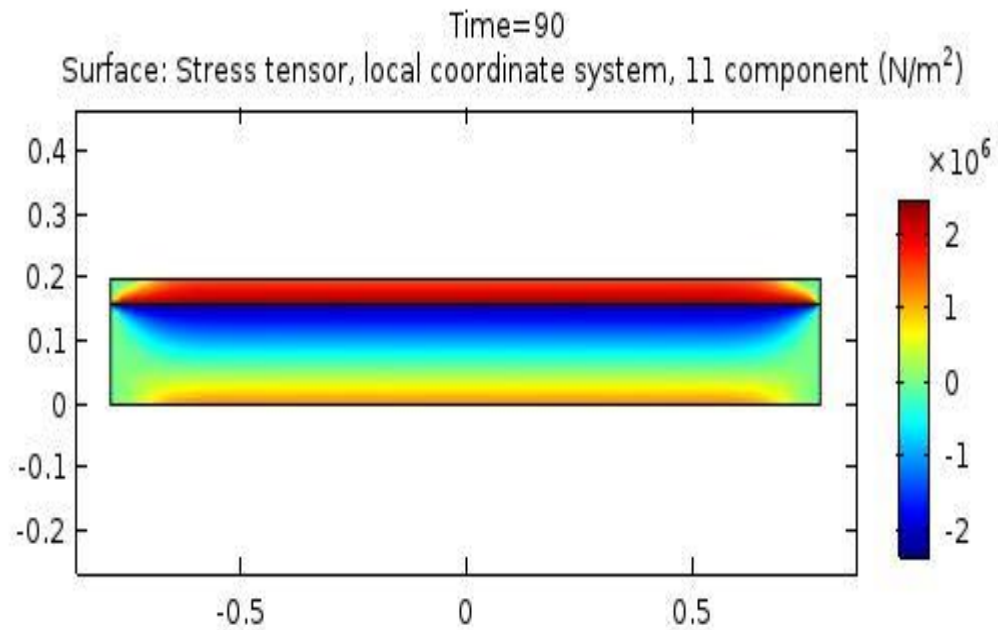


Figure 5.10 Stress Distribution σ_{xx} (90 days)

The variation of the stresses σ_{yy} at the interface along the length of repair is demonstrated in Figure 5.11; the σ_{yy} stresses are changed from tensile to zero stress at a distance (18 in) from the edge. However, in the case of higher shrinkage strain, the compressive stress will develop significantly. Then, the edge of the overlay repair system includes zone is subjected to σ_{yy} (peeling stresses) as shown in Figure 5.12.

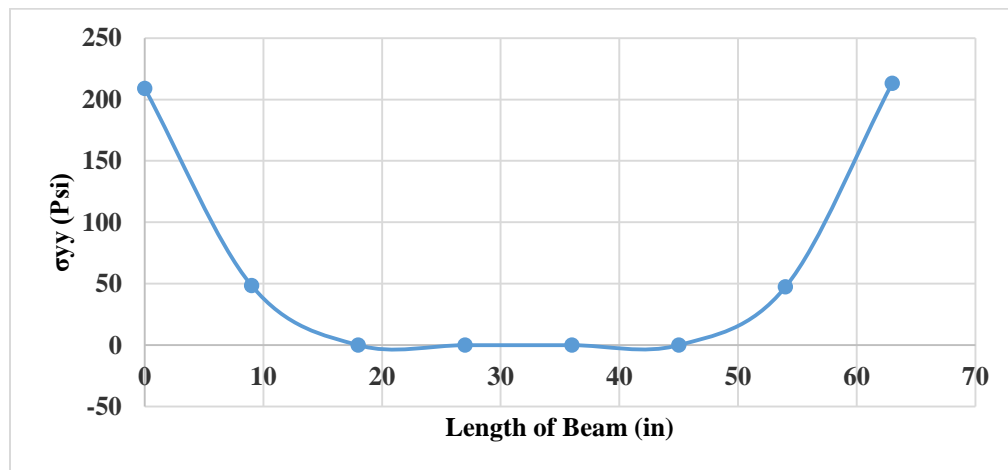


Figure 5.11 Variation of Stresses σ_{yy} Along the Length at the Bottom of the Overlay (t=90)

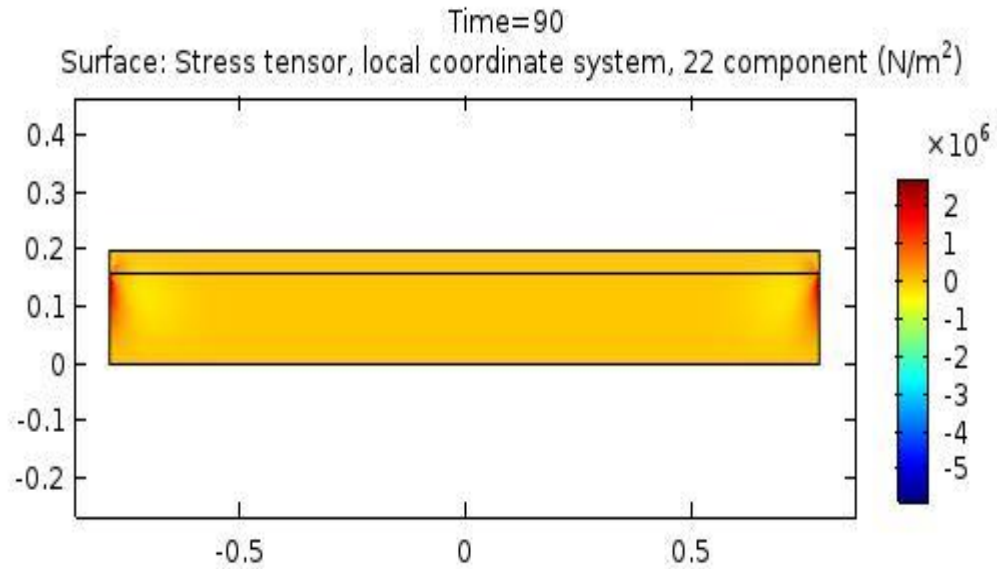


Figure 5.12 Stress Distribution σ_{yy} (90 days)

Figure 5.13 and 5.14 illustrates the σ_{xy} stresses along the length of the beam at the interface. Significant shear stress starts from the repair edge and decreases to zero at the middle of the overlay. Consequently, combined the tensile and shear stresses lead to existing interface failure zone.

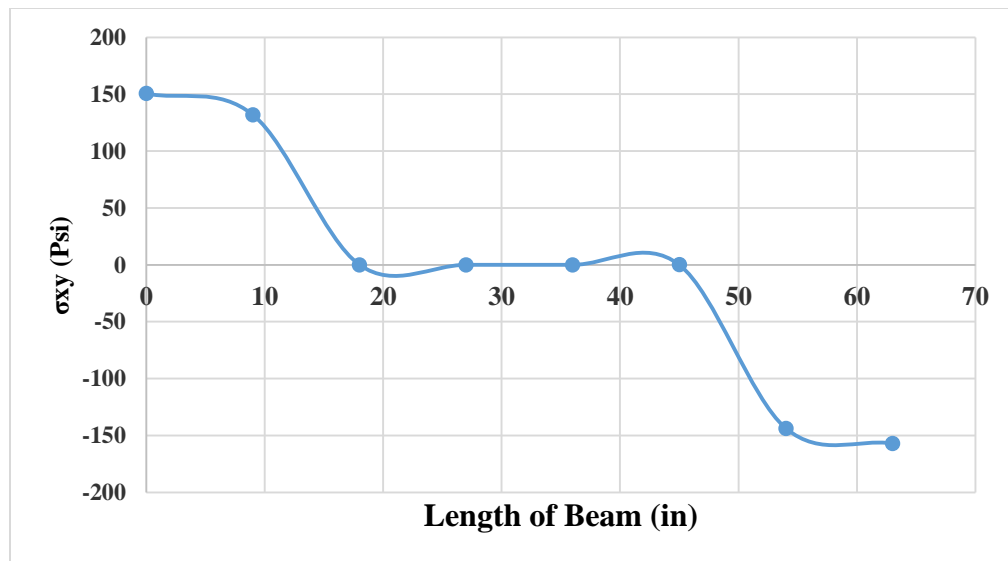


Figure 5.13 Variation of Stresses σ_{xy} Along the Length at the Bottom of the Overlay at

(t=90)

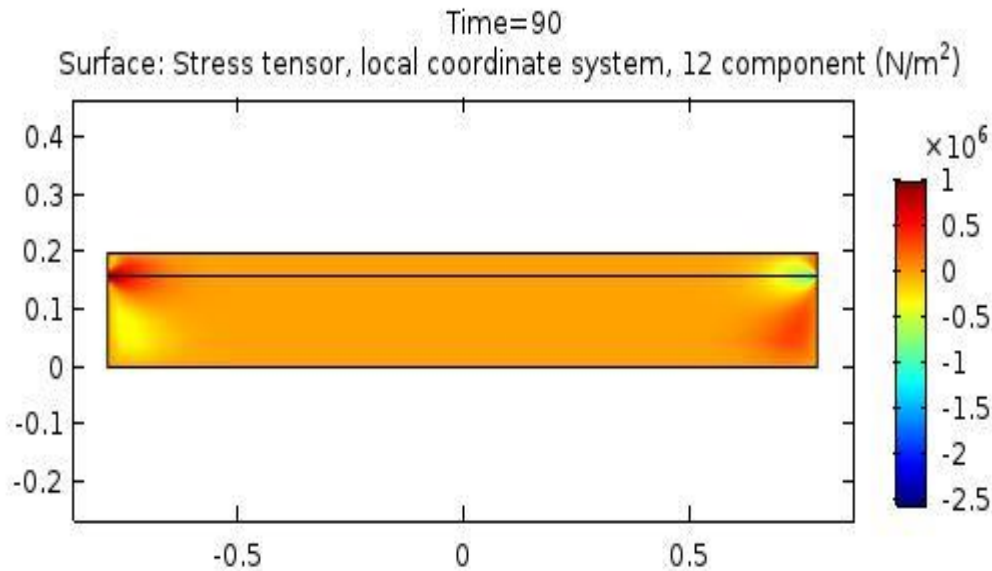


Figure 5.14 Stress Distribution σ_{xy} (90 days)

5.4.1.3 Prediction of Stresses due to Creep Effect

For the repair layer, E_r is lowered to the half to reflect its tensile creep characteristics of the repair material (Shazali et al. 2000). Figure 5.15 showed σ_{xx} variation along the length of the beam at time 90 days due to shrinkage and creep effect. It was observed that the stress σ_{xx} prediction is underestimated due to shrinkage and creep effect compared to the results due to the shrinkage effect only as shown in Figure 5.16. Figure 5.17 and 5.18 demonstrates the variation of σ_{yy} and σ_{xy} respectively along the length of the beam, Figures 5.19 and 5.20 illustrate the contour σ_{yy} and σ_{xy} stress distribution. It has been noticed the results coincides with that explained previously regarding σ_{xx} .

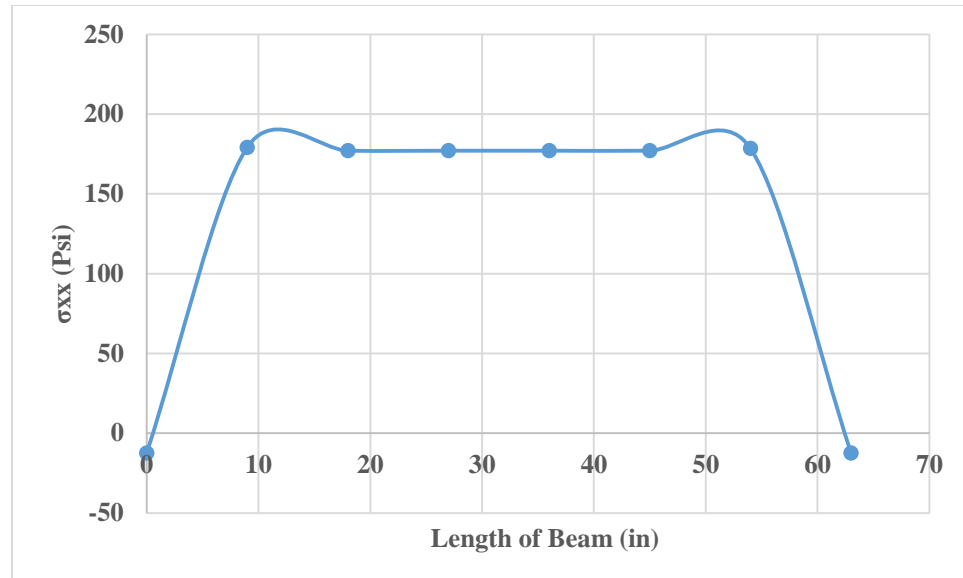


Figure 5.15 Variation of Stress σ_{xx} Along the Length at the Top of the Overlay (t=90) due to Shrinkage and Creep Effect

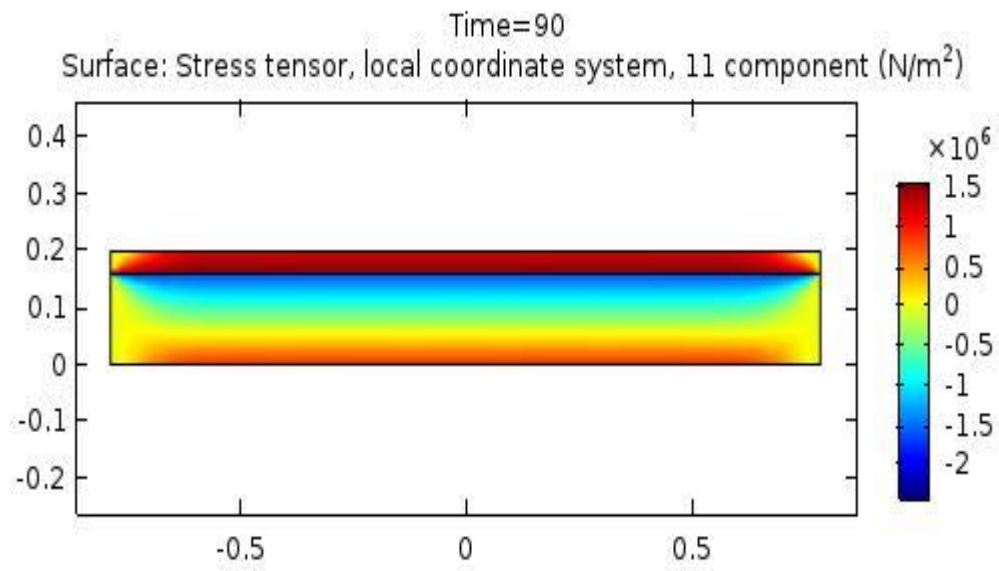


Figure 5.16 Stress Distribution σ_{xx} (90 days) Due to Shrinkage and Creep Effect

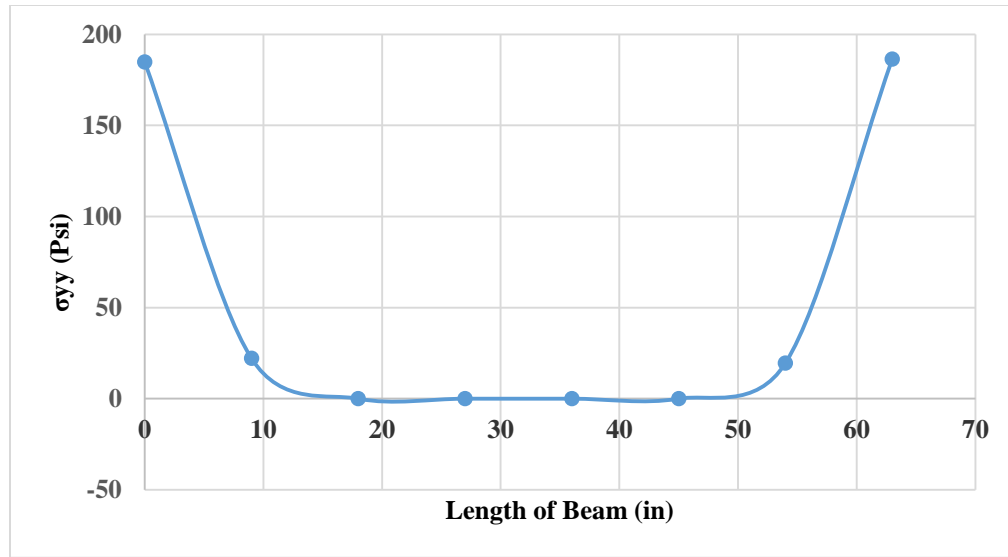


Figure 5.17 Variation of Stress σ_{yy} Along the Length at the bottom of the Overlay (t=90) Due to Shrinkage and Creep Effect.

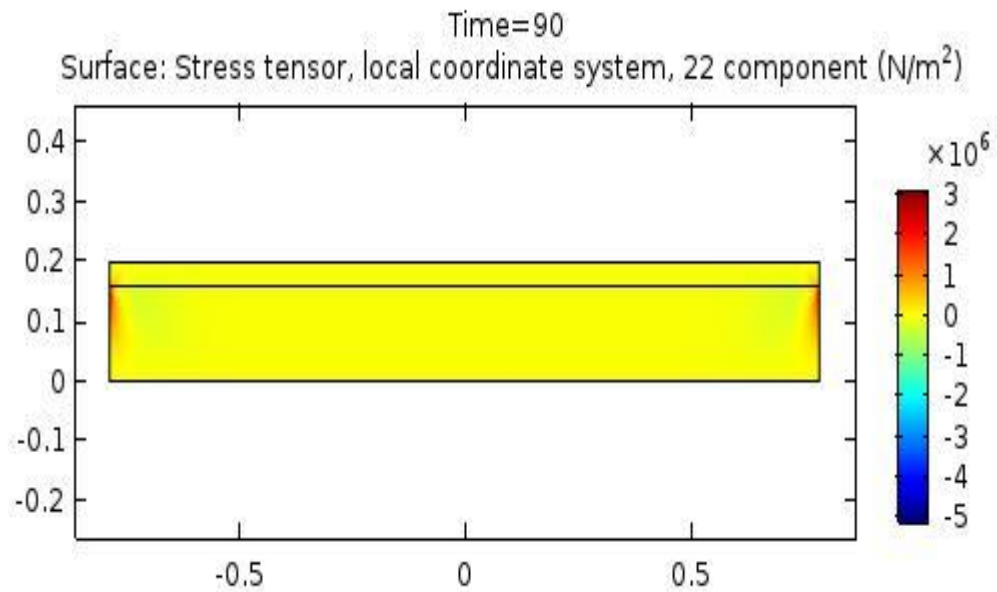


Figure 5.18 Stress Distribution σ_{yy} (90 days) Due to Shrinkage and Creep Effect

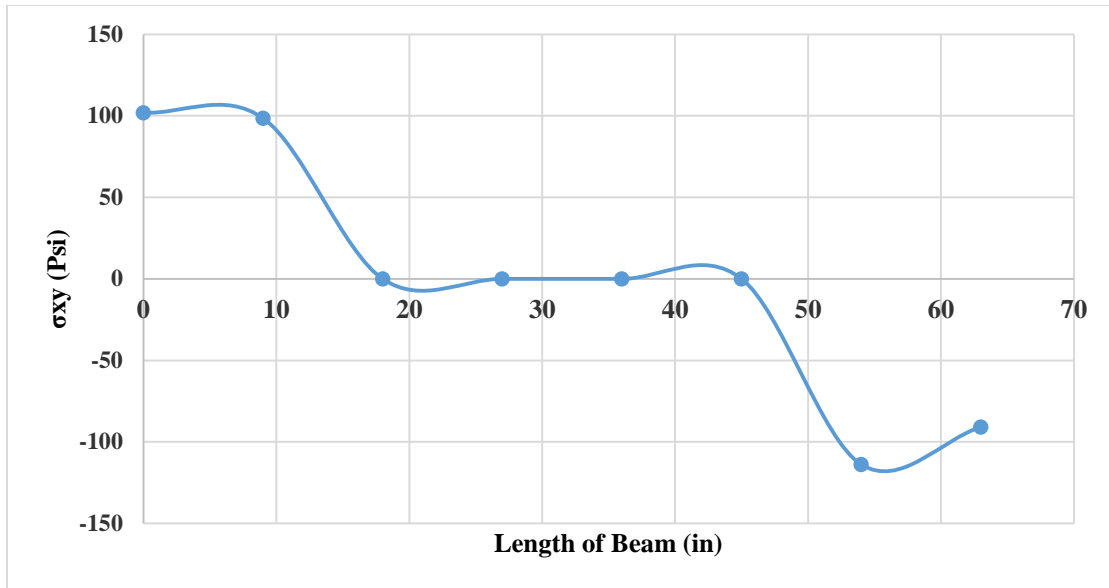


Figure 5.19 Variation of Stress σ_{xy} Along the Length at the bottom of the Overlay (t=90) due to Shrinkage and Creep Effect

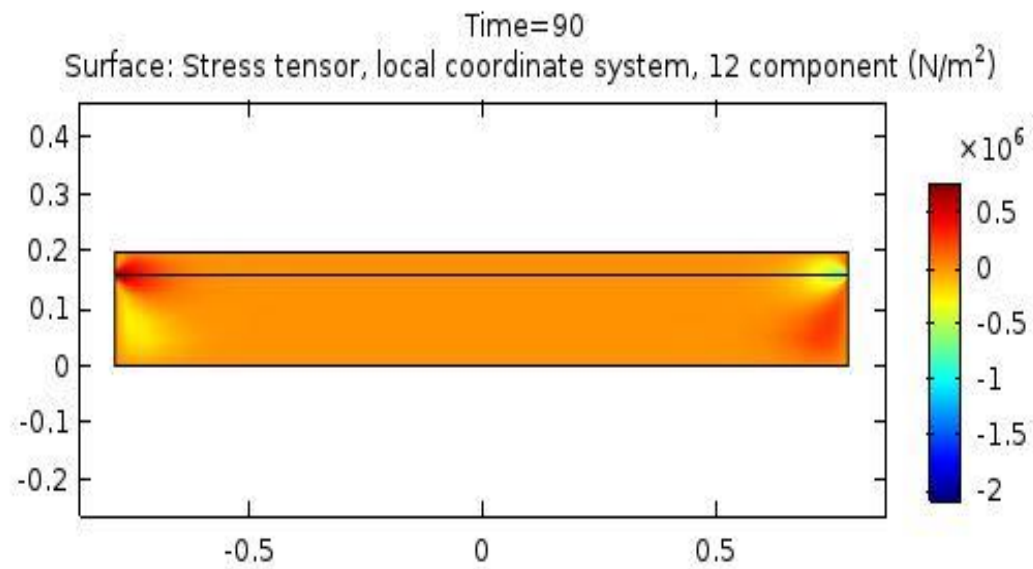


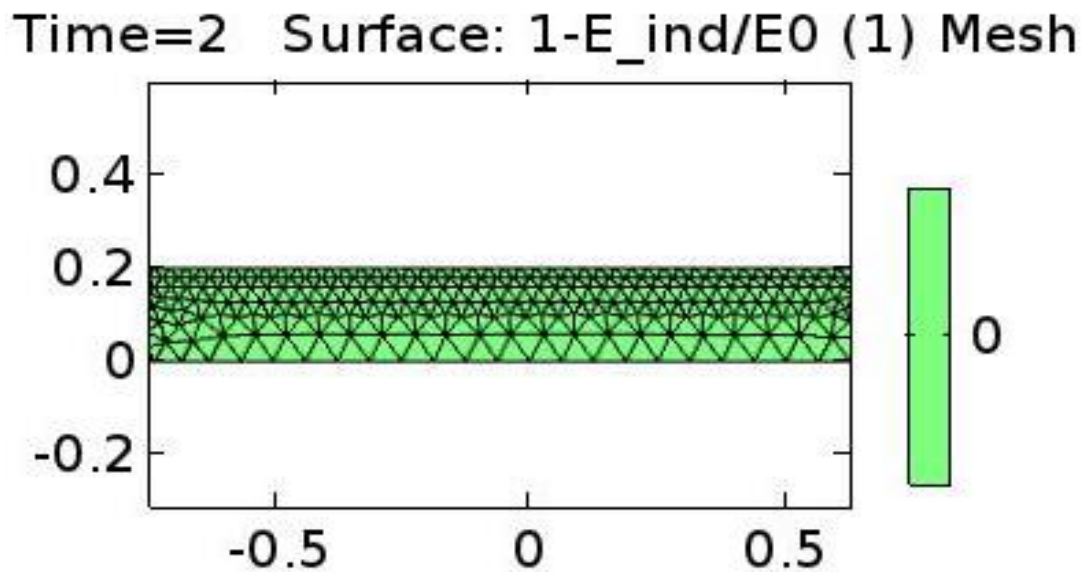
Figure 5.20 Stress Distribution σ_{xy} (90 days) Due to Shrinkage and Creep Effect

5.4.1.2 CASE B

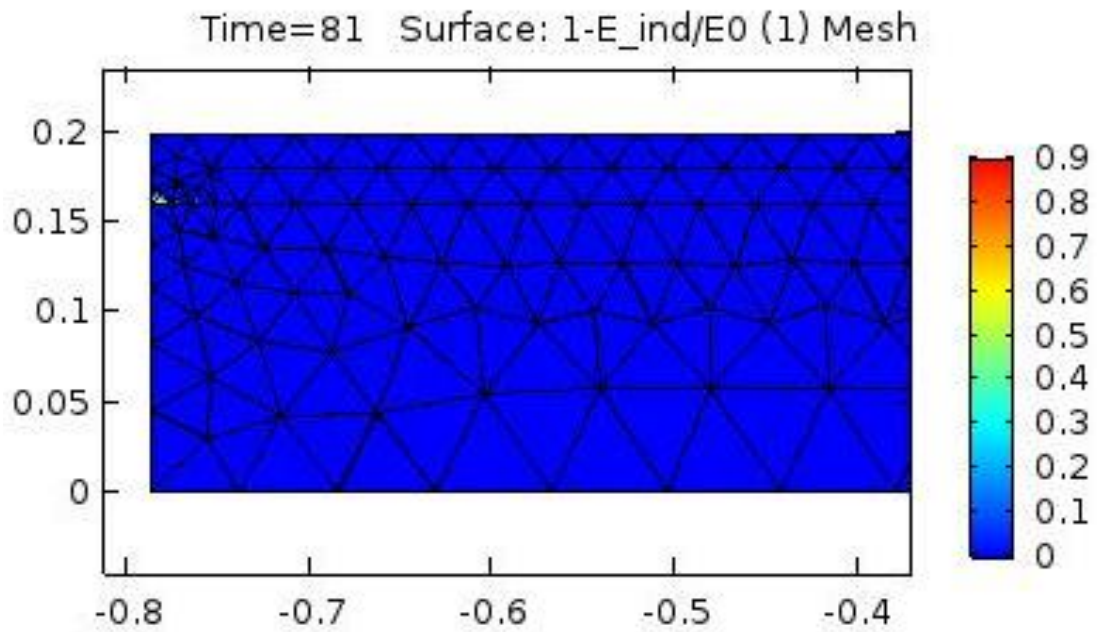
This case was assumed to examine the ability of the model to predict shrinkage cracking and how the DF is working. A simulation of the overlay repair system with a high

shrinkage value was conducted by assuming the free shrinkage strain of the overlay is greater than 290 microstrains at 28 days. For this purpose, the RH was decreased to 50% to get a value of 381 microstrains at 28 days for the free shrinkage for the overlay.

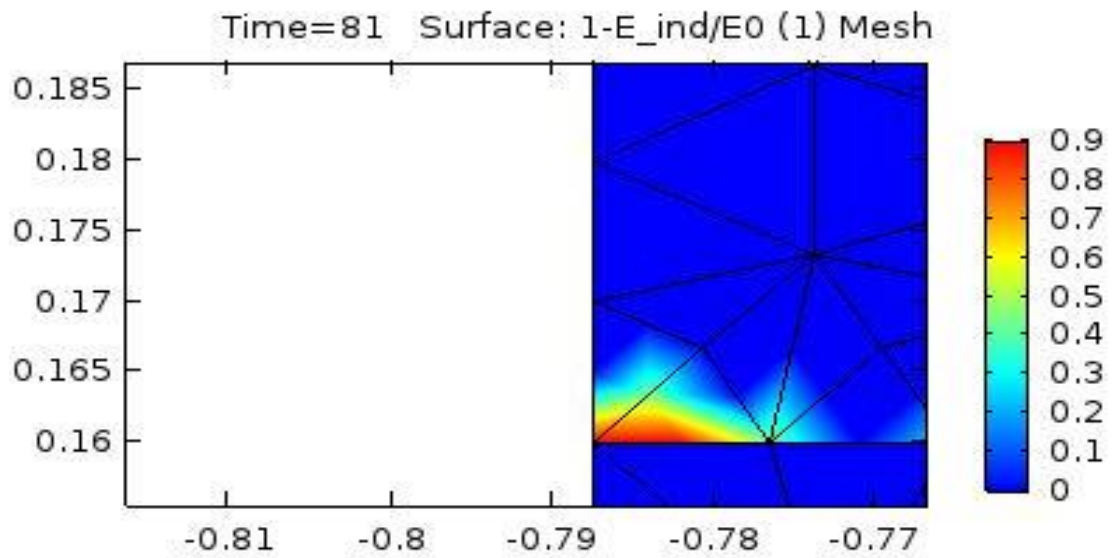
Figures 5.21a, 5.21b, 5.22c, and 5.21.d show how the DF is gradually changed and the crack is formed. Figure 5.21a shows the DF at 2 days. It can be seen that the DF value is equal to 1 and no crack is initiated yet. On the other hand, Figure 5.21b shows the DF value decreased, and hence, the crack has been initiated at 81 days. Figure 5.21c is a magnification of the formed crack shown in Figure 5.21b. At the end of the analysis, the cracks have been propagated towards the inside of the specimen as illustrated in Figure 5.21d.



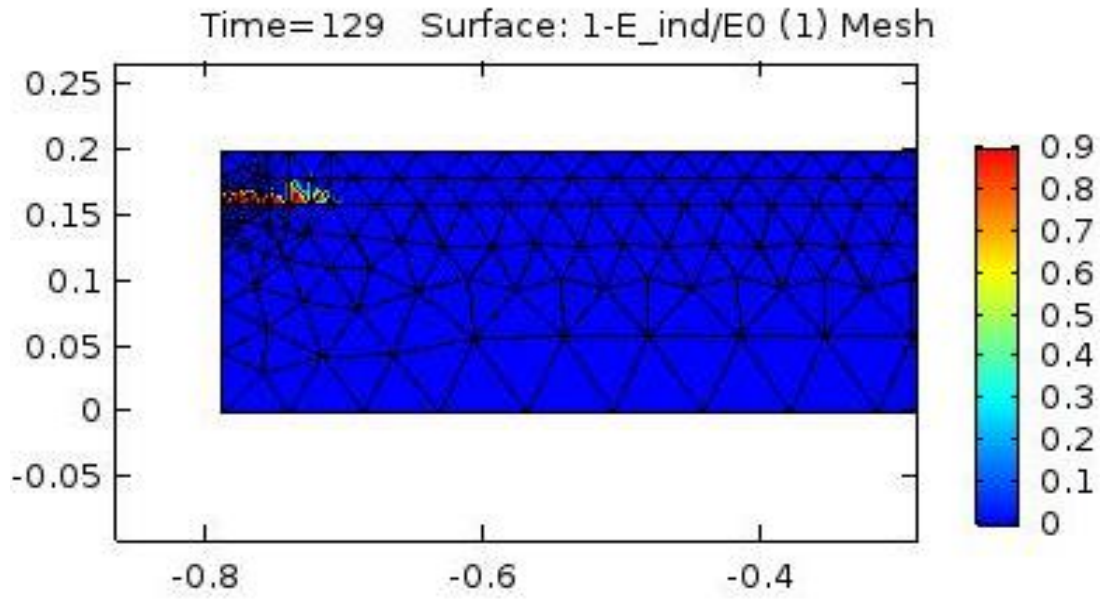
(a) The DF at 2 Days



(b) The DF at 81 Days



(c) DF at 81 Days- Magnification of the Crack



(d) The DF at 129 Days

Figure 5.21 DF During the Analysis Period

5.4.2 The Experimental was Carried out by Casting of Nine Composite Prisms

The composite prisms were demonstrated previously in chapter 3. The mean correction factors for a given model (C) are shown in Table 5.3 Linear correlations between measured and predicted shrinkage values in terms of the slope of the correction and the correlation factor (R^2) for the investigated mixtures. In general, the R^2 values for the modified models higher than those of the original models. This indicates a better prediction of the experimental shrinkage values was achieved.

Table 5.3 Predicted vs. Modified Statics Values Determined Using ACI Model

| Mixture Designation | Prediction Model | | Modified Model | | |
|---------------------|------------------|----------------|----------------|----------------|------|
| | slope | R ² | slope | R ² | C |
| C1R | 0.51 | 0.91 | 0.91 | 0.97 | 1.64 |
| C1S25 | 0.65 | 0.94 | 1.00 | 0.99 | 1.71 |
| C1S50 | 0.67 | 0.93 | 1.03 | 0.97 | 1.45 |
| C1C25 | 0.65 | 0.95 | 0.99 | 0.99 | 1.60 |
| C2R | 0.43 | 0.85 | 0.92 | 0.97 | 2.69 |
| C2S25 | 0.57 | 0.94 | 0.99 | 0.97 | 1.93 |
| C2B50 | 0.53 | 0.93 | 0.99 | 0.96 | 2.24 |
| QR | 1.32 | 0.87 | 1.00 | 0.99 | 1.75 |
| QS25 | 1.35 | 0.87 | 1.34 | 0.92 | 1.03 |

5.4.2.1 Cracking Predictions

At an early age, the concrete tensile strain capacity usually between 100-250 microstrains. Hence, the concrete cannot resist stresses due to expected drying shrinkage of 500 microstrains or more and crack initiates regardless of how low is the concrete slump and water-cement ratio (Holcim, 1999). The cracking strain can be obtained using the following equation:

$$\varepsilon_t = \frac{f_t}{E}$$

where: f_t : Tensile splitting strength; E: Modulus of elasticity; and ε_t : Cracking strain.

Table 5.4 shows the cracking strain and the comparison between the profile strain for the repaired composites from the experiment and the FEM. The model showed a good agreement with experiment. During the experiment, the cracks were observed using a digital microscope. Up to 56 days, the cracks were only found in the composite prism repaired with C2R. Indeed, the crack was initiated at 28 days in the FEM compared with 32 days in the experiment as shown in Figure 5.22.

To approve the plain stress assumption, a comparison between plain-stress and plain-stress was made and demonstrated in Table 5.5. As expected, the values from plane-strain and plane-stress analysis form an upper and lower bound, respectively. The difference between the two boundaries is very small. Hence, the assumption of the plane stress is close to the experiment.

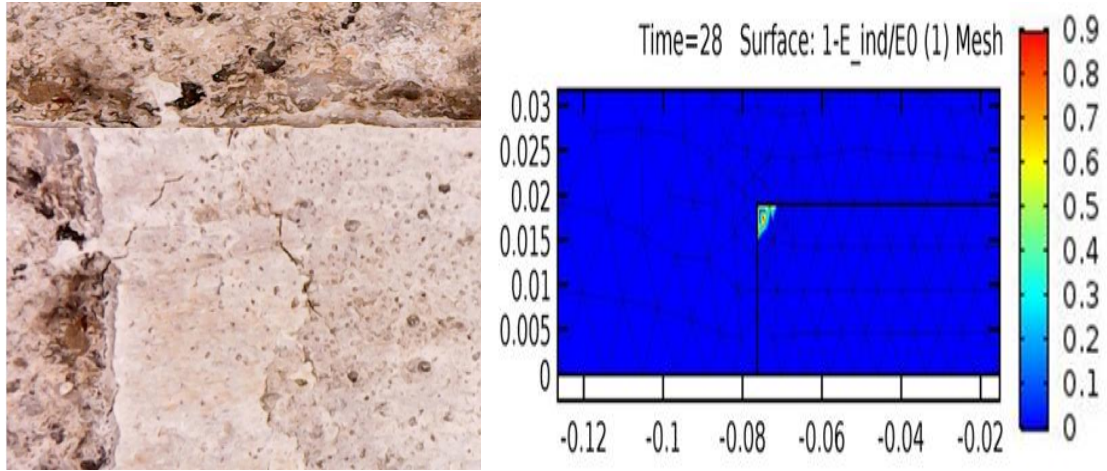
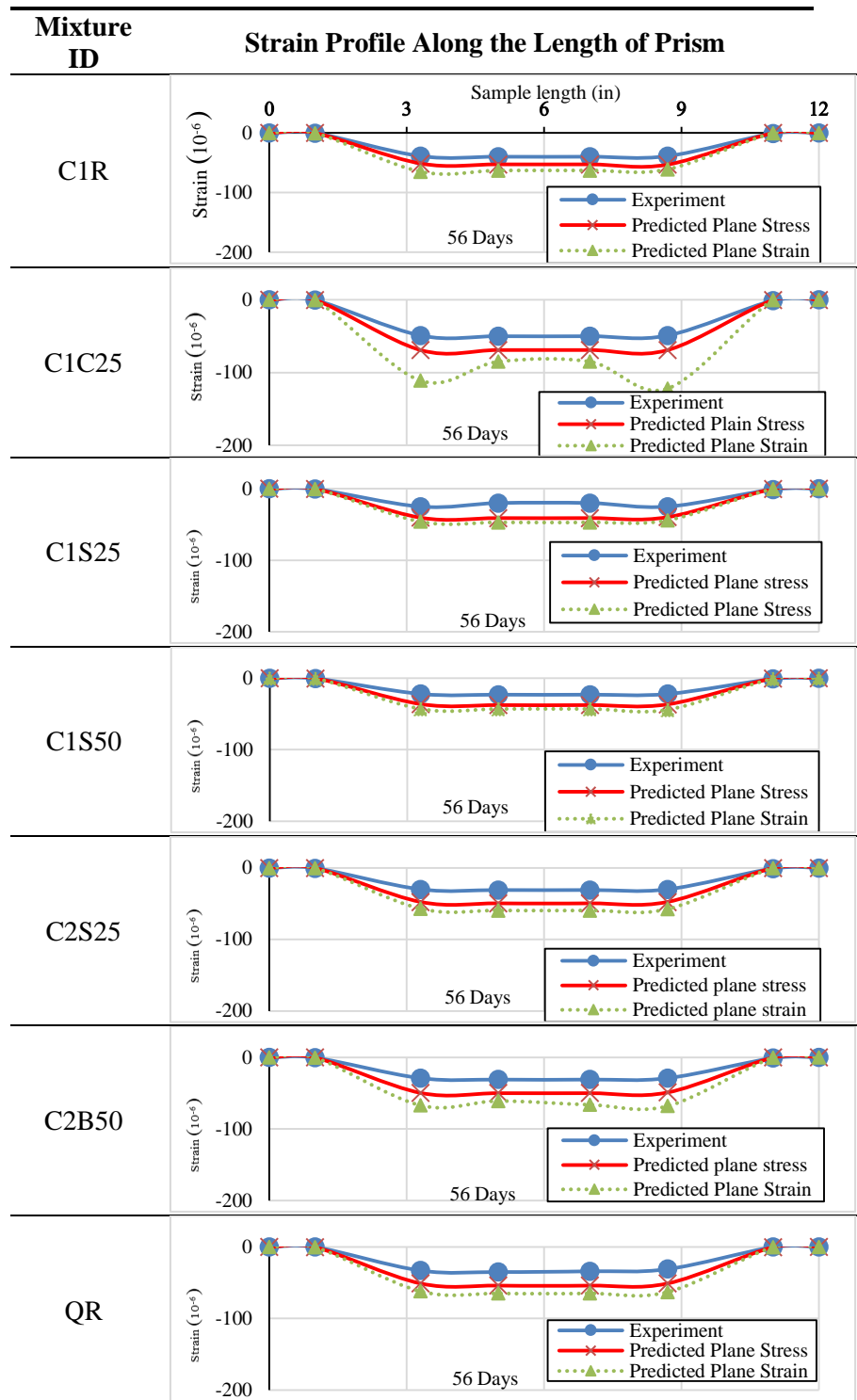


Figure 5.22 Cracks in Composite Prism Repaired by C2R: a) Experiment at 32 days, b) FEM at 28 days

Table 5.4 Strain Profile and Cracking Strain

| Mixture ID | Strain Profile Along the Length of Prism | Cracking Strain (microstrains) |
|------------|--|--------------------------------|
| C1R | <p>Sample length (mm)</p> <p>microstrain</p> <p>56 Days</p> <p>Experiment</p> <p>Predicted</p> | 119 |
| C1C25 | <p>56 Days</p> | 114 |
| C1S25 | <p>56 Days</p> | 127 |
| C1S50 | <p>56 Days</p> | 117 |
| C2R | <p>29 Days</p> | 168 |
| C2S25 | <p>56 Days</p> | 193 |
| C2B50 | <p>56 Days</p> | 193 |
| QR | <p>56 Days</p> | 133 |
| Q25S | <p>56 Days</p> | 140 |

Table 5.5 Strain Profile for the Experiment, Plane-stress, and Plane-strain



5.4.3 Parametric Studies

Based on the experimental work that was carried out, results were compared to the finite element analysis. For more extensive studies to explore the effect of sensitive factors on the repair success of the structural member incorporating shrinkage, there is a need for a parametric study. A prism repaired with C2R was selected to apply all the parametric study and evaluate the effects, which represent the critical case due to the presence of a small crack. The investigated parameters are; Dimension of the repair system (Dr) such as Length of the repair (Lr) and Thickness of the repair material (Tr), Elastic modulus of elasticity of the repair material (Er), and Shape of the repair (Sr) as shown in Figure 5.23.

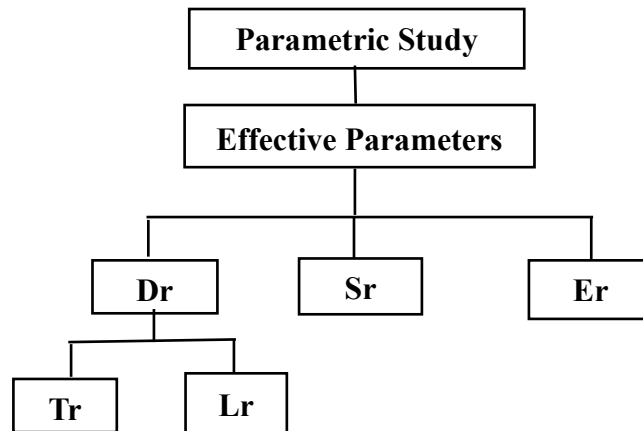


Figure 5.23 Flowchart for the Parametric Study

5.4.3.1 Dimension of the Repair

5.4.3.1.1 Thickness of the Repair (Tr)

The thickness of repair material is varied depending on how much thickness of the unsounded concrete we need to remove during the cleaning process of the damaged concrete member. Different thickness of the repair part in the composite repair system was examined during this parametric study. Three values of thickness were studied (reference

thickness 0.75, 0.8, and 0.9 in). Also, Figures 5.24, 5.25, and 5.26 show how the cracking tendency decreased with increase in the thickness of the repair. This indicates that the tendency for cracking increases in the thinner repair material. Also, Figure 5.27 shows how the tensile stresses decreased with repair thickness increases (Beushausen, 2006).

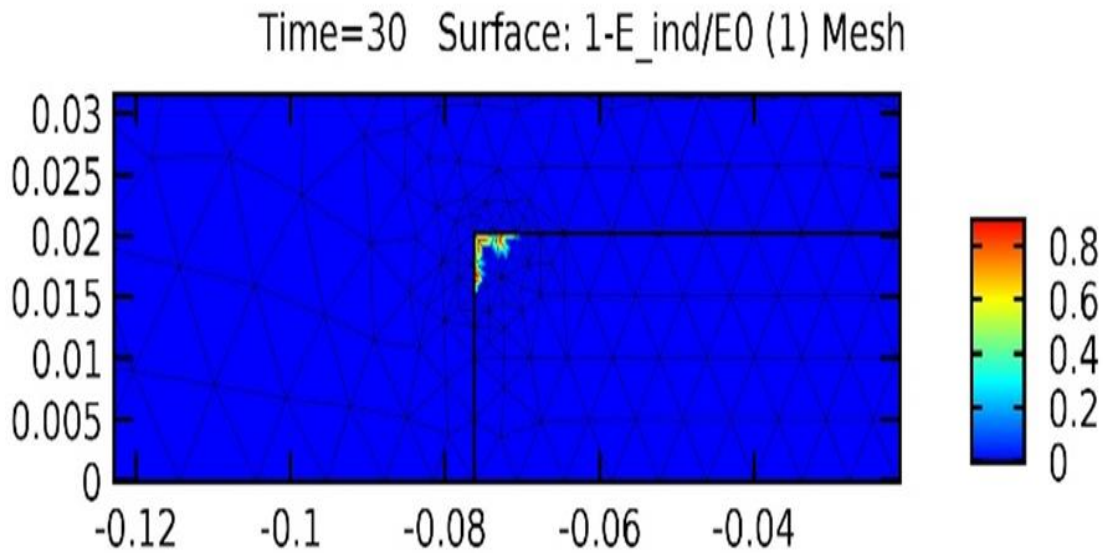


Figure 5.24 Reference Repair Thickness (0.75 in)

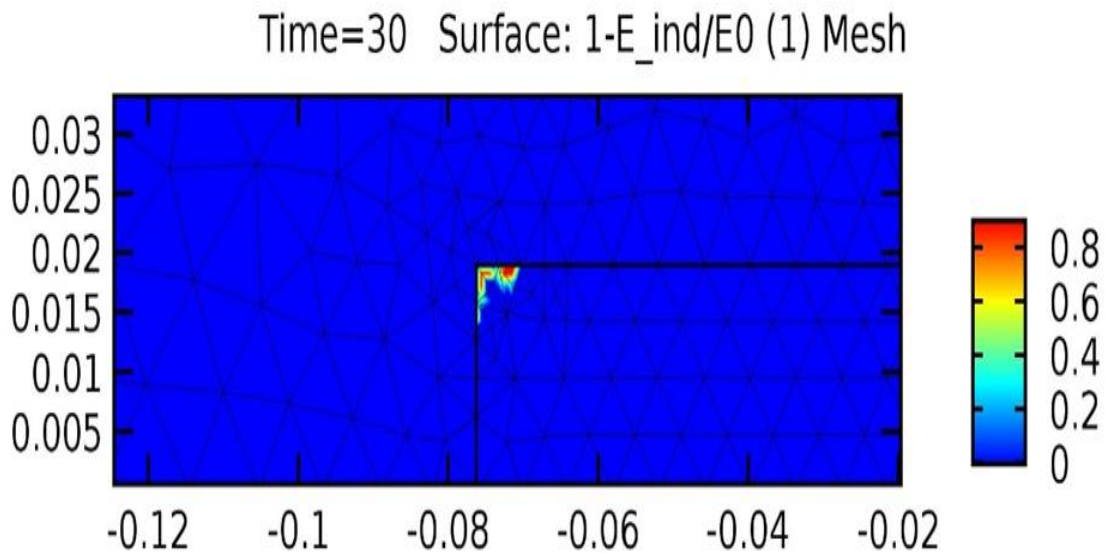


Figure 5.25 Repair Thickness (0.80 in)

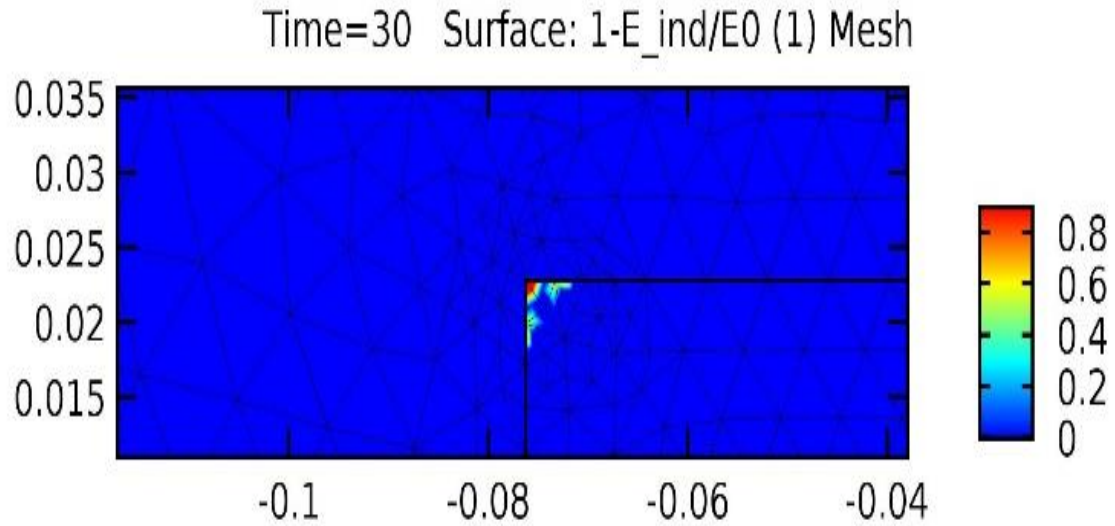


Figure 5.26 Repair Thickness (0.90 in)

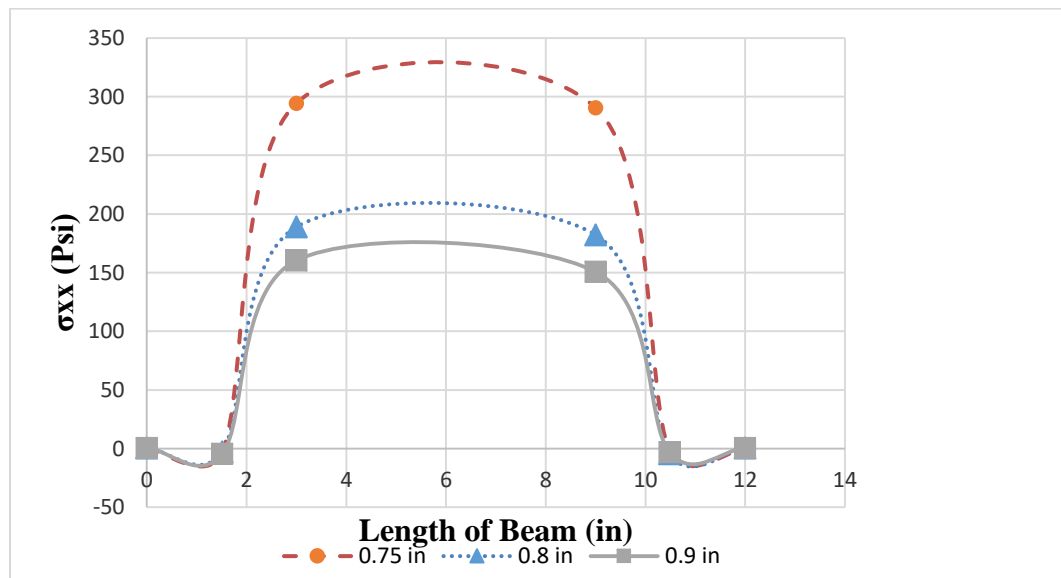
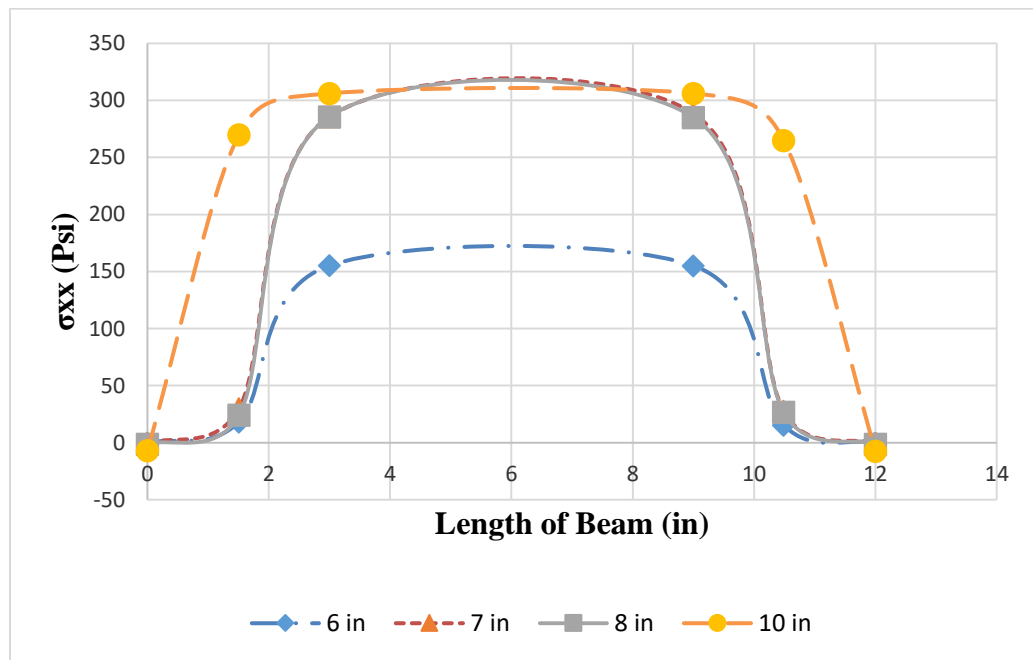


Figure 5.27 Tensile Stresses at 24 Days Varied with Repair Thickness

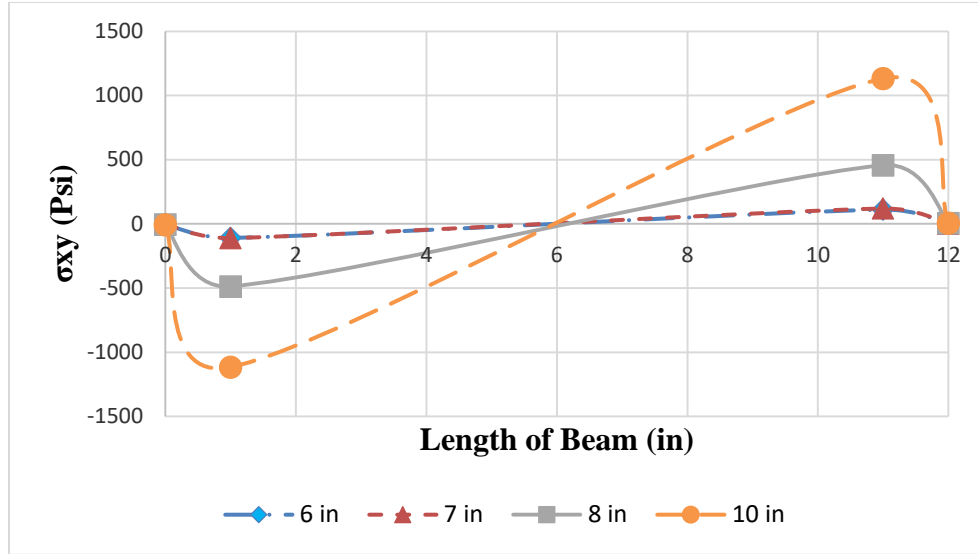
5.4.3.1.2 Length of the Repair (L_r)

Silfwerbrand (1997) concluded that the tensile stress in the repair material and the shear stress at the interface increases with the length of the repair layer increases. The same finding was concluded as shown in Figure 5.28. The tensile stress increase with length

repair increasing significantly up to (7 in) of the repair length. Beyond this value, there is a slight increase in tensile strength, and σ_{xx} reaches the maximum value of 306 Psi. In other words, the shrinkage of the repair material is governed by critical length. That means if the repair length exceeds the critical length, no more considered as a control factor. While for shear stresses, the opposite trend was observed that the shear stresses increased significantly in repair length longer than (7 in) as shown in Figure 5.29. Figures 5.31, 5.32, and 5.33 show that the cracking tendency represented by damage factor decreasing starting from E, 0.95E, and 0.9E respectively.



Figures 5.28 Tensile Stress at 24 Days Varied with Length of Repair



Figures 5.29 Shear Stress at 24 Days at Interface Varied with Length of Repair
5.4.3.2 Modulus of Elasticity (E_r)

MacDonald et al., [2002] concluded that the repair material with a low modulus of elasticity is less tendency for cracking and delamination due to the stress relaxation. As shown in Figure 5.30, the strain decrease with the decrease in the modulus of elasticity.

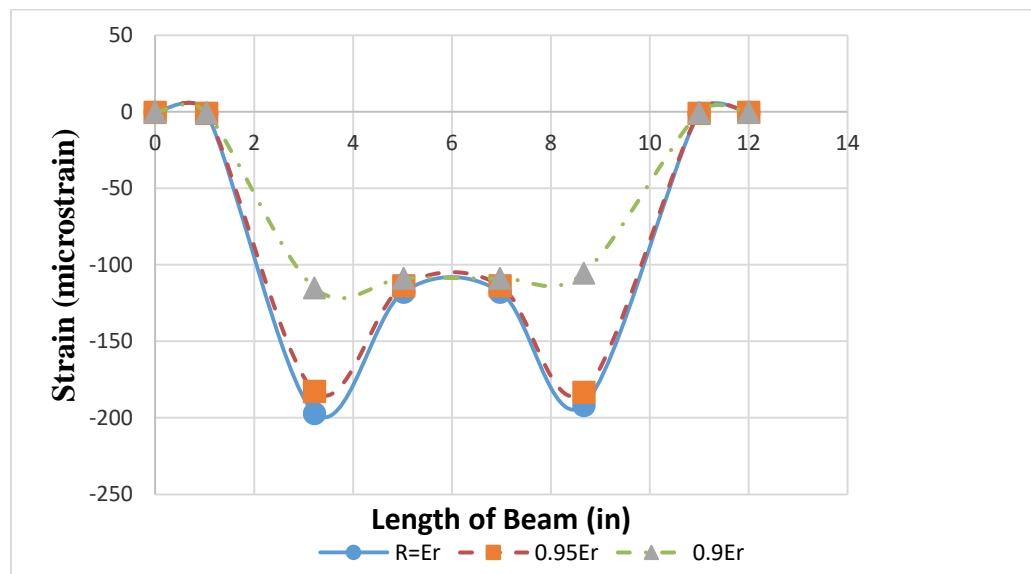


Figure 5.30 Strain Variation at 24 Days Due to the modulus of Elasticity Variation

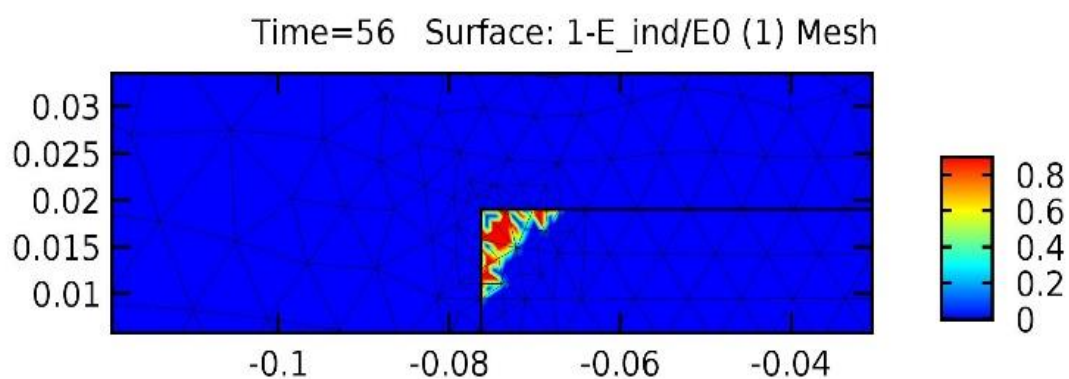


Figure 5.31 Repair Damage Factor with 1.0 E

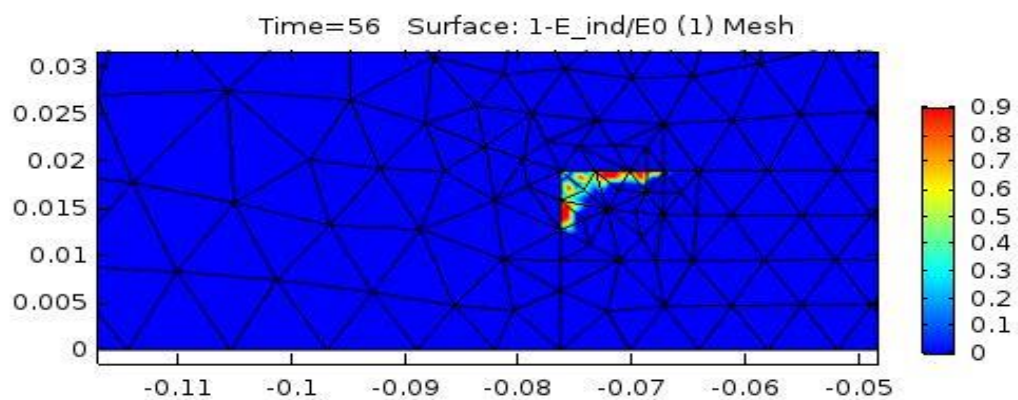


Figure 5.32 Repair Damage Factor with 0.95E

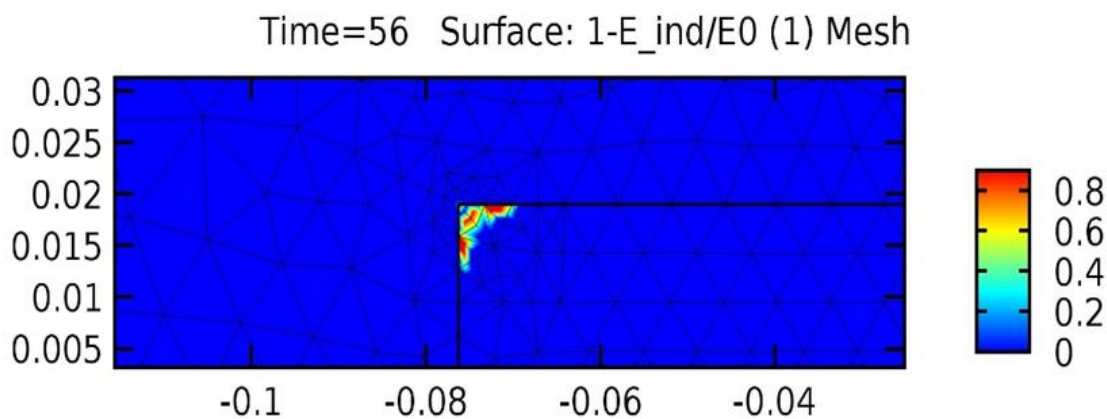


Figure 5.33 Repair Damage Factor with 0.9E

5.4.3.3 The Shape of Repair (Sr)

In general, the damaged concrete sections have non-uniform shapes and irregular edges, which increase the concentration of stresses due to shrinkage. Consequently, cracking tendency increased. To avoid the critical condition of the repair shape, the simple layout of the repair system as shown in Figure 5.34 is required such as the rectangular or trapezoidal shapes. (Emmons,1993; ACI Repair Manual, 1999).

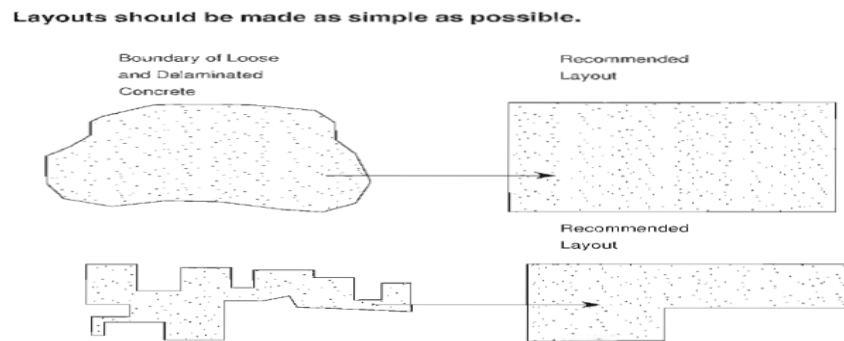


Figure 5.34 Suggestions for Layouts

Figure 5.35 showed the strain along the length of the beam in the repair part at the interface, the strain in the case which the shape of repair is trapezoidal less than rectangle shape. Therefore the cracking tendency due to excessive stresses is concentrated at the corner near to the interface between the repair and substrate in the rectangular shape. Figure 5.36 and Figure 5.37 demonstrate the crack distribution in the case of rectangular and trapezoidal shapes, respectively.

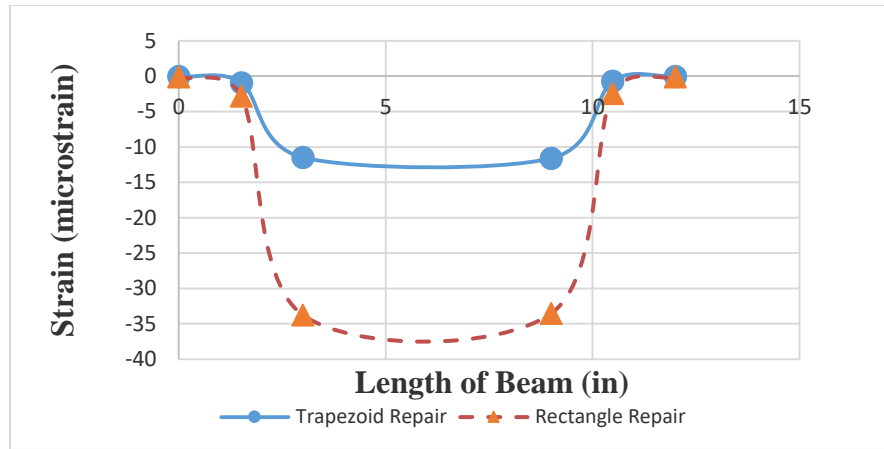


Figure 5.35 Strain Along the Length of the Beam at the Interface

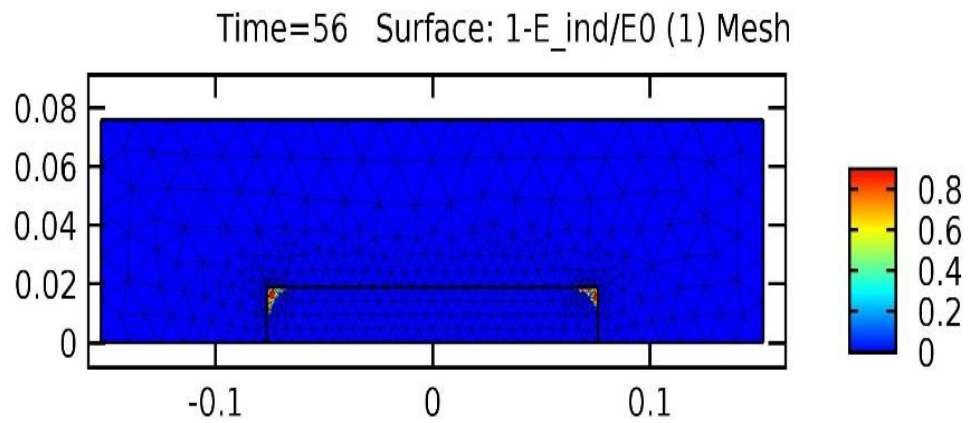


Figure 5.36 Crack Distribution in Rectangle Shape Repair

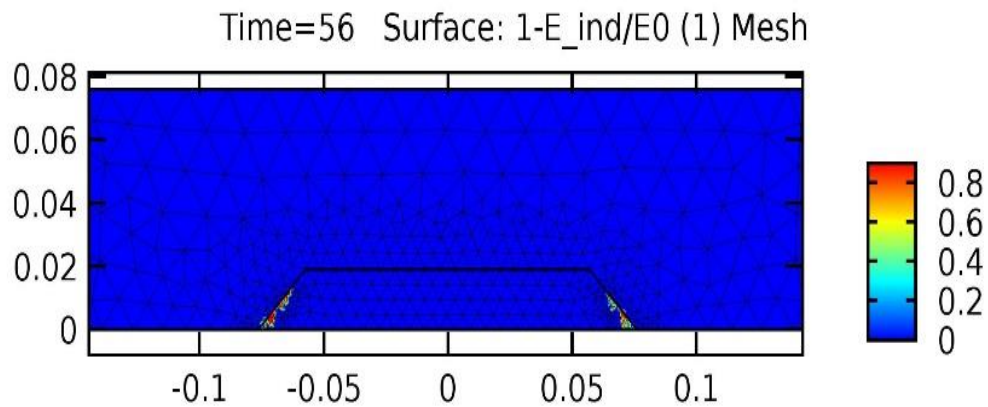


Figure 5.37 Crack Distribution in Trapezoidal Shape Repair

CHAPTER 6 CONCLUSIONS

6.1 CONCLUSIONS

In this dissertation, high early strength fiber reinforced rapid set materials (HES-FR-RSM) were developed for concrete repair applications in transportation infrastructures with low cracking potential. Three types of rapid set prepackaged repair materials were developed. The designed mixtures have included three types of fibers (steel, basalt, and carbon) with different volume fractions. The research also included developing a finite element model (FEM) that could describe the real structural behavior. Based on the experimental and analytical results, the following conclusions can be drawn:

- 1- The optimized HES-FR-RSM mixtures are flowable and can be casted easily with no or little compaction if needed. These mixtures can achieve high early strength at 4hrs.
- 2- The incorporation of CF affects the concrete workability for the Q mixtures in comparison with SF and BF. Therefore, the maximum fiber percent for the designed mixtures should not exceed 0.75 for SF, BF, and CF for the C1, C2, and Q mixtures. While 0.25 of CF for the Q mixtures.
- 3- The use of fiber in HES-FR-RSM has increased the compressive strength slightly for optimized mixtures at 28 days in comparison with RSM mixture. The compressive strength was also slightly increased with the increase of fiber content.
- 4- The addition of fibers increases the splitting tensile strength of the developed mixtures significantly. The percentage increase in splitting tensile strength was found to be increased with the increase in fiber content. The results showed that the tensile strength for HES-FR-RSM containing 0.5% of BF, SF, and CF fibers was

increased by 42.3, 10, and 7%, respectively for CTS1 mixtures. On the other hand, the maximum percentage increase for CTS2 with 0.5% of BF was 56.3%. This improvement is mainly due to the higher tensile strength of BF compared to those of SF and CF (702, 413, and 100 ksi respectively). The Q mixtures showed a slight increase in the compressive and tensile strength with an increasing percentage of SF volume fraction. The modulus of rupture also increased with the increase of fiber percentage. The maximum values for flexural strength were 2015, 2012, and 2178 psi for C1S0.5, C1B0.25, and C1C0.25, respectively. While for C2R2 were 2178, and 2292 psi for C2S0.5, and C2B0.25, respectively. For Q mixtures, the QS0.5 was the maximum value (1950 psi). The addition of fiber resulted in a slight increase in the modulus of elasticity for some mixtures.

- 5- Most of the optimized mixtures showed low cracking tendency due to the low free shrinkage and high tensile values. The results showed that the mixtures contain SF in three types of products exhibited lower shrinkage compared to mixtures contain CF and BF. It is important to mention a decrease in the percentage reduction of free shrinkage as SF content increases by about 36% and 30% for C1S50 and C1S25 compared with the reference (C1R), respectively. The best performance mixture was C1S50 with 268 microstrain, which is less than the tensile strain capacity of concrete. Consequently, limits the shrinkage strains to the tensile strain capacity of concrete. While for CF, the reduction percentage was 29% for C1C50 mixture. On the other hand, BF did not show significant shrinkage reduction. For CTS2 mixtures, the reduction percentage was 13% for C2S25. While, no significant reduction was observed in the other volume fraction or other fiber types. For Q mixtures, there is no significant shrinkage reduction compared to the reference

mixture. The mixtures that showed free drying shrinkage lower than 500 microstrains are QR, QS25, and QS50.

- 6- HES-FR-RSM can be suitable for a wide range of concrete repair applications in transportation infrastructures with significantly short time, while greatly improving durability and reducing future maintenance.
- 7- The developed model provides a new approach to introduce restrained shrinkage by using strain module in COMSOL instead of moisture diffusion. The model can transfer the free shrinkage measured in the lab and apply it to the repair system to predict the repair material behavior under restraint condition.
- 8- The developed model is a good basic tool to study the effects of free shrinkage of the repair materials on the repaired composite; hence make the selecting repair materials easiest for the engineers for practical purpose. The model is also capable of simulating the crack initiations.

APPENDICES

APPENDIX A MANUFACTURER PRODUCT SPECIFICATIONS

1. CEMENT ALL MULTI-PURPOSE REPAIR MATERIAL & NON-SHRINK GROUT

DESCRIPTION

Rapid Set® CEMENT ALL® is a high-performance, fast-setting, multipurpose concrete repair material, and non-shrink grout. Durable in wet environments, CEMENT ALL is a blend of Rapid Set hydraulic cement and specially graded fine aggregates. CEMENT ALL is non-metallic, and no chlorides are added. Mix CEMENT ALL with water to produce a workable, high-quality material that is ideal where rapid strength gain and high durability are desired. CEMENT ALL sets in 15 minutes and achieves structural strength in 1 hour.

USES

Use CEMENT ALL for general and structural concrete repair, doweling and anchoring, industrial grouting, formed work, vertical and horizontal trowel applications. CEMENT ALL is ideal for airport, highway, industrial and marine applications.

ENVIRONMENTAL ADVANTAGES

Use CEMENT ALL to reduce your carbon footprint and lower your environmental impact. Production of Rapid Set cement emits far less CO₂ than portland cement. Contact your representative for LEED values and environmental information.

APPLICATION

Apply CEMENT ALL in thicknesses from featheredge to 4" (10 cm). For heavy loads and vehicle traffic, minimum thickness will vary. Not intended for high heat applications above 300°F (149°C). For deeper sections, use Rapid Set® Mortar Mix or Rapid Set® Concrete Mix. For overlay applications, a minimum of one test section should be prepared to evaluate the suitability of the materials and procedures.

SURFACE PREPARATION

For repairs, application surface shall be clean, sound and free from any materials that may inhibit bond, such as oil, asphalt, curing compound, acid, dirt, and loose debris. Roughen surface and remove all unsound material. Apply CEMENT ALL to a surface that is thoroughly saturated with no standing water.

MIXING

The use of a power-driven mechanical mixer, such as a mortar mixer or a drill-mounted mixer, is recommended. Organize work so that all personnel and equipment are in place before mixing. Use clean potable water. CEMENT ALL may be mixed using 3 to 5 quarts (2.8 L to 4.7 L) of water per 55-lb (25-kg) bag. Use less water to achieve higher strengths. Do not exceed 5 quarts (4.7 L) of water per bag. For increased fluidity and workability, use Rapid Set® FLOW Control® plasticizing admixture from the Rapid Set® Concrete Pharmacy®. Place the desired quantity of mix water into the mixing container. While the mixer is running, add CEMENT ALL. Mix for the minimum amount of time required to achieve a lump-free, uniform consistency (usually 1 to 3 minutes). Do not retemper.

PLACEMENT

CEMENT ALL may be placed using traditional construction methods. Organize work so that all personnel and equipment are ready before placement. Place, consolidate and screed quickly to allow for a maximum finishing time. Use a method of consolidation that eliminates air voids. Do not wait for bleed water; apply the final finish as soon as possible. CEMENT ALL may be troweled, floated, or broom finished. On flat work, do not install in layers. Install full-depth sections and progress horizontally. Do not install on frozen surfaces. To extend working time, use Rapid Set® SET Control® retarding admixture from the Concrete Pharmacy or cold mix water. CEMENT ALL may be applied in temperatures ranging from 45°F to 90°F (7°C to 32°C).

CURING

Water cure all Rapid Set® CEMENT ALL® installations by keeping exposed surfaces wet for a minimum of 1 hour. Begin curing as soon as the surface starts to lose its moist sheen. When experiencing extended setting time due to cold temperature or the use of retarder, longer curing times may be required. The objective of water curing shall be to maintain a continuously wet surface until the product has achieved sufficient strength.

COLD WEATHER

Environmental and material temperatures below 70°F (21°C) may delay setting time and reduce the rate of strength gain. Lower temperatures will have a more pronounced effect. Thinner sections will be more significantly affected. To compensate for cold temperatures, keep material warm, use heated mix water, and follow ACI 306 Procedures for Cold Weather Concreting.

WARM WEATHER

Environmental and material temperatures above 70°F (21°C) may speed setting time and increase the rate of strength gain. Higher temperatures will have a more pronounced effect. To compensate for warm temperatures, keep material cool, use chilled mix water, and follow ACI 305 Procedures for Hot Weather Concreting. The use of SET Control retarding admixture from the Concrete Pharmacy will help offset the effects of high temperatures.

YIELD & PACKAGING

CEMENT ALL is available in 55-lb, 25-lb and 10-lb (25-kg, 11.3-kg and 4.5-kg) sizes. One 55-lb (25-kg) bag of CEMENT ALL will yield approximately 0.5 ft³.

SHELF LIFE

CEMENT ALL has a shelf life of 12 months when stored properly in a dry location, protected from moisture, out of direct sunlight, and in an undamaged package.

USER RESPONSIBILITY

Before using CTS products, read current technical data sheets, bulletins, product labels and safety data sheets. It is the user's responsibility to review instructions and warnings for any CTS products before use.

2. MORTAR MIX High-Strength Structural Repair Mortar DESCRIPTION

Rapid Set® MORTAR MIX is a high-performance, fast-setting, multipurpose repair material. Durable in wet environments, MORTAR MIX is a blend of Rapid Set hydraulic cement and quality aggregates. MORTAR MIX is non-metallic, and no chlorides are added. Mix MORTAR MIX with water to produce a workable, high-quality mortar material that is ideal where fast strength gain, high durability, and low shrinkage are desired. MORTAR MIX sets in 15 minutes and achieves structural strength in 1 hour.

USES

Use MORTAR MIX for general and structural concrete repair, construction of pavements, stucco and plaster repair, one-coat exterior plaster, underlayments and formed work. MORTAR MIX is a versatile product that is suitable for vertical and overhead applications. For freeze thaw durability, in some geographical areas, MORTAR MIX contains an air-entraining admixture.

ENVIRONMENTAL ADVANTAGES

Use MORTAR MIX to reduce your carbon footprint and lower your environmental impact. Production of Rapid Set cement emits far less CO₂ than portland cement. Contact your representative for LEED values and environmental information.

APPLICATION

Apply MORTAR MIX in thicknesses from 1/2" to 6" (1.2 cm to 15.2 cm). For thicker applications, use Rapid Set® Concrete Mix. Not intended for high heat applications above 300°F (149°C). For overlay applications, a minimum of one test section should be prepared to evaluate the suitability of the materials and procedures.

SURFACE PREPARATION

For repairs, application surface shall be clean, sound and free from any materials that may inhibit bond, such as oil, asphalt, curing compound, acid, dirt and loose debris. Roughen surface and remove all unsound material. Apply MORTAR MIX to a thoroughly saturated surface with no standing water.

MIXING

The use of a power-driven mechanical mixer, such as a mortar mixer or a drill-mounted mixer, is recommended. Organize work so that all personnel and equipment are

in place before mixing. Use clean potable water. MORTAR MIX may be mixed using 3 to 5 quarts (2.8 L to 4.7 L) of water per 55-lb (25-kg) bag. Use less water to achieve higher strengths. Do not exceed 5 quarts (4.7 L) of water per bag. For increased fluidity and workability, use Rapid Set® FLOW Control® plasticizing admixture from the Rapid Set® Concrete Pharmacy®. Place the desired quantity of mix water into the mixing container. While the mixer is running, add MORTAR MIX. Mix for the minimum amount of time required to achieve a lump-free, uniform consistency (usually 1 to 3 minutes). Do not retemper.

PLACEMENT

MORTAR MIX may be placed using traditional construction methods. Organize work so that all personnel and equipment are ready before placement. Place, consolidate and screed quickly to allow for a maximum finishing time. Use a method of consolidation that eliminates air voids. Do not wait for bleed water; apply the final finish as soon as possible. MORTAR MIX may be troweled, floated or broom finished. On flat work, do not install in layers. Install full-depth sections and progress horizontally. To extend working time, use Rapid Set® SET Control® retarding admixture from the Concrete Pharmacy or cold mix water. Do not install on frozen surfaces. MORTAR MIX may be applied in temperatures ranging from 45°F to 90°F (7°C to 32°C).

CURING

Water cure all Rapid Set® MORTAR MIX installations by keeping exposed surfaces wet for a minimum of 1 hour. Begin curing as soon as the surface starts to lose its moist sheen. When experiencing an extended setting time due to cold temperature or the

use of retarder, longer curing times may be required. The objective of water curing shall be to maintain a continuously wet surface until the product has achieved sufficient strength.

COLD WEATHER

Environmental and material temperatures below 70°F (21°C) may delay setting time and reduce the rate of strength gain. Lower temperatures will have a more pronounced effect. Thinner sections will be more significantly affected. To compensate for cold temperatures, keep material warm, use heated mix water, and follow ACI 306

Procedures for Cold Weather Concreting.

WARM WEATHER

Environmental and material temperatures above 70°F (21°C) may speed setting time and increase the rate of strength gain. Higher temperatures will have a more pronounced effect. To compensate for warm temperatures, keep material cool, use chilled mix water, and follow ACI 305 Procedures for Hot Weather Concreting. The use of Rapid Set® SET Control retarding admixture from the Rapid Set® Concrete Pharmacy will help offset the effects of high temperatures.

YIELD & PACKAGING

MORTAR MIX is available in 55-lb and 25-lb (25-kg and 11.3-kg) sizes. One 55-lb (25-kg) bag of MORTAR MIX will yield approximately 0.5 ft³.

SHELF LIFE

MORTAR MIX has a shelf life of 12 months when stored properly in a dry location, protected from moisture, out of direct sunlight, and in an undamaged package.

USER RESPONSIBILITY

Before using CTS products, read current technical data sheets, bulletins, product labels and safety data sheets. It is the user's responsibility to review instructions and warnings for any CTS products prior to use.

3. QUIKRETE® RAPID ROAD REPAIR® - EXTENDED PRODUCT DESCRIPTION

QUIKRETE Rapid Road Repair® - Extended is a very high strength, rapid hardening concrete designed to repair concrete highways, bridge decks, concrete parking lots and concrete floors needing repairs exceeding 2" (50mm) in depth.

PRODUCT USE

QUIKRETE Rapid Road Repair® - Extended is made from special blended cement with carefully graded sand and gravel to provide a permanent patch. It also contains alkali-resistant glass fibers for improved flexural performance essential for applications of severe vibration as in the repair of bridge decks. In most cases, traffic can be resumed 90 minutes after patching. QUIKRETE Rapid Road Repair®

- Extended can be used to replace sections of streets or highways, runways or taxiways of airports and other applications where a quick return to service is desired.

SIZES

- QUIKRETE Rapid Road Repair - Extended - 80 lb (36.2 kg) bags

YIELD

- Each 80 lb (36.2 kg) bag of QUIKRETE Rapid Road Repair® - Extended will yield approximately 0.6 cu ft (17 L).

TECHNICAL DATA

APPLICABLE STANDARDS

- ASTM C39/C39M Standard Test Method for Compressive Strength of Cylindrical Concrete Specimens
- ASTM C143 Standard Test Method for Slump of Hydraulic Cement Concrete
- ASTM C191 Standard Test Method for Time of Setting of Hydraulic Cement by Vicat Needle
- ASTM C928 Standard Specification for Packaged, Dry, Rapid-Hardening Cementitious Materials for Concrete Repairs

SURFACE PREPARATION

- Remove all spalled areas and areas of unsound concrete where repair is to occur.
- If rusty reinforcing steel is present, it must be abrasive blasted to remove rust. Remove enough material to completely expose the reinforcing steel.
- The hole should have a vertical edge of 2" (51 mm) or more, formed by use of a pneumatic jackhammer or sawing. Holes should be chipped out to create a new, sound substrate.
- After the chipping process is completed, the repair area must be cleaned by water blasting or other suitable method.
- Dampen holes with clean water before patching. No puddles of water should be left in the hole.

MIXING

- Use approximately 6 pints (2.8 L) of potable water per 80 lb (36.2 kg) bag; sparingly add water as required to achieve a slump of 3-5 inches (76-127 mm). Do not exceed 7 pints (3.3 L) of water.
- All tools and equipment used in the mixing and finishing process should be clean

- Place water in the mixer. While concrete or mortar mixer is running, add contents of the bag
- Mix 4 to 5 minutes. The mix will appear stiffer than normal concrete
- Place in a wheelbarrow or other transporting vehicle. Place the mixture immediately after the mixing is completed

APPLICATION

- The hole should be filled by placing material full depth, from one end to the other to eliminate partial depth lifts between batches.
- Consolidate the material in the hole by vibration, hand tamping or chopping with a shovel. This is particularly important around the edges.
- Screed and finish patches with hand tools to create a surface finish equivalent to the existing slab finish.

CURING

No curing membranes or compounds are required. Traffic can be allowed over the patch in approximately 90 minutes if the temperature is 70 degrees F (21 degrees C) or above. Cure under ambient conditions. Do not moist cure.

REFERENCES

- AASHTO (2014) *AASHTO LRFD Bridge Design Specifications*, SI Units, 7rd edition, Interim Revisions, American Association of State Highway and Transportation Officials.
- Abbasnia, R., Godossi, P. & Ahmadi, J. 2005. *Prediction of restrained shrinkage based on restraint factors in patching repair mortar*. Cement and Concrete Research 35: 1909–1913.
- Abdulhameed, H. 2005. “Fiber Reinforced High Performance Concrete Incorporating Calcined Clay Pozzolan Cement” , M.Sc. thesis, University of Technology.
- Abdulhameed, H. 2010. “*Evaluation of Pozzolan Repair Materials by Different Test Methods*”, Iraqi Journal for Mechanical and Materials Engineering, special Issue (A).pp. 1-14.
- Abdulhameed, H. 2018 “Experimental and analytical study of fiber-reinforced self-consolidating concrete as a repair material”, Ph.D. dissertation, Rutgers University.
- Abdulhameed, H., Nassif, H. & Khayat, K., (2018). “Use of Fiber-Reinforced Self-Consolidating Concrete to Enhance Serviceability Performance of Damaged Beams”. Transportation Research Record: Journal of the Transportation Research Board.
- ACI 318 (2014) *Building Code Requirements for Structural Concrete and Commentary*, ACI Manual of Concrete Practice, American Concrete Institute, Farmington Hills, Michigan.
- ACI 209.2R-08. (2008). *Guide for modeling and calculating shrinkage and creep in hardened concrete*. Farmington Hills, MI.
- ACI 209.1R-05 . (2005). *Report on Factors Affecting Shrinkage and Creep of Hardened Concrete*. , 12.
- ACI Committee 546. 2004. “*Concrete Repair Guide*.” ACI 546R-04. In Concrete Repair Manual, 4th ed., 663–715. Farmington Hills, MI: ACI/ICRI.
- ACI Committee 224. 2001. *Control of cracking in concrete structures*. ACI 224R-01, American Concrete Institute, Farmington Hills, Michigan: 43 pages.
- ACI Committee 224.2R. 2004. *Cracking of concrete members in direct tension*. ACI 224R-04, American Concrete Institute, Farmington Hills, Michigan: 12 pages.
- ACI (American Concrete Institute) and ICRI (International Concrete Repair Institute). (1999). “*Concrete Paving Technology—Guidelines for Partial Depth Repair*.” In Concrete Repair Manual, 467–478. Farmington Hills, MI: ACI/ICRI.
- Al-Manaseer, A., & Prado, A. (2015). Statistical comparisons of creep and shrinkage prediction models using RILEM and NU-ITI databases. ACI Materials Journal, 112(1), 125.
- Austin, S. and Robins, P.J., (1993), “Development of a patch test to study the behavior of shallow concrete patch repairs,” Magazine of Concrete Research, Vol. 45, pp. 221-229.

Austin, S., Robins, P., and Pan, Y., (1995), "Tensile Bond Testing of Concrete Repairs," *Materials and Structures*, Vol. 28, pp. 249-259.

Alexander, K. M., Bruere, G. M., & Ivanusec, I. (1980). The creep and related properties of very high-strength superplasticized concrete. *Cement and Concrete Research*, 10(2), 131-137.

Babaei, K., and Purvis, R., (1994) "Prevention of Cracks in Concrete Bridge Decks: Report on Laboratory Investigation of Concrete Shrinkage," Research Project No. 89-01, Pennsylvania Department of Transportation, Harrisburg, Pa.

Banthia, N., & Gupta, R. (2006). Repairing with fiber-reinforced concrete. *Concrete international*, 28(11), 36-39.

Barde, Amit D., Swathi Parameswaran, Todd Chariton, W. Jason Weiss, Menashi D. Cohen, and Scott Andrew Newbolds. (2006). Evaluation of rapid setting cement-based materials for patching and repair. Final Report FHWA/IN/JTRP, Indiana Department of Transportation and U.S. Department of Transportation.

Bentz, D. P., & Weiss, W. J. (2008). REACT: reducing early-age cracking today. *Concrete Plant International*, 3, 56-61.

Beushausen, H., & Alexander, M. G. 2007. Localised strain and stress in bonded concrete overlays subjected to differential shrinkage. *Materials and structures*, 40(2): 189-199.

CEB-FIP MC 1990 (1993), Design code, Comité Euro-International du Béton, Fédération Internationale de la Précontrainte, Edit. TELFORD, T., 1st Edition, London, 437 p.

Cusson, D., Qian, S., & Hoogeveen, T. (2006). Field performance of concrete repair systems on highway bridge. *ACI materials journal*, 103(5), 366.

Qi, C., Weiss, J., & Olek, J. (2003). Characterization of plastic shrinkage cracking in fiber reinforced concrete using image analysis and a modified Weibull function. *Materials and Structures*, 36(6), 386-395.

Cement and Concrete Association of Australia. 2002. *Drying Shrinkage of Cement and Concrete*, P6, July.

Czarnecki, L., Garbacz, A., Lukowski, P., & Clifton, J. R. (1999). *Polymer composites for repairing of portland cement concrete: compatibility project* (No. NIST Interagency/Internal Report (NISTIR)-6394).

Dela, B. F. (2000). Eigenstresses in hardening concrete. *DTU Department of Structural Engineering and Materials, V. Series R*, (64).

Emmons, P. H. (1993), "Concrete Repair and Maintenance Illustrated", Construction Publishers and Consultants, Kingston, MA, pp. 100-136.

Emberson, N. K., & Mays, G. C. (1990). Significance of property mismatch in the patch repair of structural concrete Part 1: Properties of repair systems. *Magazine of Concrete Research*, 42(152), 147-160.

Toledo Filho, R. D., & Sanjuan, M. A. (1999). Effect of low modulus sisal and polypropylene fibre on the free and restrained shrinkage of mortars at early age. *Cement and Concrete Research*, 29(10), 1597-1604.

COMSOL. "Finite Element Mesh Refinement Definition and Techniques". *COMSOL site*, <https://www.comsol.com/multiphysics/mesh-refinement>. Accessed July. 10, 2017.

Federal Highway Administration (FHWA). 1999. "Manual of Practice: Materials and Procedures for Repair of Partial-Depth Spalls in Concrete Pavements," Federal Highway Administration (FHWA), p. 135.

Ghazy, A., Bassuoni, M. T., Maguire, E., & O'Loan, M. (2016). Properties of Fiber-Reinforced Mortars Incorporating Nano-Silica. *Fibers*, 4(1), 6.

Görander, N. I. C. L. A. S., & Halldén, C. H. R. I. S. T. O. P. H. E. R. (2015). Crack Width Profiles for Fibre-reinforced Concrete Elements with Conventional Reinforcement. In *Tech. rep., Master thesis*. Chalmers University of Technology Göteborg, Sweden.

Hearn, N. (1999). Effect of shrinkage and load-induced cracking on water permeability of concrete. *ACI materials journal*, 96, 234-241.

Hassan, M. S., Mansi, A. S., and Abdul-Hameed, H. A. (2010). "Factors Affecting Compatibility between (S.B.R) Polymer Repair Materials and Concrete Substrate", 2010, Baghdad, Iraq. *Engineering & Technology, the scientific journal of the University of Technology*, 28(14), 4853-4865.

Hadidi, R., & Saadeghvaziri, M. A. (2005). Transverse cracking of concrete bridge decks: State-of-the-art. *Journal of Bridge Engineering*, 10(5), 503-510.

Hearn, N. (1999). Effect of shrinkage and load-induced cracking on water permeability of concrete. *ACI materials journal*, 96, 234-241.

Kassimi, F. (2013). *Development and performance of fiber-reinforced self-consolidating concrete for repair applications*. Ph.D. Dissertation, University of Sherbrooke, Canada.

Kristiawan, S. A. (2013). Performance Criteria to Assess Shrinkage Cracking Tendency in Concrete Overlay. *Procedia Engineering*, 54, 82-100.

Key Facts about America's Surface Transportation System and Federal Funding. The Road Information Program (TRIP), Washington, DC. www.tripnet.org/docs/TRIP_National_Fact_Sheet_April_2012.pdf. Accessed April, 2012.

Kumar, G, A., Kumar, Sh, N., (2014). Creep of Concrete. *International Journal of Engineering Development and Research*, 4(2), 3800-3802.

Kurtz, S., Balaguru, P., Consolazio, G. R., & Maher, A. (1997). *Fast Track Concrete for Construction Repair* (No. FHWA NJ 2001-015).

Li, V. C., Horii, H., Kabele, P., Kanda, T., & Lim, Y. M. (1998). Repair and retrofit with Engineered Cementitious Composites. *AEDIFICATIO Publishers, Fracture Mechanics of Concrete Structures*, 3, 1715-1726.

- Lamond, J. F., & Pielert, J. H. (2006, April). Significance of tests and properties of concrete and concrete-making materials. West Conshohocken, PA: ASTM.
- Lee, K. M., Lee, H. K., Lee, S. H., & Kim, G. Y. (2006). Autogenous shrinkage of concrete containing granulated blast-furnace slag. *Cement and Concrete Research*, 36(7), 1279-1285.
- Leivo, M. and Holt, E., (1997) "Autogenous Volume Changes at Early Ages," In Self-Desiccation and It's Importance in Concrete, B. Persson and G. Fagerlund, editors, Lund University, Lund Institute of Technology, Report TVBM-3075, Lund, Sweden, pp.88-98.
- Lemaitre, J. (2012). *A course on damage mechanics*. Springer Science & Business Media.
- Lepech, M., & Li, V. C. (2005). Water permeability of cracked cementitious composites.
- Luković, M., Šavija, B., Schlangen, E., Ye, G., & van Breugel, K. (2016). A 3D lattice modelling study of drying shrinkage damage in concrete repair systems. *Materials*, 9(7), 575.
- Lybas, J. & Sozen, M. 1977. Effect of beam strength and stiffness on dynamic behaviour of reinforced concrete coupled walls. Civil Engineering. Studies, Structural Research Series (44). University of Illinois, Urbana.
- Mindess S., Young J.F. and Darwin, D. (2003). Concrete, Second Edition, Pearson Education Inc., Upper Saddle River, NJ, 644 pp.
- Mangat, P. S., & Azari, M. M. (1984). A theory for the free shrinkage of steel fibre reinforced cement matrices. *Journal of materials science*, 19(7), 2183-2194.
- Matthews, S. (2007). CONREPNET: Performance-based approach to the remediation of reinforced concrete structures: Achieving durable repaired concrete structures. *Journal of Building Appraisal*, 3(1), 6-20.
- McDonald, D. B., & Roper, H. (1991). FACTORS INFLUENCING RELATIVE-HUMIDITY IN CONCRETE-DISCUSSION. *Magazine of Concrete Research*, 43(157), 305-307.
- McDonald, J. E., Vaysburd, A. M., & Poston, R. W. (1999). Performance criteria for dimensionally compatible repair materials. In *Infrastructure regeneration and rehabilitation improving the quality of life through better construction. International conference* (pp. 751-765).
- McDonald, J.E., Vaysburd, A.M., Emmons, P.H., Poston, R.W. & Kenser, K.E. 2002. Selecting durable repair materials: performance criteria-summary. *Concr. Int.* 24: 37-44.
- Grzybowski, M., & Shah, S. P. (1990). Shrinkage cracking of fiber reinforced concrete. *Materials Journal*, 87(2), 138-148.
- Mehta, P. K. (1986), "Concrete: Structure, Properties, and Materials", Prentice-Hall, Englewood Cliffs, New Jersey, pp. 353-367.
- Mehta P.K., and Meterio P.1. 2006. *Concrete Microstructure, Properties, and Materials*, Third Edition, New York, McGraw-Hill Companies, Inc.
- Mangat, P. S., and Azri, M. M. (1988). "Shrinkage of steel fiber reinforced cement composites." *Mat. and Struct.*, Paris, 21, 163–171.

- Mangat, P. S., & Azari, M. M. (1984). A theory for the free shrinkage of steel fibre reinforced cement matrices. *Journal of materials science*, 19(7), 2183-2194.
- Mansi, A. S. 2010. "Bond Strength Assessment for Different Types of Repair Materials", Baghdad, Iraq. *Engineering & Technology, the scientific journal of the University of Technology*, 28(21). 6325-6336.
- Martinola, G., Sadouki, H., & Wittmann, F. H. (2001). Numerical model for minimizing risk of damage in repair system. *Journal of materials in civil engineering*, 13(2), 121-129.
- Omar W., Makhtar A.M., Lai T.P., Omar R., and Kwong N.M. , 2008. *Creep, Shrinkage and Elastic Modulus of Malaysian Concrete*, Final Report-Project, No: LPIPMICREAMiUPP 02-02-06-09-23.
- Paillere, A., Buil, M., & Serrano, J. J. (1989). Effect of fiber addition on the autogenous shrinkage of silica fume. *Materials Journal*, 86(2), 139-144.
- Parrott, L. J. (1988). Moisture profiles in drying concrete. *Advances in cement research*, 1(3), 164-170.
- Termkhajornkit, P., Nawa, T., Nakai, M., & Saito, T. (2005). Effect of fly ash on autogenous shrinkage. *Cement and Concrete Research*, 35(3), 473-482.
- Poston, R. W., Kesner, K., McDonald, J. E., Vaysburd, A. M., & Emmons, P. H. (2001). Concrete repair material performance—Laboratory study. *Materials Journal*, 98(2), 137-147.
- Pickett, G. (1956, January). Effect of aggregate on shrinkage of concrete and a hypothesis concerning shrinkage. In *Journal Proceedings* (Vol. 52, No. 1, pp. 581-590).
- Pattnaik, R.R., 2006, "Investigation Into Compatibility Between Repair Materials and Substrate Concrete Using Experimental and Finite Element Methods", University, United States: PhD Dissertation, Graduate School of Clemson.
- Raoufi, K., Bernard, E. S., & Weiss, W. J. (2010). Shrinkage cracking behavior of fiber reinforced concrete: as assessed using the restrained ring test. *Journal of ASTM International*, 7(7), 1-15.
- Rahman, M. K., Baluch, M. H., & Al-Gadhib, A. H. 2000. Simulation of shrinkage distress and creep relief in concrete repair. *Composites Part B: Engineering*, 31(6), 541-553.
- Yuan, Y., Li, G., & Cai, Y. (2003). Modeling for prediction of restrained shrinkage effect in concrete repair. *Cement and concrete research*, 33(3), 347-352.
- Sajedi, S., Razavizadeh, A., Minaii, Z., Ghassemzadeh, F., & Shekarchi, M. (2011). A rational method for calculation of restrained shrinkage stresses in repaired concrete members. *Concrete Solutions*, 461.
- Sajedi, S., Ghassemzadeh, F., Harsini, I., Shekarchi, M., & Mohammadi, B. Behavior of bonded concrete overlays under restrained shrinkage.
- Shah, S. P., Krguller, M. E., & Sarigaphuti, M. (1992). Effects of shrinkage-reducing admixtures on restrained shrinkage cracking of concrete. *Materials Journal*, 89(3), 289-295.

- Sahmaran, M., Li, M., & Li, V. C. (2007). Transport properties of engineered cementitious composites under chloride exposure. *Materials Journal*, 104(6), 604-611.
- See, H. T., Attiogbe, E. K., & Miltenberger, M. A. (2003). Shrinkage cracking characteristics of concrete using ring specimens. *Materials Journal*, 100(3), 239-245.
- Smadi, M. M., Slate, F. O., & Nilson, A. H. (1987). Shrinkage and creep of high-, medium-, and low-strength concretes, including overloads. *Materials Journal*, 84(3), 224-234.
- Swamy, R. S., and Stavrides, H. (1979). "Influence of fiber reinforcement on restraining shrinkage and cracking." *J. ACI*, 75, 443-460.
- See, H.T., Attiogbe, E.K. & Miltenberger M.A. 2003. Shrinkage cracking characteristics of concrete using ring specimens. *ACI Materials Journal* 100(3): 239-245.
- Shah, S. P., & Weiss, W. J. (2000). High performance concrete: strength, permeability, and shrinkage cracking. In *PCI/FHWA/FIB International Symposium on High Performance Concrete Precast/Prestressed Concrete Institute Federal Highway Administration Federation Internationale du Beton*.
- Selby, R. G. (1993). Three-dimensional constitutive relations for reinforced concrete. *Publ. Dept of Civil Engrg., Univ. of Toronto*.
- Silfwerbrand, J. 1997. Stresses and strains in composite concrete beams subjected to differential shrinkage, *ACI Structural Journal* 94: 347-353.
- Shin, H. C. (2000). *Early age behavior of bonded concrete overlays due to shrinkage and thermal changes*.
- Shazali, M.A., Rahman, M.K., and Baluch, M.H. (Sep 2012). Shrinkage stress damage effect in concrete patch repair. *Concrete Repair, Rehabilitation and Retrofitting III*; Proc. ICCRRR., Capetown, South Africa., Sep 2012:1071-1076.
- Tazawa, E. I. (Ed.). (1999). Autogenous shrinkage of concrete. CRC Press.
- Tazawa, E. I., & Miyazawa, S. (1995a). Influence of cement and admixture on autogenous shrinkage of cement paste. *Cement and concrete research*, 25(2), 281-287.
- Tazawa, E., Miyazawa, S., & Shigekawa, K. (1991). Macroscopic shrinkage of hardening cement paste due to hydration. In *CAJ proceedings of Cement and Concrete* (Vol. 45, p. 528).
- Tazawa, E. I., & Miyazawa, S. (1995). Experimental study on mechanism of autogenous shrinkage of concrete. *Cement and Concrete Research*, 25(8), 1633-1638.
- Tokuda, H., Shoya. M., Kawakami. M.; and Kagaya. M. 1981. "Applications of Super plastixirers to Reduce Shrinkage and Thermal Cracking of Concrete" Developments in the use of superplasticizers, SP 68. American Concrete Institute. Farmington Hills. Mich. pp. 101-120.
- Vaysburd, A. M., Emmons, P. H., Mailvaganam, N. P., McDonald, J. E., & Bissonnette, B. (2004). Concrete repair technology—A revised approach is needed. *Concrete international*, 26(1), 58-65.

- Vaysburd, A. M., Brown, C. D., Bissonette, B., & Emmons, P. H. (2004). Realcrete” versus “Labcrete. *Concrete international*, 26(2), 90-94.
- Weiss, W. J., Yang, W., & Shah, S. P. (1998). Shrinkage cracking of restrained concrete slabs. *Journal of Engineering Mechanics*, 124(7), 765-774.
- Wang, K., & Lomboy, G. (2016). Developing Green, Highly Flowable, Rapid Set, High-Performance Concrete for Pavement Patch Repair.
- Weiss, W. J., & Shah, S. P. (1997). Recent trends to reduce shrinkage cracking in concrete pavements. In *Proceedings of the 1997 Airfield Pavement Conference*. ASCE.
- Wipf, T. J., Klaiber, F. W., & Raker, E. J. (2004). *Effective Structural Concrete Repair-Volume 3 of 3: Evaluation of Repair Materials for Use in Patching Damaged Concrete* (No. Iowa DOT Project TR-428 (Volume 3)).
- Weiss, W. J., Yang, W., & Shah, S. P. (1998). Shrinkage cracking of restrained concrete slabs. *Journal of Engineering Mechanics*, 124(7), 765-774.
- Yang, Z., Brown, H., Huddleston, J., & Seger, W. (2016). Performance evaluation of rapid-set prepackaged cementitious materials for rehabilitation of surface distress of concrete transportation structures. *PCI Journal*, 61(2).
- Yang, Q., Zhu, B., Zhang, S., & Wu, X. (2000). Properties and applications of magnesia–phosphate cement mortar for rapid repair of concrete. *Cement and concrete Research*, 30(11), 1807-1813.
- Yuan, Y. S., & Marosszeky, M. (1994). Restrained shrinkage in repaired reinforced concrete elements. *Materials and structures*, 27(7), 375-382.
- Zhang, J., & Li, V. C. (2001). Influences of fibers on drying shrinkage of fiber-reinforced cementitious composite. *Journal of engineering mechanics*, 127(1), 37-44.
- Zhou, J., Ye, G., Schlangen, E. & Breugel, K. 2008. Modelling of stresses and strains in bonded concrete overlays subjected to differential volume changes. *Theoretical and Applied Fracture Mechanics* 49: 199–205.